LASER GENERATED THERMOELASTIC WAVES IN FINITE AND INFINITE TRANSVERSELY ISOTROPIC CYLINDERS

by

RAVI CHITIKIREDDY

A THESIS SUBMITTED TO THE FACULTY OF GRADUATE STUDIES OF

THE UNIVERSITY OF MANITOBA

IN PARTIAL FULFILLMENT OF THE REQUIREMENTS OF THE DEGREE OF

DOCTOR OF PHILOSOPHY

DEPARTMENT OF CIVIL ENGINEERING

UNIVERSITY OF MANITOBA

WINNIPEG

Abstract

This thesis presents a theoretical study of thermoelastic guided waves in cylinders in the context of Lord-Shulman generalized theory of thermoelasticity. Two different methods were formulated to study dispersion relations in infinite cylinders. One of them is a Semi Analytical Finite Element (SAFE) method and the other is an analytical method. In the SAFE method, the dispersion equation has been formulated as a generalized eigenvalue problem by treating radial displacement and temperature with a one dimensional finite element model through the thickness of the cylinder. In the analytical method, displacement potentials are introduced to obtain the dispersion relations of guided wave modes. This method is applicable to isotropic cylinders and has been developed primarily to cross check the SAFE formulation. Frequency spectra obtained by both methods for an isotropic cylinder have shown excellent agreement with each other. Since the SAFE method can be used for an anisotropic composite cylinder, guided wave modes for anisotropic and composite cylinders are presented.

Transient analysis of ultrasonic guided waves generated by concentrated heating of the outer surface of an infinite anisotropic hollow cylinder has also been studied. The SAFE method is employed to model the response of a circular cylinder due to a pulsed laser focused on its surface. Green's functions were constructed numerically by superposition of guided wave modes in frequency and wave number domains. Time histories of the propagating modes are then calculated by applying an inverse Fourier transformation in the time domain. Transient radial displacements of longitudinal and flexural modes of a transversely isotropic silicon nitride (Si_3N_4) cylinder are presented.

Propagation of thermoelastic waves in a circular annulus and in finite length circular cylindrical shells have also been investigated. The SAFE method is used to simulate the guided wave modes in the cylinder. Frequency spectra obtained by the SAFE formulation, for a finite length transversely isotropic cylinder (isothermal case), are validated by comparing the numerical results with relevant publications. Frequency spectra for axisymmetric and asymmetric modes in a silicon nitride finite cylinder with both ends insulated and restrained by frictionless rigid walls are presented. The plain strain problem of circumferential guided waves is also studied and the results are validated for an isothermal case.

Acknowledgement

I would like to express my heartfelt gratitude to my advisor Prof. A. H. Shah for his invaluable guidance, constant encouragement and support during the research. He was always there to help me at all stages of my work and I have always admired him not only just as a good professor but also as a very good person and extremely disciplined researcher. I would also like to express my gratitude towards my co-advisor Prof. H. Bai for his guidance throughout the progress of my work. He has been extremely helpful to me at all stages of my work.

My deep appreciation also goes to Prof. S. K. Datta, University of Colorado, USA, for his readiness to help and have fruitful discussions. It was a great learning experience working with him and I feel proud to be associated with him in this work.

I wish to express my grateful thanks to Profs. N. Rattanawangcharoen and G. Bridges for serving in the examination committee and giving helpful comments. Special thanks are conveyed to Prof. Osama Mukdadi for devoting his time to serve as an external examiner.

The financial supports from the NSERC research grant of Professor A.H Shah, the Graduate Fellowship from the University of Manitoba and the Teaching Assistantship from the Department of Civil Engineering to complete this doctoral study are acknowledged gratefully.

I would also like to thank all those staff and graduate students in the Department of Civil Engineering who freely offered much friendly assistance. In addition, useful discussions were held with my colleague Mr. Darryl K. Stoyko.

I take this opportunity to thank Mrs. Arvind Shah for her moral support which was the most influential factor to complete my research. Finally, I would like to express my sincere regards to my father Satya Rao and mother Paiditalli, my wife Lakshmi, and parents-in-law for their support and continuous encouragement in my graduate studies.

TABLE OF CONTENTS

LIST OF FIGURES

LIST OF TABLES

Chapter 1

Introduction

1.1 Motivation

Nondestructive evaluation (NDE) technique is a family of specialized inspection methods that provides information about the condition and flaws of structural components without impairing their future usefulness. Inspection using NDE techniques enables the rehabilitation of degraded structures and preventing catastrophic structural failures. There are several nondestructive testing (NDT) methods available for inspection, such as liquid penetration, magnetic particles, radiography, eddy currents and ultrasonic techniques. Among all inspection methods that have been in practice, ultrasonic techniques have proven to be most amenable to on-line evaluation. This is because ultrasonic waves propagate very efficiently through the materials and are affected by discontinuities (such as cracks or voids or other changes in the mechanical and geometry properties). They provide an effective means of nondestructive characterization of material properties. Another important application of these waves is for defect detection in structural components.

There are many ways to generate and detect ultrasonic waves, among which laser based ultrasonic techniques have attracted great attention in recent years. These techniques not only

overcome the difficulty of using piezoelectric transducers on curved complex surfaces. They also provide a number of advantages over conventional ultrasonic methods, such as noncontact generation and detection of waves having a large bandwidth, and ability to operate on curved and rough surfaces (Scruby and Drain 1990). White (1963) demonstrated that ultrasonic waves can be generated in a solid by irradiating its surface by concentrated laser beams. Generally, there are two different mechanisms for such wave generation, depending on the density of energy deposited by the laser pulse. At high energy a thin surface layer of the solid melts (i.e., ablation process), this in turn gives rise to forces that generate ultrasonic waves. This process induces micro damage, which is not suitable for a NDE technique. At a low power level the surface of the material does not melt but induces a rapidly changing strain field due to the thermal expansion of the material. This strain field radiates energy as elastic waves. This is completely a thermoelastic process which causes no damage to the material surface. Therefore ultrasonic waves generated by laser irradiation in the thermoelastic regime are suitable for NDE applications.

The thermoelasticity of materials must be considered when ultrasonic waves generated by lasers are studied. Moreover, civil engineering, aeronautic and nuclear structures can be exposed to high temperatures. Therefore, the influence of thermoelasticity must be investigated to expand the application of NDT to these environments. Composite circular tubes and metallic pipes are common structural components which are used extensively in the energy and transportation industries. Damage to these components occurs due to handling, service loads and environmental

causes. Ultrasonic nondestructive techniques are being developed for the inspection of these components.

The objective of the present work is to study thermoelastic guided waves in cylinders theoretically using the generalized theory of thermoelasticity. A semi analytical finite element (SAFE) method has been developed to simulate the thermoelastic guided waves in cylinders. Also, an analytical model, applicable for an isotropic infinite cylinder is formulated to verify the guided wave modes obtained by the SAFE method. The guided thermoelastic wave modes, for an isotropic copper infinite cylinder, obtained by both methods have been compared. Dispersion of guided waves in a finite length cylinder is also investigated in this thesis using the SAFE model.

1.2 Guided Waves in Cylinders

In ultrasonic testing, early techniques used body waves later followed by guided waves. Guided waves are dispersive and multi-mode in nature. Thus, these waves can be used to generate many data points in a given frequency range. Also the speed of these waves is very sensitive to material properties. The selection of mode and frequency plays a very important role in the success of the ultrasonic NDE technique. Hence, the dispersion characteristics of these waves need to be understood. The axially symmetric vibration of harmonic waves in a homogeneous isotropic infinite cylindrical rod was investigated analytically by Pochhammer (1876) and Chree (1889). The proposed dispersion equation relates three variables. They are Poisson's ratio, angular frequency and the wave number. The dispersion equation satisfies the governing equations of motion and the traction free boundary conditions on the surface of the cylinder. Although

dispersion equations were introduced in 1876, no detailed numerical calculations for phase and group velocities were reported until 1962 due to complexity of the dispersion equation. At this time, Onoe at el, published complex wave numbers over a wide range of frequencies. Complex wave numbers represent non-propagating and evanescent modes. Propagating modes corresponding to real wave numbers are physically measurable. However, complex wave numbers are essential in studying wave scattering and the end reflection problem. They are also needed to satisfy end conditions of semi-infinite and finite cylinders.

Dispersion characteristics of elastic waves for infinitely long circular cylinders have been published by many authors. A review of literature by Soldatos (1994) contains many references related to three dimensional dynamic analyses of circular cylinders and cylindrical shells. There are many articles based on the semi-analytical finite element (SAFE) technique for the analysis of guided waves in cylinders [Nelson et al. (1971), Huang and Dong (1984), and Rattanawangcharoen et al. (1992, 1994a)]. References to many earlier works on composite cylinders can be found in the review by Datta (2000) and in the text book by Datta and Shah (2009).

Exact analytical solutions for a finite-length vibrating cylinder cannot be obtained in general. Therefore, several approximate solutions have been proposed to estimate natural frequencies of finite isotropic circular cylinders by McMahon (1964, 1970), Hutchinson (1972), Gladwell and Tahbildar (1972), and Gladwell and Vijay (1975).

When the cylinder is anisotropic, the solution of the free vibration problem becomes more complex. Lusher and Hardy (1988) employed separation of variables technique used by Morse (1954) to study the axisymmetric vibrations of transversely

isotropic cylinders and presented experimental results for sapphire rods. Heyliger (1991) estimated natural frequencies of axisymmetric modes of finite length transversely isotropic cylinders by applying the Ritz method. Chau (1994) and Honarvar et al. (2009) studied axisymmetric and asymmetric vibrations of a finite transversely isotropic cylinder using potential functions and compared their results with the experimental observations of Lusher and Hardy (1988). Chen et al. (1996) studied free vibrations of finite orthotropic thin cylindrical shells by employing shell theory. Liu and Qu (1998) studied analytically the two-dimensional problem of guided circumferential waves in a circular annulus.

All of the above studies are concerned with propagation of waves in cylinders within the framework of isothermal linear theory of elasticity but there is a very limited amount of reported work on waves in cylinders using thermoelastic theories. In the following, a literature review of works that deal with thermoelastic waves in elastic media is presented.

1.3 Literature Review

Use of generalized thermoelasticity theories to analyze thermoelastic waves generated by a pulsed laser beam has received some attention in recent years. The classical theory of heat conduction in solids treats the flux of heat as proportional to the gradient of temperature in the media. Therefore, the heat conduction equation is a parabolic partial differential equation, which predicts an infinite thermal wave speed. This assumption of infinite speed of heat propagation is contrary to the physical phenomenon. To rectify this paradox, several generalizations to the classical heat

conduction equation and the thermoelastic wave equations have been proposed. These generalizations take into account the finite wave speed of the thermal pulse travelling through the body.

Lord and Shulman (1967) (LS) presented a generalized theory of thermoelasticity for an isotropic body that was a modification of the Fourier law of heat conduction by the inclusion of a relaxation time. This then predicts a finite thermal wave speed. Other generalizations were proposed by Green and Lindsay (1972), who developed a temperature – rate dependent theory that included two relaxation times and by Green and Naghdi (1993) (GN), who introduced a thermoelasticity theory without energy dissipation. The theoretical developments of thermoelasticity with finite wave speeds are given in a monograph by Ignaczak and Ostoja – Starzewski (2010).

Since White (1963) first demonstrated the generation of ultrasonic waves in a medium by irradiating its surface by a pulsed laser beam, significant research has been done on laser ultrasonics both theoretically and experimentally. Most of these works treat the problem as isothermal with the heat source replaced by equivalent surface forces.

Spicer et al. (1990) studied laser ultrasonic waves in a thin plate theoretically and experimentally to compute the elastic moduli and the plate thickness. Rayleigh – Lamb waves in plates using the Lord – Shulman theory have been discussed by Datta and Shah (2009). References to many other works can be found in this book [see also, Sharma et al. (2000), Verma (2002), Verma and Hasebe (2001), Al-Qahtani and Datta (2004), Al-Qahtani et al. (2005), and Xu et al. (2008)].

Compared to many studies that have dealt with plates there is a very limited amount of reported work on waves in cylinders using generalized thermoelastic theories.

Dispersion of longitudinal thermoelastic wave propagation in a circular isotropic cylinder was studied by Erbay and Suhubi (1986), who considered the cylinder surface to be stress – free and at a constant temperature. Elnagar and Abd-Allah (1987) studied the influence of the initial stress on the Rayleigh wave propagation in a generalized thermoelastic cylinder. Three dimensional vibration of a homogeneous transversely isotropic thermoelastic cylindrical panel has been investigated by Sharma (2001) and Sharma and Sharma (2002). Recently, wave propagation in a thermoelastic cylinder of an arbitrary cross section has been reported by Ponnusamy (2007), who used a collocation method to study the dispersive waves.

Circumferential isothermal elastic waves in an isotropic cylinder generated by a laser pulse and their scattering by a surface defect was studied experimentally by Clorennec and Royer (2003). Pan et al. (2004, 2006) investigated theoretically and experimentally the isothermal acoustic waves generated by a laser point pulse in an isotropic and a transversely isotropic cylinder, respectively. Three dimensional Fourier transforms were used to find the dynamic displacements at the cylinder surface. Jiangong et al. (2010) studied circumferential thermoelastic waves in an orthotropic cylindrical curved plates using GN theory of thermoelasticity.

1.4 Thesis Outline

This thesis is mainly concerned with the investigation of thermoelastic guided waves in anisotropic cylinders in the context of Lord and Shulman (LS) generalized theory of thermoelasticity. A transversely isotropic silicon nitride (Si_3N_4) tube is

considered to illustrate numerical results. Amorphous and textured Si_3N_4 has been widely studied in the past for its excellent mechanical properties, such as, high resistance to thermal shock and chemical attack, high fracture toughness, and good tribological and wear properties. A good review of the processing and anisotropic properties of silicon nitride for various automotive, electronic and aerospace applications can be found in Zhu and Sakka (2008) [see also, Kitayama et al. (1999), Vogelgesang et al. (2000), and Yokota and Ibukyama (2003)]. Si_3N_4 nanorods and nanotubes have been studied in recent years (Lin, et al (2005)).

The thesis is organized in the following manner. Motivation and literature reviews are presented above in this chapter. Chapter 2 is devoted to the study of propagation characteristics of guided thermoelastic waves in infinitely long cylinders. Two different methods are used in this study: one of them is a semi analytical finite element (SAFE) method and the other is an analytical method. In the SAFE method, the cylinder is discretized in the radial direction into several coaxial circular cylinders (sub-cylinders). In the analytical method, displacement potentials are introduced to obtain dispersion relation of guided wave modes. This method is applicable to an isotropic cylinder and is intended primarily to cross check the SAFE formulation. Frequency spectra obtained by both methods for an isotropic copper cylinder have shown excellent agreement with each other. Guided wave modes are presented in this chapter for anisotropic and composite cylinders using the SAFE method.

In Chapter 3, transient radial displacement responses of guided waves generated by concentrated heating of the outer surface of an infinite anisotropic hollow cylinder are presented. Generalized thermoelastic theory proposed by Lord and Shulman is used to

model the response of a circular cylindrical shell due to a pulsed laser focused on the surface of the cylinder. In this study, the temperature dependence of thermal properties of irradiated material is neglected. A semi-analytical finite element (SAFE) method is employed to evaluate guided wave modes in the cylinder. The variation of displacement and temperature is approximated by one dimensional isoparametric finite elements in the radial direction and assumed harmonic functions in the transverse and axial directions. The cylinder is discretized into N laminas and over each lamina quadratic interpolation polynomials are used to approximate the displacement and the temperature field in the radial direction. The variational principle is used to derive the governing displacement equations of motion. Once the dispersion equations for guided wave modes are solved, Green's functions are constructed numerically by superposition of the guided wave modes. The obtained Green's functions are in frequency and wave number domains. The corresponding responses in the time domain are then calculated by applying inverse Fourier transformations. The heat input due to a laser pulse is assumed to decay exponentially in the radial direction and has a Gaussian profile in the axial direction. The spatial distribution of the heat source along the radial direction is calculated by consistent load formulation.

Investigation of thermoelastic guided waves in a circular annulus and in a finite length circular cylindrical shells are presented in Chapter 4. Herein, a finite cylinder with both ends restrained by frictionless rigid walls and insulated is considered for the numerical analysis. A semi-analytical finite element (SAFE) method is employed to model the guided wave modes in the cylinder using the LS generalized theory of thermoelasticity. The dispersion equation for guided waves is obtained in the form of an

eigenvalue problem. Frequency spectra obtained by the SAFE formulation, for a finite length transversely isotropic cylinder (isothermal case), are validated by comparing the numerical results with relevant publications. Also, propagating modes obtained for the (plane strain) circumferential wave propagation problem are verified with existing ones for an isotropic (isothermal) case. Numerical results are presented for both propagating and evanescent modes in a transversely isotropic silicon nitride cylinder.

In Chapter 5, conclusions of the work and a short description of possible future study are outlined.

Chapter 2

Thermoelastic Waves in Cylinders

2.1 Introduction

In this chapter, propagation of thermoelastic waves in infinite circular cylinders has been studied in the context of LS (Lord and Shulman, 1967) generalized theory of thermoelasticity. Two different methods are used to study the dispersion characteristics of guided wave modes in the cylinder: one of them is a semi analytical finite element (SAFE) method presented by Nelson et al. (1971) and Huang and Dong (1984), and the other is an analytical method. In the SAFE method, the cylinder is discretized in the radial direction into several coaxial circular cylinders (sub-cylinders) and the radial dependence of the displacement and temperature in each sub-cylinder is approximated by quadratic interpolation polynomials. The dispersion equation of the cylinder in the form of an eigenvalue problem is formulated by applying a principle of variation. In the analytical method, the guided wave modes of a circular cylinder are expressed as functions of Bessel's functions. The SAFE formulation is validated by comparing its numerical results of an isotropic copper cylinder with that of analytical method. Since the

SAFE method can also be used for anisotropic and composite cylinders, numerical results are presented for a silicon nitride (anisotropic) cylinder and a two layered composite cylinder.

2.2 Description of the Problem

Consider an infinite thermoelastic cylinder with inner radius r_i and outer radius r_o in the cylindrical coordinate system (r, θ, z) with the origin at the center of the cross section of the cylinder as shown in Fig. 2.1. The inner and outer surfaces of the cylinder are traction free and the cylinder is initially at uniform temperature T_0 in the undisturbed state. The direction of wave propagation is in axial direction, *z*.

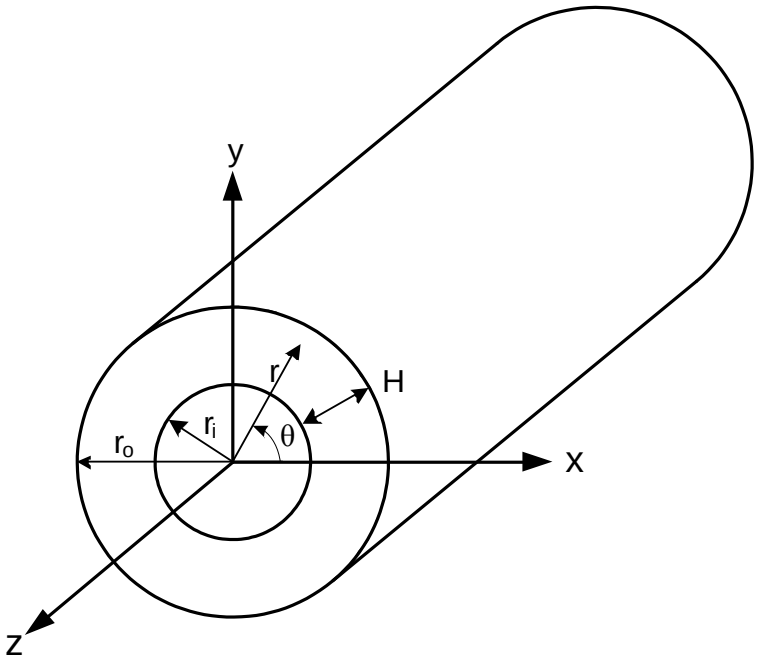

Figure 2.1: Geometry of the cylinder

2.3 Governing Equations

The generalized L-S governing equations of thermoelasticity, in the absence of body forces and heat sources, are given by Al-Qahtani et al. (2004)

$$\sigma_{ij,j} = \rho \ddot{u}_i \tag{2.1}$$

$$T_0 \rho \dot{\eta} = -q_{i,i} \tag{2.2}$$

$$\sigma_{ij} = C_{ijkl} \varepsilon_{kl} - \beta_{ij} T \tag{2.3}$$

$$\rho \dot{\eta} = \beta_{ij} \dot{\varepsilon}_{ij} + \frac{\rho c_E}{T_0} \dot{T} \tag{2.4}$$

$$q_i + \tau_0 \dot{q}_i = -k_{ij} T_{,j} \tag{2.5}$$

Various physical quantities and material constants appearing in the above equations are: σ_{ij}, the components of the stress tensor; u_i, the components of the displacement; ε_{ij}, the components of the strain tensor; C_{ijkl}, the elastic constants; q_i, components of the heat flux vector; ρ, the mass density; T_0, the reference temperature; η, the entropy density; T, the temperature change; c_E, the specific heat at constant deformation; τ_0, the thermal relaxation time; β_{ij}, the thermal coefficients; k_{ij}, the coefficients of thermal conductivity. In the above equations, the superposed dot indicates the derivative with respect to time.

Nondimensional quantities, used by Al-Qahtani and Datta (2004) and many others, are only suitable for the single layer cylinder since equations of motion have a different form after normalization. Normalization which can be used for multilayered

cylinders has not been reported yet. Therefore, a set of normalized quantities is presented here and they are given by

$$
\begin{aligned}
& r_i^* = \frac{r_i}{H}, \quad u_i^* = \frac{u_i}{\delta H}, \quad T^* = \frac{T}{\bar{T}}, \quad t^* = \frac{\bar{v}}{H} t, \\
& \sigma_{ij}^* = \frac{\sigma_{ij}}{\delta \bar{c}}, \quad q_i^* = \frac{q_i}{\bar{q}}, \quad \varepsilon_{ij}^* = \frac{\varepsilon_{ij}}{\delta}, \quad \rho^* = \frac{\rho}{\bar{\rho}}, \quad c_E^* = \frac{c_E}{\bar{c}_E}, \\
& \beta_{ij}^* = \frac{\beta_{ij}}{\bar{\beta}}, \quad k_{ij}^* = \frac{k_{ij}}{\bar{k}}, \quad c_{ijkl}^* = \frac{c_{ijkl}}{\bar{c}}, \quad \tau_0^* = \frac{\bar{v}}{H} \tau_0, \quad T_0^* = \frac{T_0}{\bar{T}}
\end{aligned}
\tag{2.6}
$$

where

$$
\bar{v} = \sqrt{\frac{\bar{c}}{\bar{\rho}}}, \quad \delta = \sqrt{\frac{\bar{k}\bar{T}}{H\bar{v}\bar{c}}}, \quad \bar{q} = \frac{\bar{k}\bar{T}}{H}, \quad \bar{\beta} = \frac{\delta \bar{c}}{\bar{T}}, \quad \bar{c}_E = \frac{\bar{k}}{\bar{\rho}\bar{v}H} \tag{2.7}
$$

Two more nondimensional quantities are also defined: the wave number $\xi^* = \xi H$ and frequency $\omega^* = \frac{\omega H}{\bar{v}}$. Here $\bar{\rho}, \bar{k}, \bar{c}, H$ and $\bar{T}$ are the basic normalization quantities and the rest could be derived from them as shown above. Note that, $\bar{\rho}, \bar{k}, \bar{c}$ and $\bar{T}$ can be taken suitably depending upon the material properties of the cylinder. This non-dimensional scheme yields all dimensionless equations in the same form as their dimensional counterparts. Therefore, this normalization could be used to solve multilayer cylinders. For convenience, the superscript (*) will be dropped.

2.4 Semi-Analytical Finite Element Formulation

The Semi-Analytical Finite Element (SAFE) method was presented by Nelson, et al. (1971), and by Huang and Dong (1984) to study wave propagation problems in

anisotropic cylinders. In this method the radial displacement $\mathbf{u}$ and the temperature $\boldsymbol{T}$ are approximated by one dimensional isoparametric finite elements. The total thickness of the cylinder H is composed of cylindrical layers and each layer can have distinct thermoelastic properties and thickness. By using the SAFE method, the thickness of the cylinder is discretized into N laminas. Quadratic interpolation polynomials are used to approximate the displacement and the temperature fields over each lamina in the radial direction.

The displacement and temperature of the k^{th} lamina are expressed as

$$\begin{aligned}\mathbf{u}(r,\theta,z,t) &= \mathbf{N}_1(\zeta)\mathbf{u}^e(\theta,z,t)\\ \mathbf{T}(r,\theta,z,t) &= \mathbf{N}_2(\zeta)\mathbf{T}^e(\theta,z,t)\end{aligned} \tag{2.8}$$

and

$$r = \mathbf{N}_2(\zeta)\mathbf{R}^e \tag{2.9}$$

Here

$$\mathbf{N}_1(\zeta) = \begin{bmatrix} n_1 & 0 & 0 & n_2 & 0 & 0 & n_3 & 0 & 0 \\ 0 & n_1 & 0 & 0 & n_2 & 0 & 0 & n_3 & 0 \\ 0 & 0 & n_1 & 0 & 0 & n_2 & 0 & 0 & n_3 \end{bmatrix}, \tag{2.10}$$

$$\mathbf{N}_2(\zeta) = \begin{bmatrix} n_1 & n_2 & n_3 \end{bmatrix}$$

$$\begin{aligned}\mathbf{u}^e &= \left(u_{r1}, u_{\theta 1}, u_{z1}, u_{r2}, u_{\theta 2}, u_{z2}, u_{r3}, u_{\theta 3}, u_{z3}\right)^T,\\ \mathbf{T}^e &= \left(T_1, T_2, T_3\right)^T,\\ \mathbf{R}^e &= \left(R_b, R_m, R_f\right)^T\end{aligned} \tag{2.11}$$

In equation (2.10), the shape functions are

$$n_1 = \tfrac{1}{2}\zeta(\zeta-1), \quad n_2 = 1-\zeta^2, \quad n_3 = \tfrac{1}{2}\zeta(\zeta+1), \quad -1 \le \zeta \le 1 \tag{2.12}$$

where

$$\zeta = \frac{2r - R_b - R_f}{R_f - R_b} \qquad (R_b \le r \le R_f) \tag{2.13}$$

In equation (2.11), the nodal displacements $u_{rj}, u_{\theta j}, u_{zj}$, and temperature T_j, where j = 1, 2, 3, are taken at the inner surface $\left(r = R_b\right)$, middle layer $\left(r = R_m = \left(R_b + R_f\right)/2\right)$, and outer surface $\left(r = R_f\right)$ of the k^{th} lamina.

The strain tensor and temperature gradient are expressed as

$$\boldsymbol{\varepsilon} = \mathbf{D}_1\mathbf{u}^e + \mathbf{D}_2\mathbf{u}^e_{,\theta} + \mathbf{D}_3\mathbf{u}^e_{,z} \tag{2.14}$$

$$\mathbf{T}' = \mathbf{B}_1\mathbf{T}^e + \mathbf{B}_2\mathbf{T}^e_{,\theta} + \mathbf{B}_3\mathbf{T}^e_{,z} \tag{2.15}$$

The stress vector is given by

$$\boldsymbol{\sigma} = \mathbf{C}\left(\mathbf{D}_1\mathbf{u}^e + \mathbf{D}_2\mathbf{u}^e_{,\theta} + \mathbf{D}_3\mathbf{u}^e_{,z}\right) - \boldsymbol{\beta}\mathbf{N}_2\mathbf{T}^e \tag{2.16}$$

Matrices $\mathbf{C}, \boldsymbol{\beta}$, $\mathbf{B}_1$, $\mathbf{B}_2$, $\mathbf{B}_3$, $\mathbf{D}_1$, $\mathbf{D}_2$ and $\mathbf{D}_3$ are defined in Appendix A. The variational principle of thermoelasticity, Al-Qahtani et al. (2004), is

$$\int_{t_0}^{t_1}\int_V \left(\delta\boldsymbol{\varepsilon}^T\boldsymbol{\sigma} - \delta\mathbf{T}'^T\mathbf{K}\mathbf{T}' - \delta\mathbf{T}'^T\left(\mathbf{q} + \tau_0\dot{\mathbf{q}}\right)\right)dVdt = \int_{t_0}^{t_1}\int_V \delta\mathbf{u}^T\left(-\rho\ddot{\mathbf{u}}\right)dVdt \tag{2.17}$$

The first term in the left hand side of equation (2.17) is

$$\begin{aligned}\int_{t_0}^{t_1}\int_V \delta\boldsymbol{\varepsilon}^T\boldsymbol{\sigma}dVdt &= \int_{t_0}^{t_1}\int_V \left(\mathbf{D}_1\delta\mathbf{u}^e + \mathbf{D}_2\delta\mathbf{u}^e_{,\theta} + \mathbf{D}_3\delta\mathbf{u}^e_{,z}\right)^T\left[\mathbf{C}\left(\mathbf{D}_1\mathbf{u}^e + \mathbf{D}_2\mathbf{u}^e_{,\theta} + \mathbf{D}_3\mathbf{u}^e_{,z}\right) - \boldsymbol{\beta}\mathbf{N}_2\mathbf{T}^e\right]dVdt \\ &= \int_{t_0}^{t_1}\int_z\int_\theta \delta\mathbf{u}^{eT}\begin{bmatrix}\mathbf{K}_{11}\mathbf{u}^e + \left(\mathbf{K}_{12} - \mathbf{K}_{21}\right)\mathbf{u}^e_{,\theta} + \left(\mathbf{K}_{13} - \mathbf{K}_{31}\right)\mathbf{u}^e_{,z} \\ -\mathbf{K}_{22}\mathbf{u}^e_{,\theta\theta} - \left(\mathbf{K}_{23} + \mathbf{K}_{32}\right)\mathbf{u}^e_{,\theta z} - \mathbf{K}_{33}\mathbf{u}^e_{,zz} \\ -\mathbf{K}^e_{01}\mathbf{T}^e + \mathbf{K}^e_{02}\mathbf{T}^e_{,\theta} + \mathbf{K}^e_{03}\mathbf{T}^e_{,z}\end{bmatrix}d\theta dzdt\end{aligned} \tag{2.18}$$

The second term in equation (2.17) is

$$\begin{aligned}\int_{t_0}^{t_1}\int_V \delta\mathbf{T}'^T\mathbf{K}\mathbf{T}'\,dVdt &= \int_{t_0}^{t_1}\int_V \left(\delta\mathbf{T}^{eT}\mathbf{B}_1^T + \delta\mathbf{T}_{,\theta}^{eT}\mathbf{B}_2^T + \delta\mathbf{T}_{,z}^{eT}\mathbf{B}_3^T\right)\mathbf{K}\left(\mathbf{B}_1\mathbf{T}^e + \mathbf{B}_2\mathbf{T}_{,\theta}^e + \mathbf{B}_3\mathbf{T}_{,z}^e\right)dVdt \\ &= \int_{t_0}^{t_1}\int_z\int_\theta \delta\mathbf{T}^{eT}\left(\mathbf{g}_{11}\mathbf{T}^e - \mathbf{g}_{22}\mathbf{T}_{,\theta\theta}^e - \mathbf{g}_{33}\mathbf{T}_{,zz}^e\right)d\theta dzdt\end{aligned} \tag{2.19}$$

The third term in equation (2.17) is

$$\begin{aligned}\int_{t_0}^{t_1}\int_V \delta\mathbf{T}'^T\left(\mathbf{q} + \tau_0\dot{\mathbf{q}}\right)dVdt &= -\int_{t_0}^{t_1}\int_V \delta\mathbf{T}^T\left(\nabla\cdot\mathbf{q} + \tau_0\nabla\cdot\dot{\mathbf{q}}\right)dVdt \\ &= \int_{t_0}^{t_1}\int_V \delta\mathbf{T}^T\left(T_0\rho\dot{\eta} + \tau_0 T_0\rho\ddot{\eta}\right)dVdt \\ &= \int_{t_0}^{t_1}\int_V \delta\mathbf{T}^T\left[T_0\boldsymbol{\beta}^T\dot{\boldsymbol{\varepsilon}} + \rho c_E\dot{T} + \tau_0\left(T_0\boldsymbol{\beta}^T\ddot{\boldsymbol{\varepsilon}} + \rho c_E\ddot{T}\right)\right]dVdt \\ &= \int_{t_0}^{t_1}\int_z\int_\theta \delta\mathbf{T}^{eT}\left[\begin{array}{l}\left(\mathbf{f}_1\dot{\mathbf{u}}^e + \mathbf{f}_2\dot{\mathbf{u}}_{,\theta}^e + \mathbf{f}_3\dot{\mathbf{u}}_{,z}^e + \mathbf{m}_0\dot{\mathbf{T}}^e\right) + \\ \tau_0\left(\mathbf{f}_1\ddot{\mathbf{u}}^e + \mathbf{f}_2\ddot{\mathbf{u}}_{,\theta}^e + \mathbf{f}_3\ddot{\mathbf{u}}_{,z}^e + \mathbf{m}_0\ddot{\mathbf{T}}^e\right)\end{array}\right]d\theta dzdt\end{aligned} \tag{2.20}$$

The right hand side of equation (2.17) has the form

$$\int_{t_0}^{t_1}\int_V \delta\mathbf{u}^T\left(-\rho\ddot{\mathbf{u}}\right)dVdt = \int_{t_0}^{t_1}\int_z\int_\theta \delta\mathbf{u}^{eT}\left(-\mathbf{M}\ddot{\mathbf{u}}^e\right)d\theta dzdt \tag{2.21}$$

The element matrices appearing in equations (2.18) – (2.21) are defined in Appendix A.

Equating the coefficients of $\delta\mathbf{u}^e$ in equation (2.17) to zero gives the following equation

$$\begin{aligned}&\mathbf{M}\ddot{\mathbf{u}}^e + \mathbf{K}_{11}\mathbf{u}^e - \mathbf{K}_{01}\mathbf{T}^e + \left(\mathbf{K}_{12} - \mathbf{K}_{21}\right)\mathbf{u}_{,\theta}^e + \mathbf{K}_{02}\mathbf{T}_{,\theta}^e \\ &+\left(\mathbf{K}_{13} - \mathbf{K}_{31}\right)\mathbf{u}_{,z}^e + \mathbf{K}_{03}\mathbf{T}_{,z}^e - \mathbf{K}_{22}\mathbf{u}_{,\theta\theta}^e - \left(\mathbf{K}_{23} + \mathbf{K}_{32}\right)\mathbf{u}_{,\theta z}^e - \mathbf{K}_{33}\mathbf{u}_{,zz}^e = 0\end{aligned} \tag{2.22}$$

Similarly, equating the coefficients of $\delta\mathbf{T}^e$ in equation (2.17) yields

$$\begin{aligned}&\tau_0\mathbf{f}_1\ddot{\mathbf{u}}^e+\tau_0\mathbf{m}_0\ddot{\mathbf{T}}^e+\tau_0\mathbf{f}_2\ddot{\mathbf{u}}^e_{,\theta}+\tau_0\mathbf{f}_3\ddot{\mathbf{u}}^e_{,z}+\mathbf{f}_1\dot{\mathbf{u}}^e+\mathbf{m}_0\dot{\mathbf{T}}^e\\&+\mathbf{f}_2\dot{\mathbf{u}}^e_{,\theta}+\mathbf{f}_3\dot{\mathbf{u}}^e_{,z}+\mathbf{g}_{11}\mathbf{T}^e-\mathbf{g}_{22}\mathbf{T}^e_{,\theta\theta}-\mathbf{g}_{33}\mathbf{T}^e_{,zz}=0\end{aligned}\tag{2.23}$$

Combining equations (2.22) and (2.23), and assembling the element matrices into global matrices lead to the following governing equations of motion,

$$\begin{aligned}&\mathbf{H}_1\ddot{\mathbf{V}}+\mathbf{H}_2\ddot{\mathbf{V}}_{,\theta}+\mathbf{H}_3\ddot{\mathbf{V}}_{,z}+\mathbf{H}_4\dot{\mathbf{V}}+\mathbf{H}_5\dot{\mathbf{V}}_{,\theta}+\mathbf{H}_6\dot{\mathbf{V}}_{,z}\\&+\mathbf{H}_7\mathbf{V}+\mathbf{H}_8\mathbf{V}_{,\theta}+\mathbf{H}_9\mathbf{V}_{,z}+\mathbf{H}_{10}\mathbf{V}_{,\theta\theta}+\mathbf{H}_{11}\mathbf{V}_{,\theta z}+\mathbf{H}_{12}\mathbf{V}_{,zz}=0\end{aligned}\tag{2.24}$$

where $\mathbf{H}_i\,(i=1,2,...,12)$ are the global matrices, given in Appendix A, $\mathbf{V}$ is the global nodal displacement and temperature vector.

The harmonic wave-form solution of equation (2.24) is assumed as

$$\mathbf{V}=\mathbf{V}_0e^{i(\xi z+n\theta-\omega t)}\tag{2.25}$$

where $\mathbf{V}_0$ is the nodal amplitude vector. ξ, n and ω are the nondimensional axial wave number, the circumferential wave number and nondimensional circular frequency, respectively, and $i=\sqrt{-1}$

Substitution of equation (2.25) into equation (2.24) results a set of linear homogeneous equations

$$\begin{bmatrix}-\omega^2\left(\mathbf{H}_1+in\mathbf{H}_2+i\xi\mathbf{H}_3\right)-i\omega\left(\mathbf{H}_4+in\mathbf{H}_5+i\xi\mathbf{H}_6\right)\\+\left(\mathbf{H}_7+in\mathbf{H}_8+i\xi\mathbf{H}_9\right)-n^2\mathbf{H}_{10}-n\xi\mathbf{H}_{11}-\xi^2\mathbf{H}_{12}\end{bmatrix}\mathbf{V}_0=0\tag{2.26}$$

For integer values of *n*, two eigenvalue problems can be deduced depending on whether ξ or ω is chosen as the eigenvalue. If ξ serves as the eigenvalue with assigned values for ω, equation (2.26) gives a quadratic eigenvalue problem:

$$\left(-\xi^2\mathbf{H}_{12}+\xi\mathbf{H}_B+\mathbf{H}_A\right)\mathbf{V}_0=0 \tag{2.27}$$

where

$$\begin{aligned}\mathbf{H}_B&=-i\omega^2\mathbf{H}_3+\omega\mathbf{H}_6+i\mathbf{H}_9-n\mathbf{H}_{11}\\ \mathbf{H}_A&=-\omega^2\left(\mathbf{H}_1+in\mathbf{H}_2\right)-i\omega\left(\mathbf{H}_4+in\mathbf{H}_5\right)+\left(\mathbf{H}_7+in\mathbf{H}_8-n^2\mathbf{H}_{10}\right)\end{aligned} \tag{2.28}$$

Equation (2.27) can be converted into first order equation in the form

$$\begin{bmatrix}0 & I\\ \mathbf{H}_A & \mathbf{H}_B\end{bmatrix}\begin{Bmatrix}\mathbf{V}_0\\ \xi\mathbf{V}_0\end{Bmatrix}=\xi\begin{bmatrix}I & 0\\ 0 & \mathbf{H}_{12}\end{bmatrix}\begin{Bmatrix}\mathbf{V}_0\\ \xi\mathbf{V}_0\end{Bmatrix} \tag{2.29}$$

Solution of the generalized eigenvalue problem (2.29) gives the dispersion relation for guided thermoelastic waves in the cylinder. It also provides the initial value of the roots of equation (2.43) when Muller's method is employed to solve the exact dispersion equations for eigenvalues.

2.5 Analytical Method for an Isotropic Cylinder

For isotropic case, the material properties are

$$\begin{aligned}&c_{11}=c_{22}=c_{33}=\lambda+2\mu\\ &c_{44}=c_{55}=c_{66}=\mu\\ &c_{12}=c_{21}=c_{13}=c_{31}=c_{23}=c_{32}=\lambda\\ &k_{rr}=k_{\theta\theta}=k_{zz}=k,\ k_{r\theta}=k_{\theta z}=k_{zr}=0\\ &\beta_{rr}=\beta_{\theta\theta}=\beta_{zz}=\beta,\ \beta_{r\theta}=\beta_{\theta z}=\beta_{zr}=0\end{aligned} \tag{2.30}$$

here λ and μ are elastic (Lame) constants

The governing equations of motion for homogeneous isotropic cylinders can be expressed in terms of displacement and temperature as

$$\mu\nabla^2\mathbf{u}+(\lambda+\mu)\nabla(\nabla.\mathbf{u})-\beta\nabla T=\rho\ddot{\mathbf{u}} \tag{2.31}$$

$$k\nabla^2T-\rho c_E\left(\dot{T}+\tau_0\ddot{T}\right)=T_0\left(\beta\nabla\cdot\dot{\mathbf{u}}+\tau_0\beta\nabla\cdot\ddot{\mathbf{u}}\right) \tag{2.32}$$

Using Helmholtz resolution (Gazis, 1959), the displacement vector **u** is expressed in terms of a scalar potential ϕ and a vector potential **H**

$$\mathbf{u}=\nabla\phi+\nabla\times\mathbf{H},\quad \nabla\cdot\mathbf{H}=0 \tag{2.33}$$

Substitution of the above displacement representation into equations (2.31) and (2.32) yields the following equations of motion

$$(\lambda+2\mu)\nabla^2\phi-\rho\ddot{\phi}-\beta T=0 \tag{2.34}$$

$$k\nabla^2T-\rho c_E\left(\dot{T}+\tau_0\ddot{T}\right)=T_0\beta\left(\nabla^2\dot{\phi}+\tau_0\nabla^2\ddot{\phi}\right) \tag{2.35}$$

$$\mu\nabla^2\mathbf{H}-\rho\ddot{\mathbf{H}}=0 \tag{2.36}$$

By considering a wave-form solution,

$$\begin{aligned}\phi&=f(r)e^{i(\xi z+n\theta-\omega t)}\\ T&=h(r)e^{i(\xi z+n\theta-\omega t)}\\ \mathbf{H}&=\mathbf{g}(r)e^{i(\xi z+n\theta-\omega t)}\end{aligned} \tag{2.37}$$

Equations (2.34) and (2.35) can be simplified as

$$h = \frac{\lambda + 2\mu}{\beta} \nabla^2 f + \frac{\rho\omega^2}{\beta} f \tag{2.38}$$

$$\nabla^4 f + b_1 \nabla^2 f + b_2 f = 0 \tag{2.39}$$

where

$$b_1 = \frac{\omega^2}{c_p^2} + \frac{\rho c_E \tau}{k} + \frac{T_0 \beta^2 \tau}{k \rho c_p^2},$$

$$b_2 = \frac{\rho c_E \tau \omega^2}{k c_p^2},$$

$$c_p^2 = \frac{\lambda + 2\mu}{\rho},$$

$$\tau = i\omega + \omega^2 \tau_0,$$

$$\nabla^2 = \frac{d^2}{dr^2} + \frac{1}{r}\frac{d}{dr} - \frac{n^2}{r^2} - \xi^2$$

Solution of equation (2.39) is given by

$$f = A_1 J_n(\alpha_1 r) + A_2 Y_n(\alpha_1 r) + A_3 J_n(\alpha_2 r) + A_4 Y_n(\alpha_2 r) \tag{2.40}$$

where $\alpha_1^2 = -\left(\xi^2 + r_1\right)$, $\alpha_2^2 = -\left(\xi^2 + r_2\right)$ and $r_{1,2} = -\frac{b_1}{2} \pm \frac{1}{2}\sqrt{b_1^2 - 4b_2}$

Solution of equation (2.36) is given by

$$\begin{aligned} g_r &= B_1 J_n\left(\hat{\beta} r\right) + B_2 Y_n\left(\hat{\beta} r\right) \\ g_\theta &= i g_r \\ g_z &= C_1 J_n\left(\hat{\beta} r\right) + C_2 Y_n\left(\hat{\beta} r\right) \end{aligned} \tag{2.41}$$

where $\hat{\beta}^2 = \frac{\omega^2}{c_s^2} - \xi^2$ and $c_s^2 = \frac{\mu}{\rho}$.

The resulting displacements and temperature are then given by

$$
\begin{aligned}
u_r &= \left(f' - \xi g_r + \frac{in}{r} g_z \right) e^{i(\xi z + n\theta - \omega t)} \\
u_\theta &= \left(\frac{in}{r} f + i\xi g_r - g_z' \right) e^{i(\xi z + n\theta - \omega t)} \\
u_z &= \left[i\xi f - i g_r' - i\left(\frac{1+n}{r} \right) g_r \right] e^{i(\xi z + n\theta - \omega t)} \\
T &= \frac{\lambda + 2\mu}{\beta} \left[f'' + \frac{1}{r} f' + \left(\frac{\omega^2}{c_p^2} - \xi^2 - \frac{n^2}{r^2} \right) f \right] e^{i(\xi z + n\theta - \omega t)}
\end{aligned}
\tag{2.42}
$$

Here a prime stands for the differentiation with respect to *r*. The stresses and the gradient of the temperature are given in Appendix B.

Traction free boundary conditions on surfaces of cylinder require that the stresses at inner and outer surfaces of the cylinder are zero. For thermal boundary conditions, temperature gradients at the inner and outer surfaces of the cylinder are zero

$$
\left.
\begin{array}{c}
\sigma_{rr} = \sigma_{r\theta} = \sigma_{rz} = 0 \\
T_{,r} = 0
\end{array}
\right\} \text{at} \quad r = r_i \text{ and } r = r_o
\tag{2.43}
$$

The frequency equation results from substituting equations of the stresses and the gradient of the temperature into the boundary conditions (2.43). The resulting determinant of unknown coefficients A_1, A_2, A_3, A_4, B_1, B_2, C_1, and C_2, which yields the frequency equation, is

$$
\det\left[a_{ij} \right] = 0 \quad \left(i, j = 1, 2, \cdots, 8 \right)
\tag{2.44}
$$

where the expressions of a_{ij} can be obtained from Appendix B.

2.6 Numerical Results and Discussion

In this section, numerical results in the forms of dispersion curves (wavenumbers vs. frequency) are presented for three types of cylinders. They are 1) an isotropic cylinder, 2) a transversely isotropic cylinder, and 3) a composite cylinder. For the isotropic cylinder, the material considered is copper (Cu), and for the transversely isotropic cylinder the material is silicon nitride (Si_3N_4). The composite cylinder is taken as an inner layer of zinc (Zn) and outer layer of silicon nitride (Si_3N_4). The properties of the materials are listed in Table 2.1.

The speed of the thermal wave v_t in the *z* direction is

$$v_t = \sqrt{\frac{k_{zz}}{\rho c_E \tau_0}} \tag{2.45}$$

To the best of my knowledge, no experimental values for thermal relaxation time, τ_0, have been reported. However, Chester (1963), has suggested the following equation to calculate the approximate speed of the thermal wave:

$$v_t = \frac{v}{\sqrt{3}} \tag{2.46}$$

where $v = \sqrt{\frac{c_{33}}{\rho}}$. From the above approximate equation, the thermal relaxation time is calculated as

$$\tau_0 = \frac{3k_{zz}}{c_E c_{33}} \tag{2.47}$$

Hence, for copper, for example, the approximate value of τ_0 is 2.244×10^{-6} s. Thermal relaxation times for Zinc and Silicon Nitride are shown in the Table 2.1.

For comparison of results with and without thermoelastic effects, results for isotropic, anisotropic and composite cylinders were also obtained for the isothermal case using the SAFE method. These results are calculated by keeping ω^* $(=\Omega)$ real and ξ $(=\gamma_R + i\gamma_I)$ being complex.

Case 1: Isotropic Cylinder

An infinite copper cylinder with inner radius 0.5 m and outer radius 1.5 m is considered. Therefore, the nondimensional inner and outer radii are, $r_i = 0.5$ and $r_o = 1.5$. Material properties of copper cylinder are listed in (see Erby and Suhubi, 1986) Table 2.1. Numerical results are obtained for the axisymmetric motion ($n = 0$) by both the analytical and the SAFE methods which are presented graphically in Figs. 2.2 and 2.3. Comparison of Fig. 2.2(a) for the isothermal case with Fig. 2.2(b) including the thermal effect shows that the elastic modes are indistinguishable in the two cases. Thus, the effect of thermal coupling is found to be negligible. Mechanical displacements and temperature distribution across the thickness of the cylinder are shown in Table 2.2. From these results, it is observed that the temperature effect can be neglected completely for this case.

The lowest order elastic mode propagates at all frequencies, but the higher order modes have cutoff frequencies below which they are evanescent. Since the waves are propagating in the axial direction, the longitudinal and torsional modes are uncoupled. This is evidenced by the intersection of torsional wave branches with those of for longitudinal waves. It should be noted that torsional modes are free from temperature

effect. Complex branches, representing pure thermal modes, are shown in Fig. 2.3(b). Thermal modes are found to have very high attenuation when compared with elastic modes. Higher order thermal modes originate with high imaginary values of the wave number when $\omega^* = \Omega = 0$. It is found that the higher order thermal modes approach the first thermal mode as the frequency increases.

Flexural modes are obtained for both elastic and thermoelastic cylinders by setting $n = 1$. Flexural modes from Fig. 2.4 (b) resemble those of $n = 1$ for the isothermal case as shown in Fig. 2.4(a). Propagating and pure thermal modes are shown in Figs. 2.5(a) and 2.5(b), respectively. In this case also, pure thermal modes show the same behavior as mentioned above. Spectra obtained for the elastic and thermoelastic modes using the SAFE method were compared with those obtained from the analytic solution for an isotropic (copper) cylinder. Excellent agreement was found between both results which are shown in Figs. 2.2(b) and 2.4(b).

Case 2: Anisotropic Cylinder

In this case, an infinite cylindrical tube with thickness 1 mm and inner radius 1.5 mm is considered. Therefore, the nondimensional inner and outer radii are, $r_i = 1.5$ and $r_o = 2.5$, respectively. The material of the tube is taken to be silicon nitride (Si_3N_4), whose properties are listed in Table 2.1 (see Al-Qahtani et al. 2004). The symmetry axis of the material is aligned with the axis of the cylinder. Equation (2.28) yields dispersion curves for thermoelastic waves in a cylinder. These curves for different circumferential modes (n = 0 and 1) are computed and presented graphically in the form

of 3-D plots shown in Figs. 2.6(a) and 2.7(a). Comparisons of propagating modes for elastic and thermoelastic cylinders are shown in Figs. 2.6(b) and 2.7(b) for $n = 0$ and $n = 1$ respectively. It is noticed that the longitudinal modes are coupled with temperature but the effect is not significant, which is seen from Table 2.3. It is also found that the flexural modes are not affected significantly by the thermal effects within the frequency range considered here.

Dispersion curves for the thermal modes are also presented in a three dimensional form for n = 0 in Figs. 2.8(a) and 2.8(b). Figure 2.8(a) shows the behavior of thermal branches at a low frequency range, up to 0.12 MHz ($ie.,\ \Omega = 3.0$), and Fig 2.8(b) is for a higher range of frequency, up to 1.2 MHz ($ie.,\ \Omega = 30$). Also, non-dimensional complex wavenumbers corresponding to thermal modes at low and high frequencies are listed in Table 2.4 to indicate the attenuation associated with these modes. Thermal modes are found to have very high attenuation when compared with elastic modes and higher order thermal modes originate with high imaginary values of the wave number when $\omega^*(=\Omega) = 0$. In this case also, it is found that the higher order thermal modes approach the first thermal mode as the frequency increases.

Case 3: Composite Cylinder

The inner and outer layers of the composite cylinder are zinc and silicon nitride, respectively. Both layers of the cylinder are bonded perfectly and the thickness of each layer is 1 mm and the inner radius of the cylinder is 1.5 mm. Material properties of Zinc are listed in (see Sharma, 2001) Table 2.1. Dispersion curves, for the composite cylinder,

have been computed with $n = 0$ and presented graphically in the form of a 3-D plot shown in Fig 2.9(a). Elastic modes resemble those of the isothermal case due to small coupling effect of temperature which is seen from Fig 2.9(b). It is observed that torsional modes are completely free from temperature effect. Longitudinal modes are coupled with temperature but it is not significant which is evident from Table 2.5, showing mechanical displacements and temperature distribution across the thickness. Predominantly thermal modes are not shown here. They have similar behaviour as in the isotropic case.

2.7 Concluding Remarks

Propagation of thermoelastic waves in isotropic, anisotropic and composite cylinders has been investigated in the context of L–S generalized theory of thermoelasticity. This theory includes single thermal relaxation time in the heat conduction equation in order to model the finite speed of thermal wave. Analytical and SAFE methods are used to obtain dispersion relation for an isotropic cylinder. Numerical results obtained by these methods have shown good agreement with each other. Also, the SAFE method formulation is used to calculate dispersion relations for anisotropic and composite cylinders.

Numerical results show that a purely transverse mode is independent of temperature change and thermal modes exhibit much larger attenuation than the elastic modes. Also, it is observed that materials with a small coefficient of thermal conductivity yield larger wave numbers. Comparison of dispersion curves with that of an elastic cylinder shows that the effect of temperature on mechanical displacements is small.

Therefore, neglecting the coupling term β simplifies the analysis procedure for the above cases. Convergence of SAFE results is achieved by a fewer number of elements (25 elements). This indicates that the SAFE method is an efficient tool to analyze thermoelastic problems.

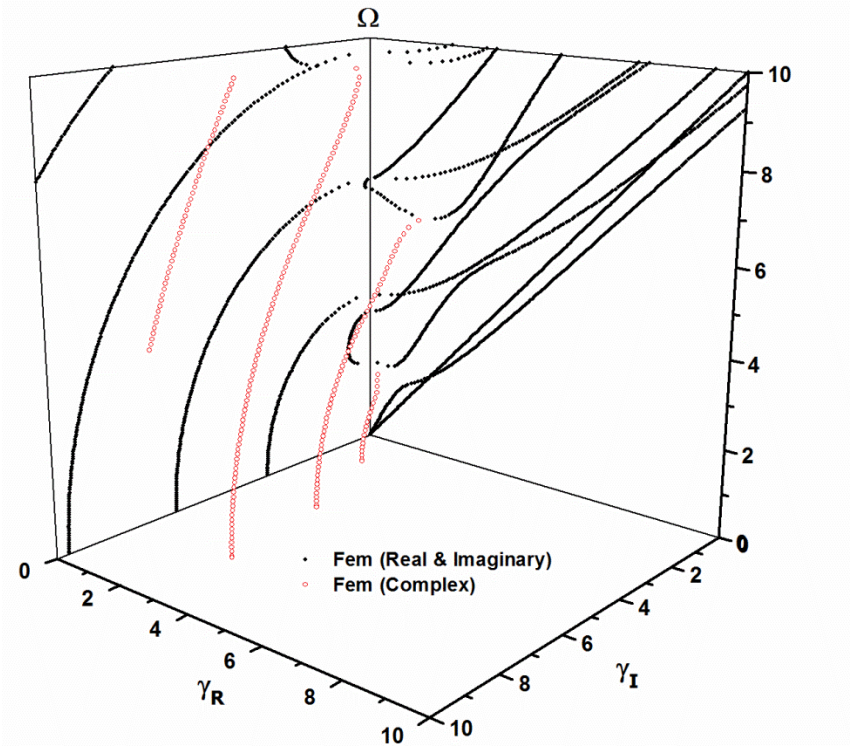

Figure 2.2(a): Three dimensional frequency spectra for an isotropic elastic cylinder with *n* = 0

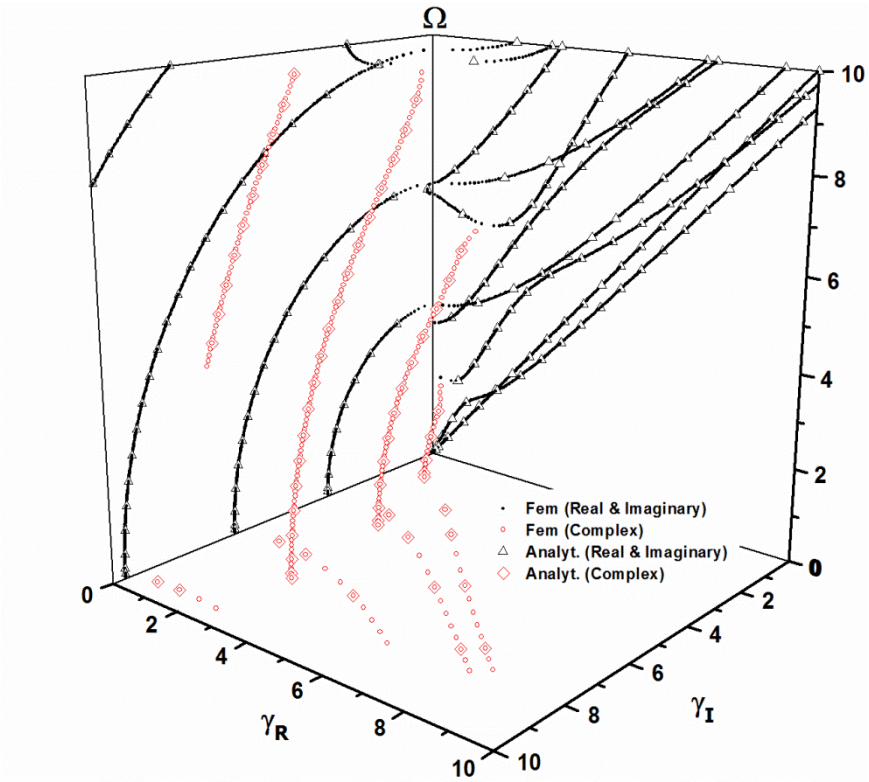

Figure 2.2(b): Three dimensional frequency spectra for an isotropic thermoelastic cylinder with n = 0

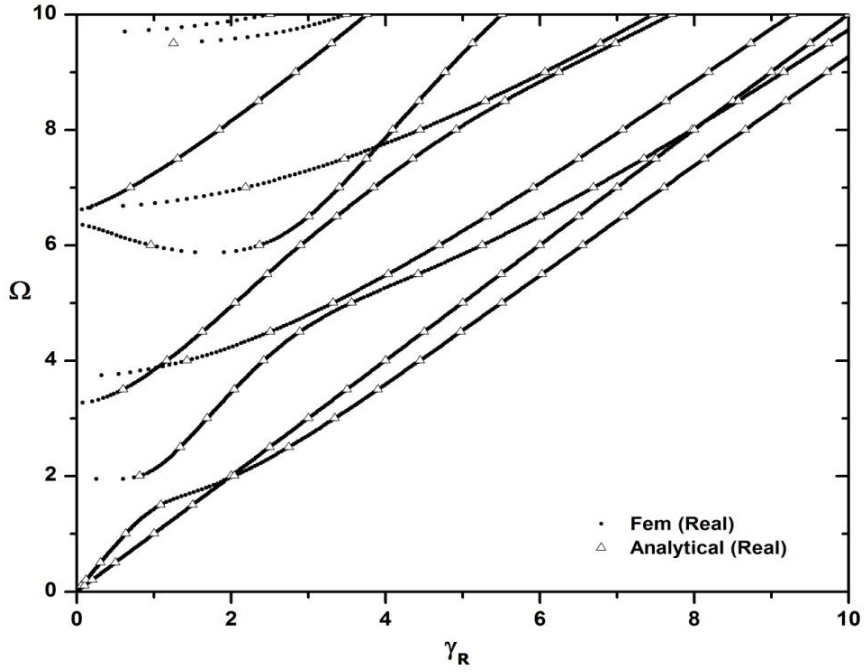

Figure 2.3(a): Two dimensional view of propagating modes of an isotropic cylinder with n = 0

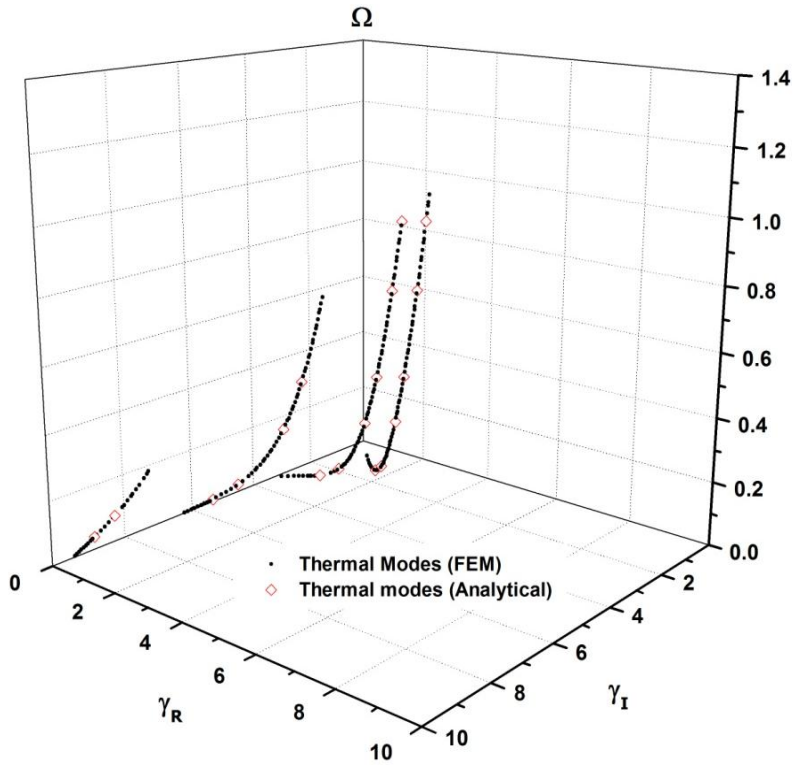

Figure 2.3(b): **T**hree dimensional view of thermal modes of an isotropic thermoelastic cylinder with n = 0

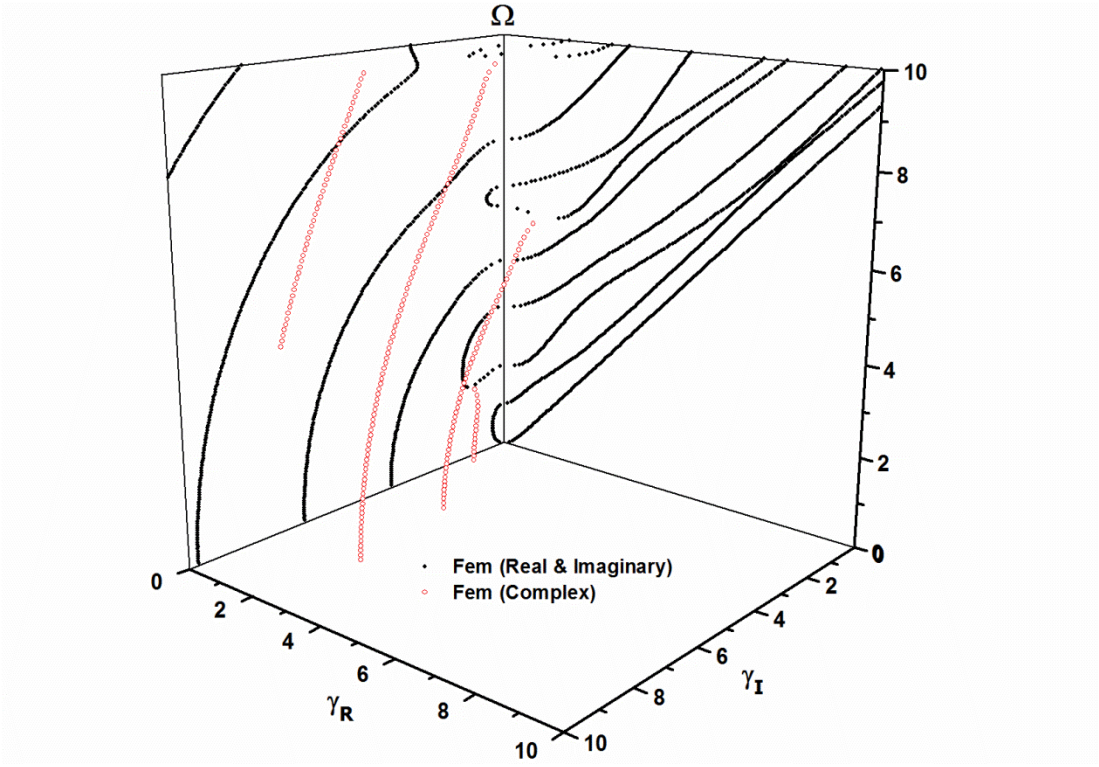

Figure 2.4(a): Three dimensional frequency spectra for an isotropic elastic cylinder with n = 1

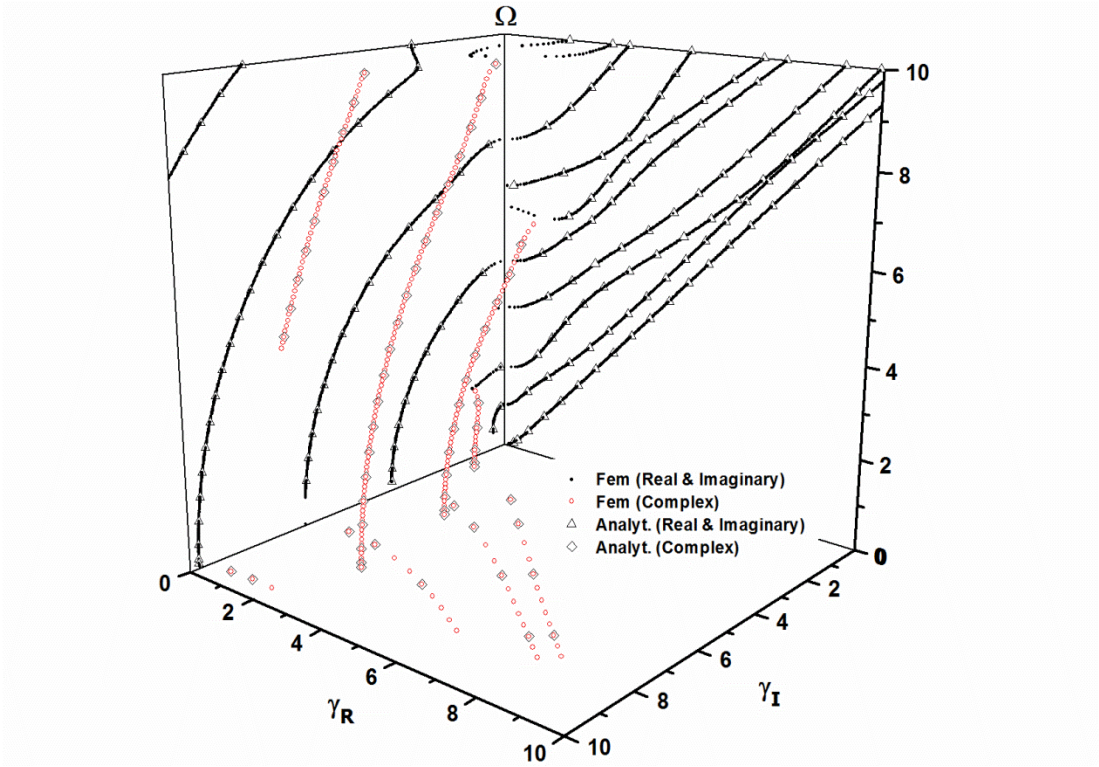

Figure 2.4(b): Three dimensional frequency spectra for an isotropic thermoelastic cylinder with n = 1

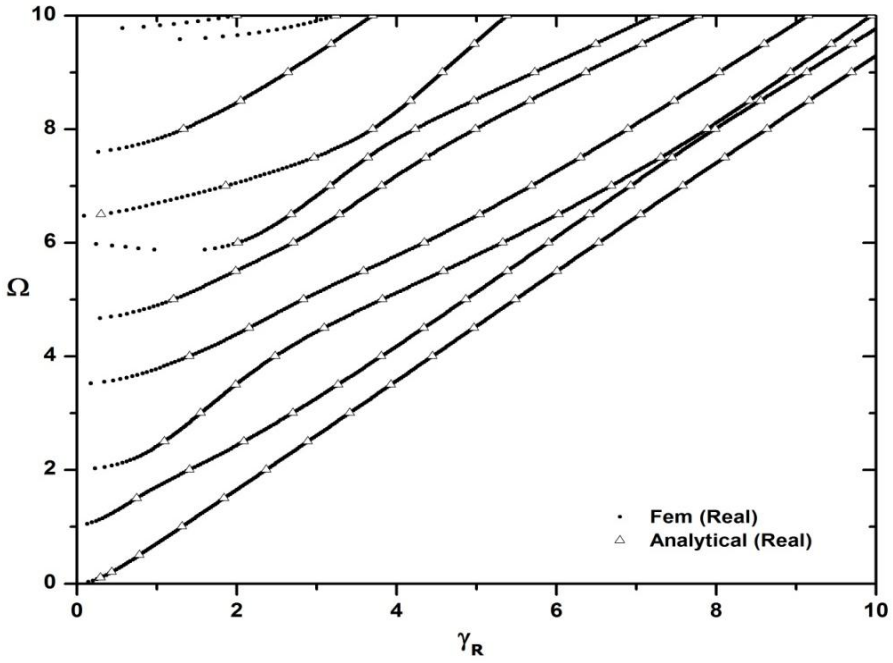

Figure 2.5(a): Two dimensional view of propagating modes of an isotropic cylinder with n = 1

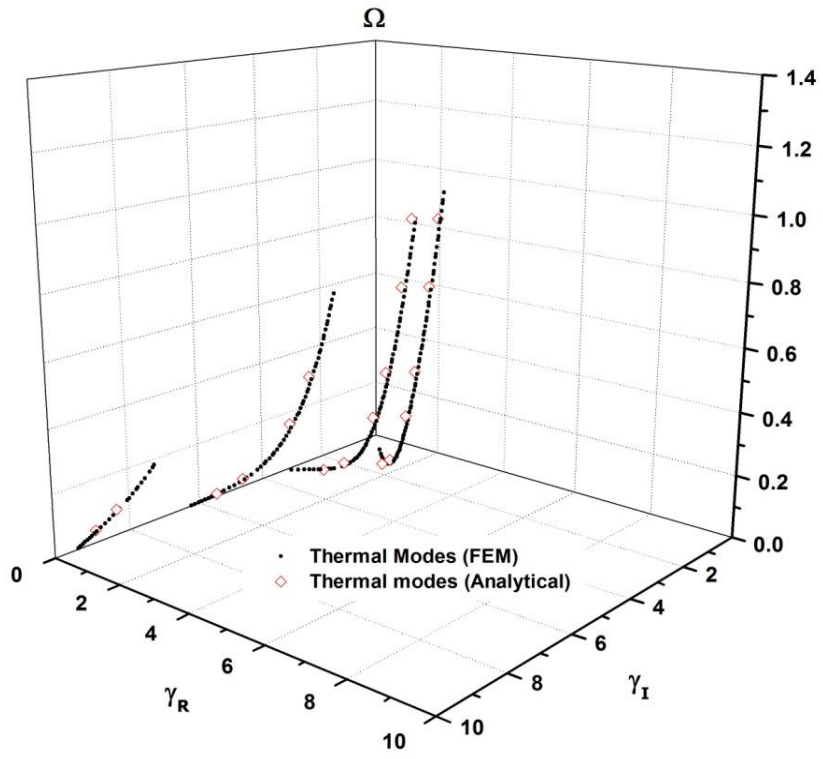

Figure 2.5(b): Three dimensional view of thermal modes of an isotropic thermoelastic cylinder with n = 1

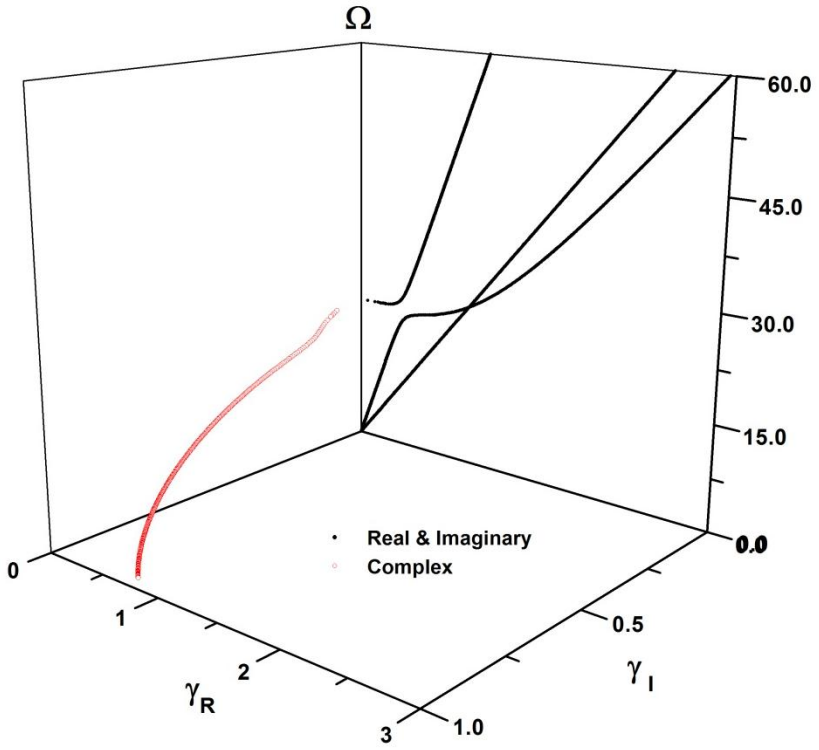

Figure 2.6(a): Frequency spectra of anisotropic thermoelastic cylinder with n = 0

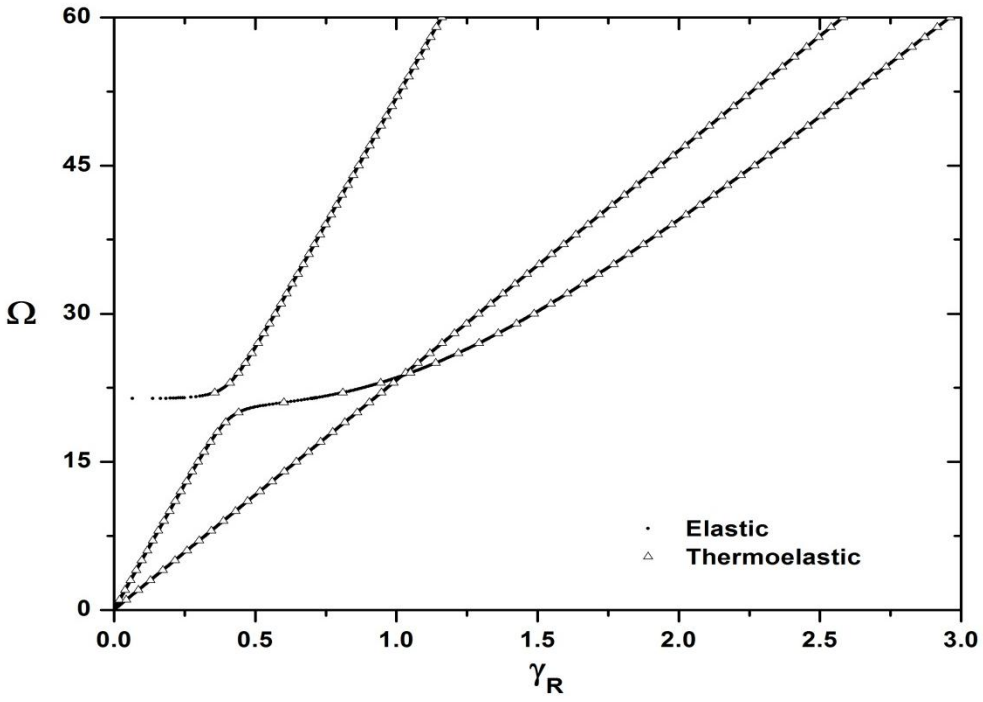

Figure 2.6(b): Comparison of propagating modes of elastic and thermoelastic anisotropic cylinders with n = 0

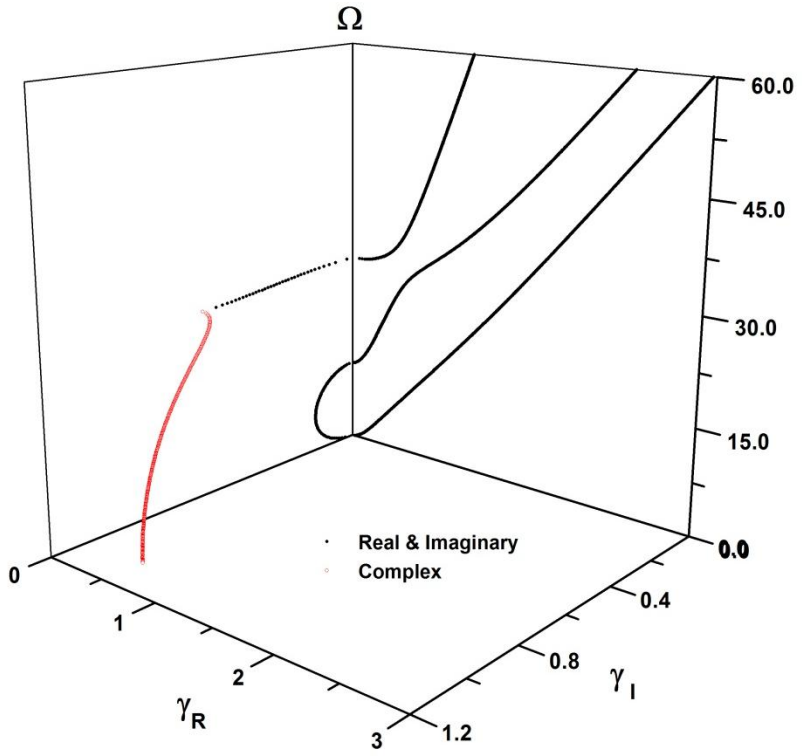

Figure 2.7(a): Frequency spectra of anisotropic thermoelastic cylinder with n = 1

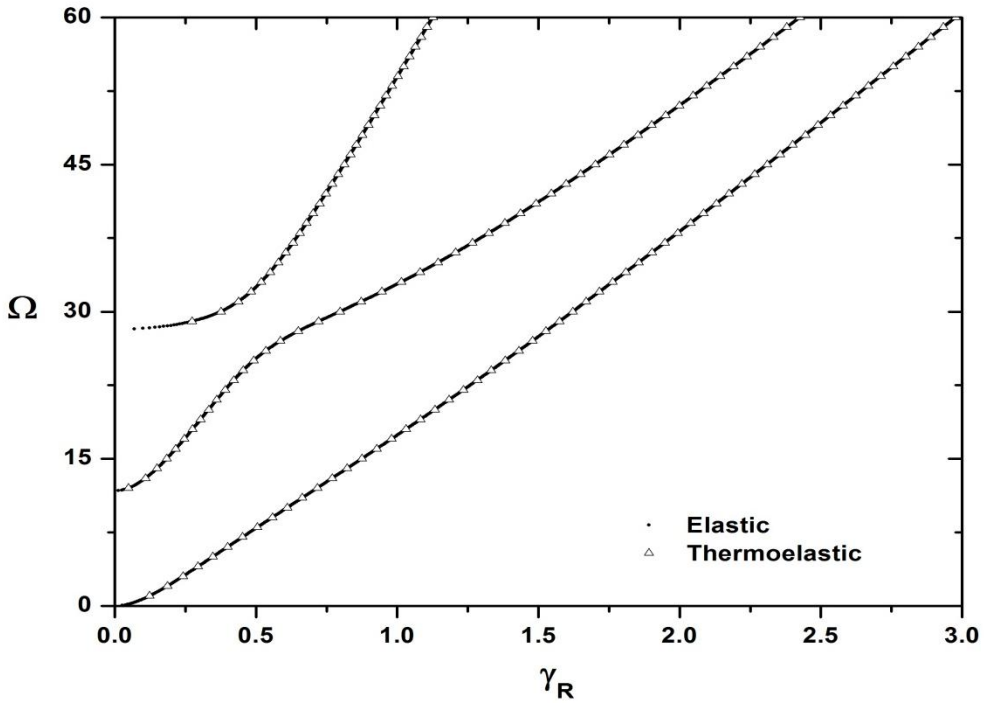

Figure 2.7(b): Comparison of propagating modes of elastic and thermoelastic anisotropic cylinders with n = 1

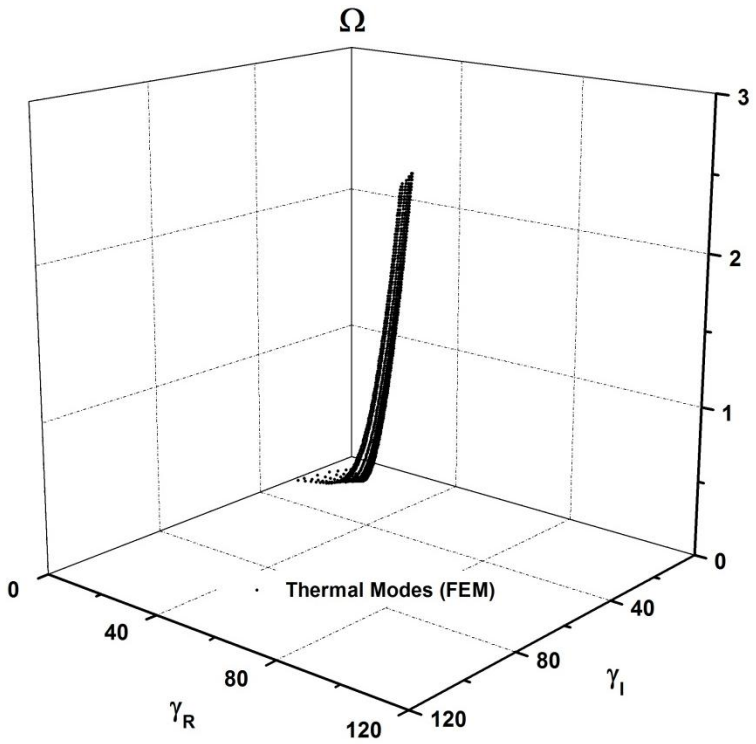

Figure 2.8(a): Three dimensional view of thermal modes of anisotropic thermoelastic cylinder with n = 0, up to nondimensional frequency $\Omega = 3.0$

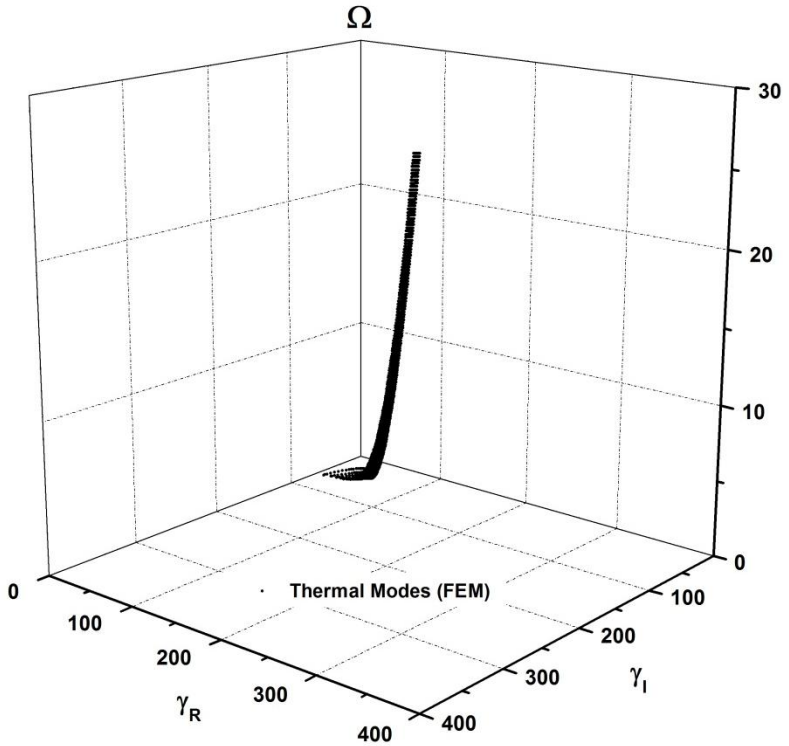

Figure 2.8(b): Three dimensional view of thermal modes of anisotropic thermoelastic cylinder with n = 0, up to nondimensional frequency $\Omega = 30.0$

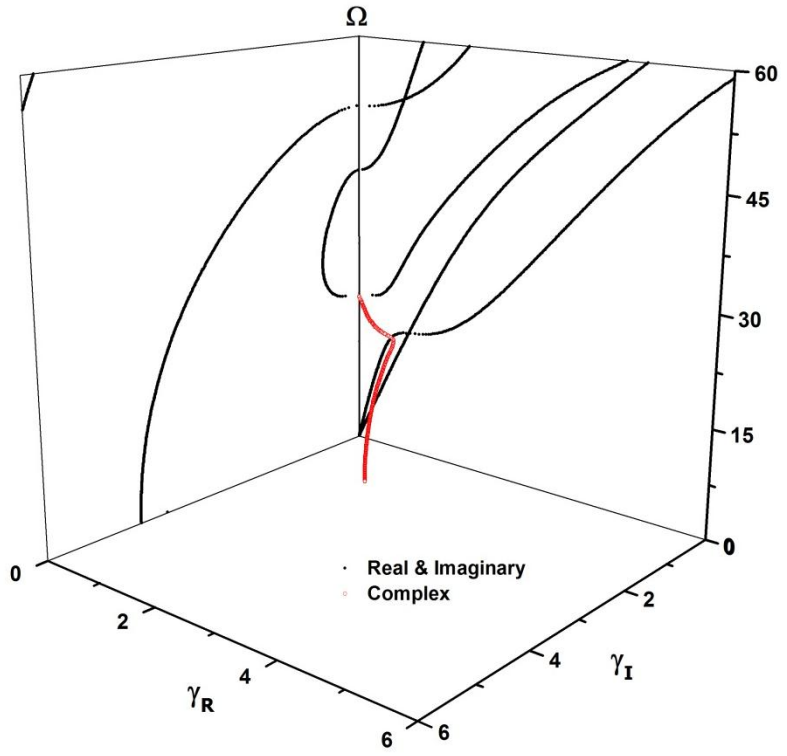

Figure 2.9(a): Frequency spectra of thermoelastic composite cylinder with $n = 0$

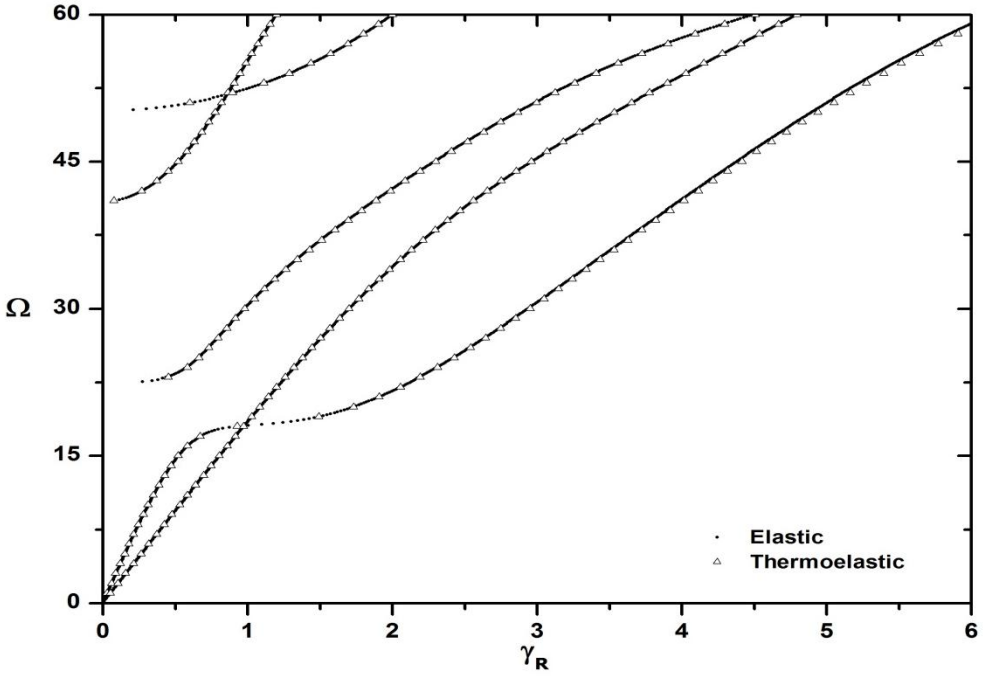

Figure 2.9(b): Comparison of propagating modes of elastic and thermoelastic composite cylinders with $n = 0$

Table 2.1: Thermomechanical properties of Copper, Zinc and Silicon Nitride

Quantity	Units	Copper	Zinc	Silicon Nitride
ρ	kg/m^3	8.96×10^3	7.14×10^3	3.20×10^3
c_{11}	N/m^2	1.66×10^{11}	1.628×10^{11}	4.33×10^{11}
c_{12}	N/m^2	8.2×10^{10}	0.362×10^{11}	1.95×10^{11}
c_{13}	N/m^2	8.2×10^{10}	0.508×10^{11}	1.27×10^{11}
c_{33}	N/m^2	1.66×10^{11}	0.627×10^{11}	5.74×10^{11}
c_{44}	N/m^2	4.2×10^{10}	0.385×10^{11}	1.08×10^{11}
β_1	$N/m^2 \,°K$	3.3×10^3	5.75×10^6	2.71×10^6
β_3	$N/m^2 \,° K$	3.3×10^3	5.17×10^6	3.22×10^6
k_{11}	$W/m \,° K$	1.13×10^4	1.24×10^2	43.5
k_{33}	$W/m \,° K$	1.13×10^4	1.24×10^2	55.4
c_E	$J/kg \,° K$	9.1×10^{-2}	3.90×10^2	0.67×10^3
$T_0 = \overline{T}$	$°K$	4.2	296	296
τ_0	s	2.244×10^{-6}	1.521×10^{-11}	4.32×10^{-13}
$\overline{\rho}$	kg/m^3	8.96×10^3	3.20×10^3	3.20×10^3
$\overline{c}$	N/m^2	4.2×10^{10}	2.00×10^8	2.00×10^8
$\overline{k}$	$W/m \,° K$	1.13×10^4	554	554

Table 2.2: First longitudinal mode of a copper cylinder with Ω = 1.0 and $\gamma_R = 0.64$

Thermoelastic Cylinder									Elastic Cylinder (i.e., without temperature effect)					
r	u_r		u_θ		u_z		T		u_r		u_θ		u_z	
	γ_R	γ_I	γ_R	γ_I	γ_R	γ_I	γ_R	γ_I	γ_R	γ_I	γ_R	γ_I	γ_R	γ_I
0.5	0	-0.0542	0	0	0.2924	0	0	-4.5×10^5	0	-0.0542	0	0	0.2924	0
0.625	0	-0.0597	0	0	0.2878	0	0	-4.6×10^5	0	-0.0597	0	0	0.2878	0
0.75	0	-0.0660	0	0	0.2827	0	0	-4.6×10^5	0	-0.0660	0	0	0.2827	0
0.875	0	-0.0725	0	0	0.2770	0	0	-4.6×10^5	0	-0.0725	0	0	0.2770	0
1	0	-0.0791	0	0	0.2707	0	0	-4.7×10^5	0	-0.0791	0	0	0.2707	0
1.125	0	-0.0856	0	0	0.2640	0	0	-4.8×10^5	0	-0.0856	0	0	0.2640	0
1.25	0	-0.0917	0	0	0.2568	0	0	-4.8×10^5	0	-0.0917	0	0	0.2568	0
1.375	0	-0.0976	0	0	0.2491	0	0	-4.9×10^5	0	-0.0976	0	0	0.2491	0
1.5	0	-0.1030	0	0	0.2411	0	0	-4.9×10^5	0	-0.1030	0	0	0.2411	0

Table 2.3: First longitudinal mode of a silicon nitride cylinder with Ω = 1.0 and $\gamma_R = 0.02$

Thermoelastic Cylinder									**Elastic Cylinder (i.e., without temperature effect)**					
r	u_r		u_θ		u_z		T		u_r		u_θ		u_z	
	γ_R	γ_I	γ_R	γ_I	γ_R	γ_I	γ_R	γ_I	γ_R	γ_I	γ_R	γ_I	γ_R	γ_I
8	0	-0.0020	0	0	0.3333	0	0	-0.0004	0	-0.0133	0	0	0.3331	0
0.625	0	-0.0022	0	0	0.3333	0	0	-0.0004	0	-0.0135	0	0	0.3330	0
0.75	0	-0.0023	0	0	0.3333	0	0	-0.0004	0	-0.0136	0	0	0.3330	0
0.875	0	-0.0025	0	0	0.3333	0	0	-0.0004	0	-0.0138	0	0	0.3330	0
1	0	-0.0027	0	0	0.3333	0	0	-0.0004	0	-0.0139	0	0	0.3329	0
1.125	0	-0.0028	0	0	0.3333	0	0	-0.0004	0	-0.0141	0	0	0.3329	0
1.25	0	-0.0030	0	0	0.3332	0	0	-0.0004	0	-0.0143	0	0	0.3329	0
1.375	0	-0.0032	0	0	0.3332	0	0	-0.0004	0	-0.0144	0	0	0.3328	0
1.5	0	-0.0033	0	0	0.3332	0	0	-0.0004	0	-0.0146	0	0	0.3328	0

Table 2.4: Nondimensional wave numbers of thermal modes at low and high frequency level

At Low Level Frequency (0.4 Hz)			**At High Level Frequency (1.2 MHz)**		
Mode Number	**Real Wave Number**	**Imaginary Wave Number**	**Mode Number**	**Real Wave Number**	**Imaginary Wave Number**
1	0.697	0.697	1	381.4302	381.4285
2	0.172	2.817	2	381.4253	381.4335
3	0.087	5.603	3	381.4099	381.4488
4	0.057	8.500	4	381.3832	381.4756
5	0.040	12.283	5	381.3318	381.5269
6	0.031	15.555	6	381.2724	381.5864
7	0.024	20.100	7	381.1661	381.6928

Table 2.5: First longitudinal mode of a composite cylinder with Ω = 1.0 and $\gamma_R = 0.030$

Thermoelastic Cylinder									**Elastic Cylinder (i.e., without temperature effect)**					
r	u_r		u_θ		u_z		T		u_r		u_θ		u_z	
	γ_R	γ_I	γ_R	γ_I	γ_R	γ_I	γ_R	γ_I	γ_R	γ_I	γ_R	γ_I	γ_R	γ_I
0.5	0	-0.0016	0	0	0.3335	0	0	-0.0004	0	-0.0016	0	0	0.3335	0
0.625	0	-0.0019	0	0	0.3335	0	0	-0.0003	0	-0.0019	0	0	0.3335	0
0.75	0	-0.0023	0	0	0.3334	0	0	-0.0004	0	-0.0022	0	0	0.3334	0
0.875	0	-0.0026	0	0	0.3333	0	0	-0.0003	0	-0.0025	0	0	0.3333	0
1	0	-0.0029	0	0	0.3331	0	0	-0.0004	0	-0.0029	0	0	0.3331	0
1.125	0	-0.0031	0	0	0.333	0	0	-0.0004	0	-0.0031	0	0	0.333	0
1.25	0	-0.0034	0	0	0.333	0	0	-0.0004	0	-0.0033	0	0	0.333	0
1.375	0	-0.0036	0	0	0.3329	0	0	-0.0004	0	-0.0036	0	0	0.3329	0
1.5	0	-0.0039	0	0	0.3329	0	0	-0.0004	0	-0.0038	0	0	0.3329	0

Chapter 3

Transient Thermoelastic Waves in an Infinite Cylinder

3.1 Introduction

This chapter presents a theoretical study of transient ultrasonic guided waves generated by concentrated heating of the outer surface of an infinite anisotropic cylinder. Generalized thermoelastic theory proposed by Lord and Shulman (1967) (LS) is used to model the response of a circular cylinder due to a pulsed laser focused on the surface of the cylinder. Zhuang et al. (1999) and Bai et al. (2004) studied Green's functions for an isothermal composite cylinder and a piezoelectric cylinder, respectively due to a steady state concentrated force with the SAFE method. A Semi-Analytical Finite Element (SAFE) method was employed, in Chapter 2, to obtain the guided thermoelastic wave modes in free cylinders. These modes are used here to construct the frequency response functions due to the laser excitation. Using integral transform techniques, the modal wave forms are obtained in frequency and wave number domains. Time histories of the propagating modes are then calculated by applying an inverse Fourier transformation in the time domain. Numerical results are presented for dispersion curves, frequency displacement response spectra and transient wave forms. Convergence and accuracy of

numerical results at high frequencies are also discussed in detail. The emphasis here is on propagation of longitudinal and flexural wave modes that are generated by the laser pulse. Many previous studies of ultrasonic waves in plates have shown that the propagating modes can be used to characterize their anisotropic properties (see Datta and Shah, 2009, Ch. 4). Recently, Gsell et al. (2000) and Gsell and Dual (2004) have used guided wave modes in composite hollow cylinders to measure the anisotropic properties of the material. As mentioned above, our attention is focused here on the characteristics of the guided modes generated by a concentrated heat source modeling a laser pulse. Transversely isotropic silicon nitride tube (Si_3N_4) is considered for numerical calculations.

3.2 Description of the Problem

Consider an infinite transversely isotropic cylinder of inner radius r_i and outer radius r_o in the cylindrical coordinate system (r, θ, z) shown in Fig. 3.1.

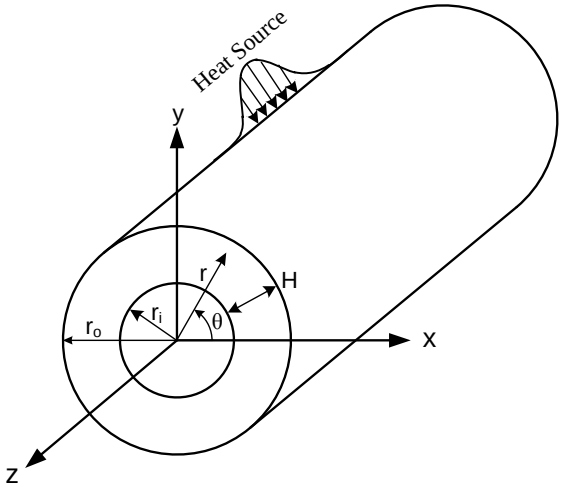

Figure 3.1: Geometry of the cylinder

The cylinder is initially in the undisturbed state with uniform temperature T_0. The inner and outer surfaces of the cylinder are traction free and the heat flux vanishes at the inner and outer surfaces in the radial direction. The cylinders outer surface is subjected to a concentrated heat source in the form of a focused laser beam.

3.3 Governing Equations

The generalized LS governing equations of thermoelasticity, in the presence of body force and heat source, are given by Al-Qahtani et al. (2005) as,

$$\sigma_{ij,j} + f_i = \rho \ddot{u}_i \tag{3.1}$$

$$T_0 \rho \dot{\eta} + Q = -q_{i,i} \tag{3.2}$$

$$\sigma_{ij} = C_{ijkl}\varepsilon_{kl} - \beta_{ij} T \tag{3.3}$$

$$\rho \dot{\eta} = \beta_{ij} \dot{\varepsilon}_{ij} + \frac{\rho c_E}{T_0} \dot{T} \tag{3.4}$$

$$q_i + \tau_0 \dot{q}_i = -k_{ij} T_{,j} \tag{3.5}$$

Various physical quantities and material constants appearing in the above equations are: σ_{ij}, the components of the stress tensor; u_i, the components of the displacement; ε_{ij}, the components of the strain tensor; C_{ijkl}, the elastic constants; q_i, components of the heat flux vector; ρ, the mass density; T_0, the reference temperature; η, the entropy density; T, the temperature change; c_E, the specific heat at constant deformation; τ_0, the thermal relaxation time; β_{ij}, the thermal coefficients; k_{ij}, the coefficients of thermal

conductivity; f_i, the body force per unit volume; Q, the heat source. In the above equations, the superposed dot indicates the derivative with respect to time.

A set of normalized quantities is presented here and they are given by

$$r_i^* = \frac{r_i}{H}, \quad u_i^* = \frac{u_i}{\delta H}, \quad T^* = \frac{T}{\bar{T}}, \quad t^* = \frac{\bar{v}}{H}t, \quad T_0^* = \frac{T_0}{\bar{T}}$$

$$\sigma_{ij}^* = \frac{\sigma_{ij}}{\delta \bar{c}}, \quad q_i^* = \frac{q_i}{\bar{q}}, \quad \varepsilon_{ij}^* = \frac{\varepsilon_{ij}}{\delta}, \quad \rho^* = \frac{\rho}{\bar{\rho}}, \quad c_E^* = \frac{c_E}{\bar{c}_E}, \tag{3.6}$$

$$\beta_{ij}^* = \frac{\beta_{ij}}{\bar{\beta}}, \quad k_{ij}^* = \frac{k_{ij}}{\bar{k}}, \quad c_{ijkl}^* = \frac{c_{ijkl}}{\bar{c}}, \quad \tau_0^* = \frac{\bar{v}}{H}\tau_0, \quad \mathrm{Q}^* = \frac{\bar{q}}{H}Q$$

where

$$\bar{v} = \sqrt{\frac{\bar{c}}{\bar{\rho}}}, \quad \delta = \sqrt{\frac{\bar{k}\bar{T}}{H\bar{v}\bar{c}}}, \quad \bar{q} = \frac{\bar{k}\bar{T}}{H}, \quad \bar{\beta} = \frac{\delta \bar{c}}{\bar{T}}, \quad \bar{c}_E = \frac{\bar{k}}{\bar{\rho}\bar{v}H} \tag{3.7}$$

Two more nondimensional quantities are defined: the wave number $\xi^* = \xi H$ and frequency $\omega^* = \frac{\omega H}{\bar{v}}$. Here $\bar{\rho}, \bar{k}, \bar{c}, H$ and $\bar{T}$ are the basic normalization quantities and the rest can be derived from them as shown above. Note that, $\bar{\rho}, \bar{k}, \bar{c}$ and $\bar{T}$ can be taken suitably depending upon the material properties of the cylinder. For convenience, the superscript (*) will be dropped.

3.4 Semi-Analytical Finite Element Formulation

In this method, the radial dependence of the displacement **u** and temperature **T** is approximated by one dimensional isoparametric finite elements. The total thickness of

the cylinder H is composed of cylindrical layers and each layer can have distinct thermoelastic properties and thickness. By using the SAFE method, the thickness of the cylinder is discretized into N laminas. Quadratic interpolation polynomials are used to approximate the displacement and temperature field over each lamina in the radial direction.

The displacements and temperature of the k^{th} lamina are expressed as

$$\begin{aligned} \mathbf{u}(r,\theta,z,t) &= \mathbf{N}_1(\zeta)\mathbf{u}^e(\theta,z,t) \\ \mathbf{T}(r,\theta,z,t) &= \mathbf{N}_2(\zeta)\mathbf{T}^e(\theta,z,t) \end{aligned} \tag{3.8}$$

and

$$r = \mathbf{N}_2(\zeta)\mathbf{R}^e \tag{3.9}$$

Here

$$\mathbf{N}_1(\zeta) = \begin{bmatrix} n_1 & 0 & 0 & n_2 & 0 & 0 & n_3 & 0 & 0 \\ 0 & n_1 & 0 & 0 & n_2 & 0 & 0 & n_3 & 0 \\ 0 & 0 & n_1 & 0 & 0 & n_2 & 0 & 0 & n_3 \end{bmatrix}, \quad \mathbf{N}_2(\zeta) = \begin{bmatrix} n_1 & n_2 & n_3 \end{bmatrix} \tag{3.10}$$

$$\begin{aligned} \mathbf{u}^e &= \left(u_{r1}, u_{\theta 1}, u_{z1}, u_{r2}, u_{\theta 2}, u_{z2}, u_{r3}, u_{\theta 3}, u_{z3}\right)^T, \\ \mathbf{T}^e &= \left(T_1, T_2, T_3\right)^T, \\ \mathbf{R}^e &= \left(R_b, R_m, R_f\right)^T \end{aligned} \tag{3.11}$$

In equation (3.10), the shape functions are

$$n_1 = \tfrac{1}{2}\zeta(\zeta-1), \quad n_2 = 1-\zeta^2, \quad n_3 = \tfrac{1}{2}\zeta(\zeta+1), \quad -1 \le \zeta \le 1 \tag{3.12}$$

where

$$\zeta = \frac{2r - R_b - R_f}{R_f - R_b} \qquad (R_b \le r \le R_f) \tag{3.13}$$

In equation (3.11), the nodal displacements $u_{rj}, u_{\theta j}, u_{zj}$, and temperature T_j, where j = 1, 2, 3, are taken at the inner surface $\left(r = R_b\right)$, middle layer $\left(r = R_m = \left(R_b + R_f\right)/2\right)$, and outer surface $\left(r = R_f\right)$ of the k^{th} lamina.

The strain tensor and temperature gradient are expressed as

$$\boldsymbol{\varepsilon} = \mathbf{D}_1\mathbf{u}^e + \mathbf{D}_2\mathbf{u}^e_{,\theta} + \mathbf{D}_3\mathbf{u}^e_{,z} \tag{3.14}$$

$$\mathbf{T}' = \mathbf{B}_1\mathbf{T}^e + \mathbf{B}_2\mathbf{T}^e_{,\theta} + \mathbf{B}_3\mathbf{T}^e_{,z} \tag{3.15}$$

The stress vector is given by

$$\boldsymbol{\sigma} = \mathbf{C}\left(\mathbf{D}_1\mathbf{u}^e + \mathbf{D}_2\mathbf{u}^e_{,\theta} + \mathbf{D}_3\mathbf{u}^e_{,z}\right) - \boldsymbol{\beta}\mathbf{N}_2\mathbf{T}^e \tag{3.16}$$

Matrices **ε, σ, C**, **β** , $\mathbf{B}_1$, $\mathbf{B}_2$, $\mathbf{B}_3$, $\mathbf{D}_1$, $\mathbf{D}_2$ and $\mathbf{D}_3$ are defined in Appendix A. The variational principle of thermoelasticity, Al-Qahtani et al. (2005), is

$$\int_{t_0}^{t_1}\int_V \left(\delta\boldsymbol{\varepsilon}^T\boldsymbol{\sigma} - \delta\mathbf{T}'^T\mathbf{K}\mathbf{T}' - \delta\mathbf{T}'^T\left(\mathbf{q} + \tau_0\dot{\mathbf{q}}\right)\right)dVdt = \int_{t_0}^{t_1}\int_V \delta\mathbf{u}^T\left(\mathbf{f} - \rho\ddot{\mathbf{u}}\right)dVdt \tag{3.17}$$

The first term in the left hand side of equation (3.17) is

$$\begin{aligned}\int_{t_0}^{t_1}\int_V \delta\boldsymbol{\varepsilon}^T\boldsymbol{\sigma}dVdt &= \int_{t_0}^{t_1}\int_V \left(\mathbf{D}_1\delta\mathbf{u}^e + \mathbf{D}_2\delta\mathbf{u}^e_{,\theta} + \mathbf{D}_3\delta\mathbf{u}^e_{,z}\right)^T\left[\mathbf{C}\left(\mathbf{D}_1\mathbf{u}^e + \mathbf{D}_2\mathbf{u}^e_{,\theta} + \mathbf{D}_3\mathbf{u}^e_{,z}\right) - \boldsymbol{\beta}\mathbf{N}_2\mathbf{T}^e\right]dVdt \\ &= \int_{t_0}^{t_1}\int_z\int_\theta \delta\mathbf{u}^{eT}\begin{bmatrix}\mathbf{K}_{11}\mathbf{u}^e + \left(\mathbf{K}_{12} - \mathbf{K}_{21}\right)\mathbf{u}^e_{,\theta} + \left(\mathbf{K}_{13} - \mathbf{K}_{31}\right)\mathbf{u}^e_{,z} \\ -\mathbf{K}_{22}\mathbf{u}^e_{,\theta\theta} - \left(\mathbf{K}_{23} + \mathbf{K}_{32}\right)\mathbf{u}^e_{,\theta z} - \mathbf{K}_{33}\mathbf{u}^e_{,zz} \\ -\mathbf{K}^e_{01}\mathbf{T}^e + \mathbf{K}^e_{02}\mathbf{T}^e_{,\theta} + \mathbf{K}^e_{03}\mathbf{T}^e_{,z}\end{bmatrix}d\theta dzdt\end{aligned} \tag{3.18}$$

The second term is

$$\int_{t_0}^{t_1}\int_V \delta\mathbf{T}'^T\mathbf{K}\mathbf{T}'\,dVdt = \int_{t_0}^{t_1}\int_V \left(\delta\mathbf{T}^{eT}\mathbf{B}_1^T + \delta\mathbf{T}_{,\theta}^{eT}\mathbf{B}_2^T + \delta\mathbf{T}_{,z}^{eT}\mathbf{B}_3^T\right)\mathbf{K}\left(\mathbf{B}_1\mathbf{T}^e + \mathbf{B}_2\mathbf{T}_{,\theta}^e + \mathbf{B}_3\mathbf{T}_{,z}^e\right)dVdt$$
$$= \int_{t_0}^{t_1}\int_z\int_\theta \delta\mathbf{T}^{eT}\left(\mathbf{g}_{11}\mathbf{T}^e - \mathbf{g}_{22}\mathbf{T}_{,\theta\theta}^e - \mathbf{g}_{33}\mathbf{T}_{,zz}^e\right)d\theta dzdt \tag{3.19}$$

The third term is

$$\int_{t_0}^{t_1}\int_V \delta\mathbf{T}'^T\left(\mathbf{q} + \tau_0\dot{\mathbf{q}}\right)dVdt = -\int_{t_0}^{t_1}\int_V \delta\mathbf{T}^T\left(\nabla\cdot\mathbf{q} + \tau_0\nabla\cdot\dot{\mathbf{q}}\right)dVdt$$
$$= \int_{t_0}^{t_1}\int_V \delta\mathbf{T}^T\left(T_0\rho\dot{\eta} + Q + \tau_0 T_0\rho\ddot{\eta} + \tau_0\dot{Q}\right)dVdt$$
$$= \int_{t_0}^{t_1}\int_V \delta\mathbf{T}^T\left[T_0\boldsymbol{\beta}^T\dot{\boldsymbol{\varepsilon}} + \rho c_E\dot{T} + Q + \tau_0\left(T_0\boldsymbol{\beta}^T\ddot{\boldsymbol{\varepsilon}} + \rho c_E\ddot{T} + \dot{Q}\right)\right]dVdt \tag{3.20}$$
$$= \int_{t_0}^{t_1}\int_z\int_\theta \delta\mathbf{T}^{eT}\begin{bmatrix}\left(\mathbf{f}_1\dot{\mathbf{u}}^e + \mathbf{f}_2\dot{\mathbf{u}}_{,\theta}^e + \mathbf{f}_3\dot{\mathbf{u}}_{,z}^e + \mathbf{m}_0\dot{\mathbf{T}}^e\right) + \\ \tau_0\left(\mathbf{f}_1\ddot{\mathbf{u}}^e + \mathbf{f}_2\ddot{\mathbf{u}}_{,\theta}^e + \mathbf{f}_3\ddot{\mathbf{u}}_{,z}^e + \mathbf{m}_0\ddot{\mathbf{T}}^e\right) + \mathbf{Q}_{th}^e\end{bmatrix}d\theta dzdt$$

The right hand side of equation (3.17) has the form

$$\int_{t_0}^{t_1}\int_V \delta\mathbf{u}^T\left(\mathbf{f} - \rho\ddot{\mathbf{u}}\right)dVdt = \int_{t_0}^{t_1}\int_z\int_\theta \delta\mathbf{u}^{eT}\left(\mathbf{f}^e - \mathbf{M}\ddot{\mathbf{u}}^e\right)d\theta dzdt \tag{3.21}$$

The element matrices appearing in equations (3.18) - (3.21) are defined in Appendix A.

Equating the coefficients of $\delta\mathbf{u}^e$ in equation (3.17) to zero gives the following equation

$$\mathbf{M}\ddot{\mathbf{u}}^e + \mathbf{K}_{11}\mathbf{u}^e - \mathbf{K}_{01}\mathbf{T}^e + \left(\mathbf{K}_{12} - \mathbf{K}_{21}\right)\mathbf{u}_{,\theta}^e + \mathbf{K}_{02}\mathbf{T}_{,\theta}^e$$
$$+\left(\mathbf{K}_{13} - \mathbf{K}_{31}\right)\mathbf{u}_{,z}^e + \mathbf{K}_{03}\mathbf{T}_{,z}^e - \mathbf{K}_{22}\mathbf{u}_{,\theta\theta}^e - \left(\mathbf{K}_{23} + \mathbf{K}_{32}\right)\mathbf{u}_{,\theta z}^e - \mathbf{K}_{33}\mathbf{u}_{,zz}^e = \mathbf{f}^e \tag{3.22}$$

Similarly, equating the coefficients of $\delta\mathbf{T}^e$ in equation (3.17) yields

$$\begin{aligned}&\tau_0\mathbf{f}_1\ddot{\mathbf{u}}^e+\tau_0\mathbf{m}_0\ddot{\mathbf{T}}^e+\tau_0\mathbf{f}_2\ddot{\mathbf{u}}^e_{,\theta}+\tau_0\mathbf{f}_3\ddot{\mathbf{u}}^e_{,z}+\mathbf{f}_1\dot{\mathbf{u}}^e+\mathbf{m}_0\dot{\mathbf{T}}^e\\&+\mathbf{f}_2\dot{\mathbf{u}}^e_{,\theta}+\mathbf{f}_3\dot{\mathbf{u}}^e_{,z}+\mathbf{g}_{11}\mathbf{T}^e-\mathbf{g}_{22}\mathbf{T}^e_{,\theta\theta}-\mathbf{g}_{33}\mathbf{T}^e_{,zz}=\mathbf{Q}^e\end{aligned}\tag{3.23}$$

Combining equations (3.22) and (3.23), and assembling the element matrices into global matrices lead to the following governing equations of motion,

$$\begin{aligned}&\mathbf{H}_1\ddot{\mathbf{V}}+\mathbf{H}_2\ddot{\mathbf{V}}_{,\theta}+\mathbf{H}_3\ddot{\mathbf{V}}_{,z}+\mathbf{H}_4\dot{\mathbf{V}}+\mathbf{H}_5\dot{\mathbf{V}}_{,\theta}+\mathbf{H}_6\dot{\mathbf{V}}_{,z}\\&+\mathbf{H}_7\mathbf{V}+\mathbf{H}_8\mathbf{V}_{,\theta}+\mathbf{H}_9\mathbf{V}_{,z}+\mathbf{H}_{10}\mathbf{V}_{,\theta\theta}+\mathbf{H}_{11}\mathbf{V}_{,\theta z}+\mathbf{H}_{12}\mathbf{V}_{,zz}=\mathbf{F}\end{aligned}\tag{3.24}$$

where $\mathbf{H}_i\,(i=1,2,...,12)$ are the global matrices, given in Appendix A, $\mathbf{V}$ is the global nodal displacement and temperature vector and $\mathbf{F}$ is a load vector defined by

$$\mathbf{F}=\begin{bmatrix}\mathbf{f}^e\\\mathbf{Q}^e\end{bmatrix}\tag{3.25}$$

Traction free boundary conditions on the surfaces of cylinder require that the stresses at the inner and outer surfaces of the cylinder are zero

$$\sigma_{rr}=\sigma_{r\theta}=\sigma_{rz}=0\quad\text{at}\quad r=r_i\text{ and }r=r_o\tag{3.26}$$

Thermal boundary conditions are considered as

$$T_{,r}=0\quad\text{at}\quad r=r_i\text{ and }r=r_o\tag{3.27}$$

Thermal boundary conditions imply that heat does not flow into or out of the system via the boundaries. Initial conditions are specified as

$$\mathbf{V}=\dot{\mathbf{V}}=0\quad\text{at}\quad\text{time, }t=0\tag{3.28}$$

3.5 Solution Procedure for Steady State Loading

In equation (3.25), the force vector $\mathbf{F}$ and the response $\mathbf{V}$ are assumed to be time harmonic with frequency ω. The $\theta-$dependence of the load and response can be expressed in Fourier series as:

$$\begin{aligned}\mathbf{F}(\theta,z,t) &= e^{-i\omega t}\mathbf{F}(\theta,z) = e^{-i\omega t}\sum_{n=-\infty}^{n=+\infty}\mathbf{F}_n(z)e^{in\theta} \\ \mathbf{V}(\theta,z,t) &= e^{-i\omega t}\mathbf{V}(\theta,z) = e^{-i\omega t}\sum_{n=-\infty}^{n=+\infty}\mathbf{V}_n(z)e^{in\theta}\end{aligned} \tag{3.29}$$

Substitution of equation (3.29) into (3.24) yields a system of ordinary differential equations with Fourier coefficients $\mathbf{V}_n$ in terms of *z*. For each circumferential wave number(n), we obtain

$$\begin{aligned}&\mathbf{H}_{12}\mathbf{V}_{n,zz} + \left(-\omega^2\mathbf{H}_3 - i\omega\mathbf{H}_6 + \mathbf{H}_9 + in\mathbf{H}_{11}\right)\mathbf{V}_{n,z} - \\ &\left[\omega^2\left(\mathbf{H}_1 + in\mathbf{H}_2\right) + i\omega\left(\mathbf{H}_4 + in\mathbf{H}_5\right) - \left(\mathbf{H}_7 + in\mathbf{H}_8 - n^2\mathbf{H}_{10}\right)\right]\mathbf{V}_n = \mathbf{F}_n\end{aligned} \tag{3.30}$$

The following Fourier integral transform pairs are used to treat the *z*-dependence in equation (3.30)

$$\bar{\mathbf{V}}_n(k_n) = \int_{-\infty}^{+\infty}\mathbf{V}_n(z)e^{-ik_nz}dz \qquad \textit{and} \qquad \mathbf{V}_n(z) = \frac{1}{2\pi}\int_{-\infty}^{+\infty}\bar{\mathbf{V}}_n(k_n)e^{ik_nz}dk_n \tag{3.31}$$

Application of Fourier transformation to equation (3.30) yields the algebraic equation in terms of the transform parameter (k_n)

$$-k_n^2\mathbf{H}_{12}\bar{\mathbf{V}}_n + k_n\mathbf{H}_B\bar{\mathbf{V}}_n + \mathbf{H}_A\bar{\mathbf{V}}_n = \bar{\mathbf{F}}_n \tag{3.32}$$

where

$$\mathbf{H}_B = -i\omega^2\mathbf{H}_3 + \omega\mathbf{H}_6 + i\mathbf{H}_9 - n\mathbf{H}_{11}$$
$$\mathbf{H}_A = -\omega^2\left(\mathbf{H}_1 + in\mathbf{H}_2\right) - i\omega\left(\mathbf{H}_4 + in\mathbf{H}_5\right) + \left(\mathbf{H}_7 + in\mathbf{H}_8 - n^2\mathbf{H}_{10}\right)$$

Equation (3.32) is the governing equation for the n^{th} circumferential harmonic in the transformed domain. Note that for a free cylinder without body forces and heat sources the right hand side of equation (3.32) will be zero. Then, the homogeneous equation (3.32) leads to the eigenvalue problem for the determination of the dispersion relation between the frequency ω and the axial wave number k_n for a fixed circumferential integral wave number *n*.

The solution of equation (3.32) will be obtained in the form of an expansion in guided wave modes in the *z*-direction. For this purpose, the homogeneous equation, which is a three parameter algebraic eigen system in $\omega, n,$ and k_n is considered. If k_n serves as an eigenvalue for given values of ω and n, equation (3.32) gives a quadratic eigenvalue problem. Equation (3.32) can be converted into first order equation in the form

$$\begin{bmatrix} 0 & I \\ \mathbf{H}_A & \mathbf{H}_B \end{bmatrix} \begin{Bmatrix} \bar{\mathbf{V}}_n \\ k_n\bar{\mathbf{V}}_n \end{Bmatrix} - k_n \begin{bmatrix} I & 0 \\ 0 & \mathbf{H}_{12} \end{bmatrix} \begin{Bmatrix} \bar{\mathbf{V}}_n \\ k_n\bar{\mathbf{V}}_n \end{Bmatrix} = \begin{bmatrix} 0 \\ \bar{\mathbf{F}}_n \end{bmatrix} \quad \Rightarrow \quad \left[\mathbf{A} - k_n\mathbf{B}\right]\mathbf{U}_n = \mathbf{P}_n \qquad (3.33)$$

If the dimension of the displacement and temperature vector $\bar{\mathbf{V}}_n$ is M, then the dimension of $\mathbf{U}_n$ in equation (3.33) becomes $2M$. A non-trivial solution to the homogeneous form of equation (3.33) in terms of k_n yields $2M$ roots, denoted by k_{nm}. They represent axial wave numbers which can be real, purely imaginary or complex. A

real wave number represents a propagating wave and purely imaginary or complex wave numbers represent non-propagating (evanescent) waves.

Once the wavenumbers and wave functions are found from equation (3.33), the response due to the n^{th} circumferential mode in the Fourier series representation of applied loads can be obtained by modal summation. Associated with each eigenvalue, there are right and left eigenvectors, $\mathbf{\Phi}_{nm}^{R}$ and $\mathbf{\Phi}_{nm}^{L}$, respectively, and they satisfy the equations

$$\begin{aligned} \left[\mathbf{A}-k_n\mathbf{B}\right]\mathbf{\Phi}_{nm}^{R}&=0,\\ \left[\mathbf{A}^{T}-k_n\mathbf{B}^{T}\right]\mathbf{\Phi}_{nm}^{L}&=0. \end{aligned} \tag{3.34}$$

The right and left eigenvectors also satisfy bi-orthogonality relations

$$\mathbf{\Phi}_{nm}^{L^T}\mathbf{B}\mathbf{\Phi}_{np}^{R}=diag\left(B_{nm}\right),\qquad \mathbf{\Phi}_{nm}^{L^T}\mathbf{A}\mathbf{\Phi}_{np}^{R}=diag\left(k_{nm}B_{nm}\right) \tag{3.35}$$

where, diag ( ) denotes a diagonal matrix. The eigenvectors can also be partitioned into the following upper and lower halves represented by subscripts u and l, respectively.

$$\mathbf{\Phi}_{nm}^{R}=\begin{bmatrix}\mathbf{\Phi}_{nmu}^{R}\\ \mathbf{\Phi}_{nml}^{R}\end{bmatrix},\qquad \mathbf{\Phi}_{nm}^{L}=\begin{bmatrix}\mathbf{\Phi}_{nmu}^{L}\\ \mathbf{\Phi}_{nml}^{L}\end{bmatrix} \tag{3.36}$$

The solution of equation (3.33) is expressed by summation of right eigenvectors as

$$\mathbf{U}_n=\sum_{m=1}^{2M}U_{nm}\mathbf{\Phi}_{nm}^{R} \tag{3.37}$$

Coefficients U_{nm} are calculated by substituting equation (3.37) into equation (3.33) and using the bi-orthogonality relations (3.35). Then, the solution vector $\mathbf{U}_n$ is written as

$$\mathbf{U}_n = \sum_{m=1}^{2M} \frac{\boldsymbol{\Phi}_{mn}^{L^T} \mathbf{P}_n}{\left(k_{nm} - k_n\right) B_{nm}} \boldsymbol{\Phi}_{nm}^{R} \tag{3.38}$$

The solution vector $\bar{\mathbf{V}}_n$ in equation (3.33) , occupying the upper half of $\mathbf{U}_n$, takes the form

$$\bar{\mathbf{V}}_n = \sum_{m=1}^{2M} \frac{\boldsymbol{\Phi}_{mnl}^{L^T} \bar{\mathbf{F}}_n}{\left(k_{nm} - k_n\right) B_{nm}} \boldsymbol{\Phi}_{nmu}^{R} \tag{3.39}$$

The inverse Fourier transform of equation (3.39) gives the response, $\mathbf{V}_n\left(z\right)$, of the n^{th} circumferential harmonic in the spatial domain

$$\mathbf{V}_n\left(z\right) = \frac{1}{2\pi} \sum_{m=1}^{2M} \int_{-\infty}^{+\infty} \frac{\boldsymbol{\Phi}_{mnl}^{L^T} \bar{\mathbf{F}}_n}{\left(k_{nm} - k_n\right) B_{nm}} \boldsymbol{\Phi}_{nmu}^{R} e^{ik_n z} dk_n \tag{3.40}$$

In the above equation, $\bar{\mathbf{F}}_n, \boldsymbol{\Phi}_{mn}^{L}, \boldsymbol{\Phi}_{nm}^{R}$ and B_{nm} are independent of wave number k_n, so that the application of the Cauchy residue theorem yields the modal response $\mathbf{V}_n\left(z\right)$ in a straight forward way. The eigen data can be divided into two groups for travelling or decaying modes from the origin in $\pm z$ directions, respectively. Therefore, $\mathbf{V}_n\left(z\right)$ can be expressed as summation of motions in positive and negative directions as

$$\mathbf{V}_n\left(z,\omega\right) = -i \sum_{m=1}^{M} \frac{\boldsymbol{\Phi}_{mnl}^{L^T} \bar{\mathbf{F}}_n}{B_{nm}} \boldsymbol{\Phi}_{nmu}^{R} e^{ik_{nm} z} - i \sum_{m=M+1}^{2M} \frac{\boldsymbol{\Phi}_{mnl}^{L^T} \bar{\mathbf{F}}_n}{B_{nm}} \boldsymbol{\Phi}_{nmu}^{R} e^{-ik_{nm} z} \tag{3.41}$$

The response in the time domain is now obtained by applying an inverse Fourier transformation to equation (3.41) and is calculated numerically as

$$\mathbf{V}_n\left(z,t\right) = \frac{1}{2\pi} \int_{-\infty}^{+\infty} \mathbf{V}_n\left(z,\omega\right) e^{-i\omega t} d\omega \tag{3.42}$$

3.6 Heat Source Representation

The heat input due to the laser pulse is assumed to be of the form

$$Q = I_0 f(t)\delta(\theta) g_r(r) g_z(z) \tag{3.43}$$

where I_0 is the energy of the laser pulse. The temporal profile $f(t)$ is assumed as

$$f(t) = \frac{t}{t_0^2} e^{-\frac{t}{t_0}} \tag{3.44}$$

where t_0 is the pulse rise time. The spatial profile $g_z(z)$ is assumed to have a Gaussian profile in the *z*-direction,

$$g_z(z) = \frac{1}{\sqrt{\pi} a} e^{-\frac{z^2}{a^2}} \tag{3.45}$$

where a is the radius of the laser beam. The depth dependence, $g_r(r)$, of the pulse is taken as,

$$g_r(r) = \frac{\gamma}{r} e^{-\gamma(r_0 - r)} \tag{3.46}$$

where γ is the extinction coefficient.

Once the fundamental response functions $\mathbf{\Gamma}(z)$ are constructed due to $Q = I_0 f(t)\delta(\theta) g_r(r)\delta(z)$, the response due to the heat source Q, represented by equation (3.43), can be calculated as

$$\mathbf{v}(z_0) = \int_{-\infty}^{+\infty} \mathbf{\Gamma}(z)\, g_z(z - z_0)\, dz \tag{3.47}$$

In the present work, only the thermal load is considered for constructing the response function. Spatial representation of heat source along the radial profile in frequency domain is

$$\mathbf{Q} = I_0 \bar{f}(\omega)\delta(\theta)\delta(z)\mathbf{Q}_0 \tag{3.48}$$

where $\mathbf{Q}_0 = (Q_1,\ \ Q_2,\ \ .\ .\ .,\ \ Q_k,\ \ .\ .\ .,\ \ Q_{2N+1})^T$ and Q_k is the value of $g_r(r)$ at the k^{th} node using consistent load formulation. The solution procedure involves expansion of $\delta(\theta)$ in a Fourier series. It is well known that the Fourier series representation of $\delta-$ function does not converge. Hence, it is necessary to replace the point source by a uniform spatial pulse of intensity q_0 over a circumferential distance $2r_o\theta_0$. For equivalence of a unit concentrated source, q_0 is given by

$$\int_{-\theta_0}^{+\theta_0} q_0 r_o\, d\theta = 1 \qquad or \qquad q_0 = \frac{1}{2r_o\theta_0} \tag{3.49}$$

Therefore, the θ-dependence of $\mathbf{Q}$ in equation (3.48) is represented by a Fourier series expansion in circumferential direction as

$$\mathbf{Q} = \sum_{n=-\infty}^{n=+\infty} e^{in\theta}\mathbf{Q}_{n\theta} \tag{3.50}$$

where

$$\mathbf{Q}_{n\theta} = \frac{1}{2\pi r_o}\frac{\sin n\theta_0}{n\theta_0} I_0 \bar{f}(\omega)\delta(z)\mathbf{Q}_0 \tag{3.51}$$

The Fourier transform of $\mathbf{Q}_{n\theta}$ in the *z*-direction is

$$\bar{\mathbf{Q}}_{n\theta} = \frac{1}{2\pi r_o} \frac{\sin n\theta_0}{n\theta_0} I_0 \bar{f}(\omega) \mathbf{Q}_0 \tag{3.52}$$

Since a mechanical load is not considered here, the load vector in equation (3.32) becomes

$$\bar{\mathbf{F}}_n = \begin{bmatrix} 0 \\ \bar{\mathbf{Q}}_{n\theta} \end{bmatrix} = \frac{I_0 \bar{f}(\omega)}{2\pi r_o} \frac{\sin n\theta_0}{n\theta_0} \mathbf{F}_0 \tag{3.53}$$

where $\mathbf{F}_0 = \begin{bmatrix} 0 & \mathbf{Q}_0 \end{bmatrix}^T$. Note that Zhuang et al. (1999) considered the isothermal problem due to a mechanical point load. Substitution of equation (3.53) into equation (3.41) and considering propagation only in the $+z$ directions yields the n^{th} circumferential mode displacement and temperature response functions as

$$\mathbf{V}_n(z,\omega) = \frac{-iI_0 \bar{f}(\omega)}{2\pi r_o} \frac{\sin n\theta_0}{n\theta_0} \sum_{m=1}^{M} \frac{\mathbf{\Phi}_{mnl}^{L^T} \mathbf{F}_0}{B_{nm}} \mathbf{\Phi}_{nmu}^{R} e^{ik_{nm}z} \tag{3.54}$$

Using (3.54) in (3.50), we obtain

$$\mathbf{V}(\theta,z,\omega) = \frac{-iI_0 \bar{f}(\omega)}{2\pi r_o} \sum_{n=-\infty}^{n=+\infty} \frac{\sin n\theta_0}{n\theta_0} e^{in\theta} \sum_{m=1}^{M} \frac{\mathbf{\Phi}_{mnl}^{L^T} \mathbf{F}_0}{B_{nm}} \mathbf{\Phi}_{nmu}^{R} e^{ik_{nm}z} \tag{3.55}$$

where $\bar{f}(\omega)$ is the Fourier transform of temporal profile $f(t)$. Equation (3.55) is used in the following section to calculate the vector **V** at a given location (θ, *z*) for different frequency ω. Applying an inverse Fourier transformation to the above equation (3.55) yields the time transient response.

3.7 Numerical Results and Discussion

For Numerical results, an infinite cylindrical tube with thickness 1 mm and inner radius 1.5 mm is considered. Thus, the nondimensional inner and outer radii are, $r_i = 1.5$ and $r_o = 2.5$, respectively. The material of the tube is taken to be silicon nitride (Si_3N_4), whose properties are listed in Table 2.1 (see Al-Qahtani et al. 2005). The symmetry axis of the material is aligned with the axis of the cylinder. A schematic representation of the pulse and the frequency spectrum of $f(t)$ are shown in Figs. 3.2(a) and 3.2(b). Here, the nondimensional frequency, $\omega^* = \omega H / \bar{v}$. Figure 3.2(b) shows that the frequency content of the heat pulse is confined in the interval $(0,4)$ MHz . The pulse rise time t_0 in equation (3.44) is taken as 1 μs and the extinction coefficient γ appearing in the expression for $g_r(r)$ is taken as 10^4 m^{-1}. To calculate the response due to the source given by equation (3.43), $g_z(z)$ is first replaced by the impulse function $\delta(z)$. Once the response due to this source is found, the response due to any other function $g_z(z)$ can be evaluated by convolution (Eq. (3.47)).

For the purpose of nondimensionalization, normalizing velocity $\bar{v}$ is chosen to be 0.25 km/s. Furthermore, the normalized density ρ^* is taken to be 1. Then, the nondimensional material properties of the tube are given by

$$T_0^* = 1.0,\ \tau_0^* = 1.081\times10^{-7}$$
$$\beta_{rr}^* = 70.03,\ \beta_{\theta\theta}^* = 70.03,\ \beta_{zz}^* = 83.21$$
$$k_{rr}^* = 0.0785,\ k_{\theta\theta}^* = 0.0785,\ k_{zz}^* = 0.1, c_E^* = 967.50$$

Also, the nondimensional elastic stiffness tensor is given by

$$\mathbf{C}^{*} = \begin{bmatrix} 2165 & 975 & 635 & 0 & 0 & 0 \\ 975 & 2165 & 635 & 0 & 0 & 0 \\ 635 & 635 & 2870 & 0 & 0 & 0 \\ 0 & 0 & 0 & 540 & 0 & 0 \\ 0 & 0 & 0 & 0 & 540 & 0 \\ 0 & 0 & 0 & 0 & 0 & 595 \end{bmatrix}$$

As mentioned previously, the homogeneous solution of equation (3.33) yields dispersion curves for thermoelastic waves in a cylinder. These curves for different circumferential modes (n = 0, 1, 2, 3) are computed and presented graphically in the form of 3-D plots shown in Figs. 3.3(a) and 3.3(b). These modes are labeled as L(0,1), L(0,2), F(1,1), F(1,2) etc, using the convention employed in Alleyne et al. (1998). The series representation in equation (3.55) involves double summation: one over the number of axial modes *M* for a given circumferential mode *n* and the other over circumferential modes *n*. The first one is determined by the number of finite elements N_e used to discretize the thickness of the cylinder. θ_0, appearing in equation (3.49) has been chosen as 0.01 radians.

To test the convergence of series at high frequency $\omega^{*} = 100.0$ (~4 MHz), numerical results were calculated for different mesh sizes with N_e taken as 10, 25 and 50 keeping $|n|$ fixed at 20. Figures 3.4(a) and 3.4(b) show the variation of displacement, temperature, stress, and radial heat flux through the thickness with the number N_e. It is seen that convergence of displacements, temperature, and the stresses are achieved with 25 elements whereas, convergence of heat flux is achieved with 50 elements. As the accuracy is also related to the number of circumferential modes, the response was calculated with different $|n|$ values of 5, 10 and 20 and shown in Figs 3.5(a) and 3.5(b). It

was observed that with N_e = 50, numerical results converged with 10 circumferential modes at an observation point $\theta = 0^{\circ}$ and $z = 100H$. The heat flux distribution through the thickness of the cylinder shows sharp drops near the inner and outer surfaces of the cylinder (boundary layer like behavior) and more elements are needed near these surfaces to capture this behavior. In the 50 element model, the thickness is divided into 20 layers (10 at the outer end and 10 at the inner), each of thickness 0.0015, and 30 layers of thickness 0.0023 mm in the middle whereas, in the 25 element model, the shell is divided into 25 uniform layers of thickness 0.004 mm each.

In this chapter, the main emphasis is on the characteristics of longitudinal and flexural modes (in addition to the total response), as these modes have received a great deal of attention in nondestructive evaluation of materials (see Rose, 2004). In the frequency range 0 and 4.0 MHz, where the dominant contribution of the laser pulse considered here is limited, primarily the longitudinal modes [L(0,1), L(0,2)] and the flexural modes [F(1,1), F(2,1), F(3,1)] are excited. Group velocities of these modes were computed and are shown in Figs. 3.6(a) and 3.6(b). Figure 3.6(a) shows that at low frequencies L(0,1) mode propagates at much higher group speed than at high frequencies. It is interesting to note the speed of L(0,1) mode drops sharply to 0.97 km/s at a frequency 0.835 MHz. This frequency is very close to that of the zero group speed of the L(0,2) mode, which is 0.85 MHz.

As seen in Figs. 3.6(a) and 3.6(b), maximum group speeds of the L(0,1) and L(0,2) modes are almost the same, which is 12.80 km/s, and are attained below 4.0 MHz. Furthermore, the F(1,1), F(2,1), and F(3,1) modes propagate with the same maximum group speed of 5.70 km/s, which is attained at around 4 MHz. Also, these modes are

fairly dispersive at low frequencies. Figure 3.7(a) shows the frequency response spectrum of the radial displacement of the outer surface of the cylinder associated with the L(0,1) and L(0,2) modes at $\theta = 0^o, z = 100H$. Sharp resonances are seen at 0.835 and 0.85 MHz. Frequency resolution of 2.0 kHz was used to compute the frequency response spectra. Frequency spectra of flexural modes are presented in Fig. 3.7(b). Sharp resonance peaks are found to occur for the F(2,1) and F(3,1) near their cutoff frequency points.

Figures 3.8(a) and 3.8(b) show the transient radial displacement responses of longitudinal modes at two observation locations, $\theta = 0^\circ,\ z = 100H$, and $\theta = 0^\circ,\ z = 200H$. As mentioned above, both longitudinal modes propagate with almost the same highest group speed of 12.80 km/s. Therefore, the arrival times of these modes at the first and the second locations are about 7.8 μs and 15.6 μs , respectively. It is observed that the L(0,1) mode shows higher amplitudes than the L(0,2) mode.

Transient displacement responses of flexural modes at the same observation points, mentioned above, are shown in Figs. 3.9 and 3.10. Since these modes travel with almost the same group speeds of 5.70 km/s, they arrive at the first location in about 17.54 μs and the second location in about 35.1 μs . It is evident from Figs. 3.8(a), 3.8(b), and 3.9, 3.10 that the peak response is dominated by flexural modes when compared to that of longitudinal modes.

In order to see the difference between the response of the cylinder due to the Gaussian profile of $g_z(z)$ and that due to $\delta(z)$, transient response of the L(0,1) mode due to the Gaussian profile is computed at observation location, $\theta = 0^\circ,\ z = 100H$, and is

compared with that due to $\delta(z)$ in Fig. 3.11. Comparison of these two wave forms does not show significant differences. Figure 3.12 shows the dispersion curves for all the propagating modes within the frequency range 0 to 3.0 MHz. The time history response due to each propagating mode was computed and summed up to obtain the total response history shown in Fig. 3.13. Clearly, the total response is dominated by the flexural waves.

As mentioned before, the focus of the present study has been on the characteristics of the guided waves modes in the cylinder due to concentrated heating by a laser source. For this purpose, the cylinder is assumed to have no defects. Once the modes are calculated, they can be used to study reflection and transmission of these modes when there are localized defects like cracks, joints, corrosion pits, and others. References to such works can be found in Rattanawangcharoen et al. (1994) and Zhuang et al. (1997), Bai et al. (2001, 2002) (see also Datta and Shah, 2009, Section 6.3).

3.8 Concluding Remarks

Transient analysis of thermoelastic waves in an anisotropic circular cylindrical shell excited by a focused laser beam has been studied in this chapter. The heat input is assumed to be that due to a pulsed laser beam focused at $r = r_o,\ \theta = 0,\ z = 0$, with a radial dependence that decays with decreasing r, and is assumed to act on a small circular arc, $2r_o\theta_0,$ along the circumference. The pulse has a Gaussian distribution in the axial direction. The solution can then be used for more general dependence on *z* and θ. Pulsed laser heating generates thermal waves as well as (primarily) elastic waves. The former are strongly attenuated as they propagate along the cylinder whereas, the latter

have very small attenuation and are weakly dependent on the temperature. Thus, the laser generated elastic waves provide an efficient means of ultrasonic material characterization. They can also be used for ultrasonic NDE of defects in the structure. In this chapter, attention has been focused on the frequency and time-dependent characteristics of the guided elastic modes of propagation.

The dispersion curves and transient wave forms of propagating longitudinal and flexural modes in a silicon nitride (Si_3N_4) tube are computed numerically. Longitudinal modes travel faster than the flexural modes, the latter having larger amplitudes than the former. The transient wave forms presented here are for dominant propagating modes and the total response is found by summation of all the propagating modes in the frequency range of the pulse. It is found that the response is dominated by the flexural modes. The Semi-Analytical Finite Element (SAFE) method that has been used here can also be used for other anisotropic materials and for different thicknesses of the cylinders. It also can be used to calculate the transient displacement response at multiple locations on the cylinder. The results can be used along with experiments to characterize the anisotropic material properties.

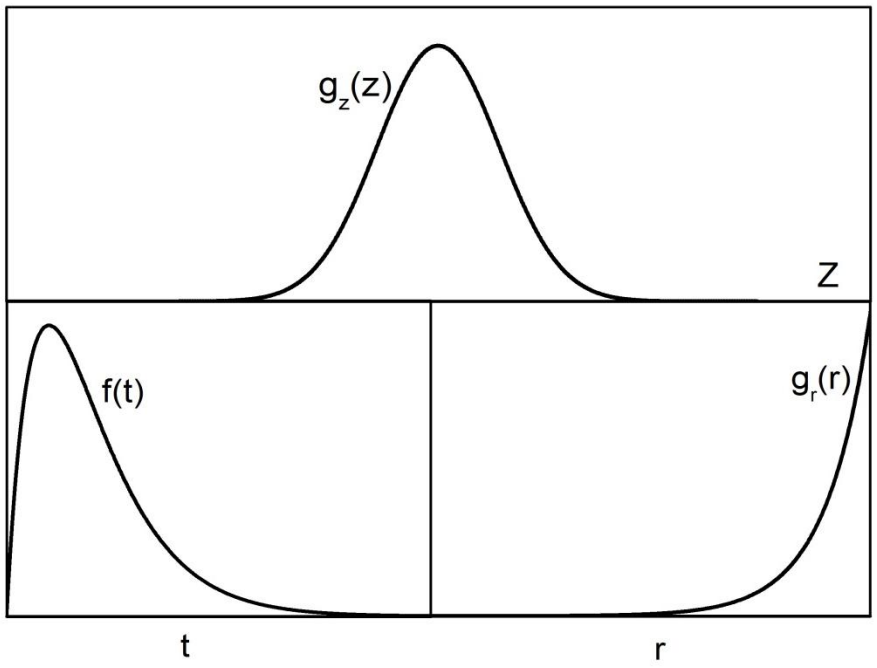

Figure 3.2(a): Temporal and spatial profiles of the heat source

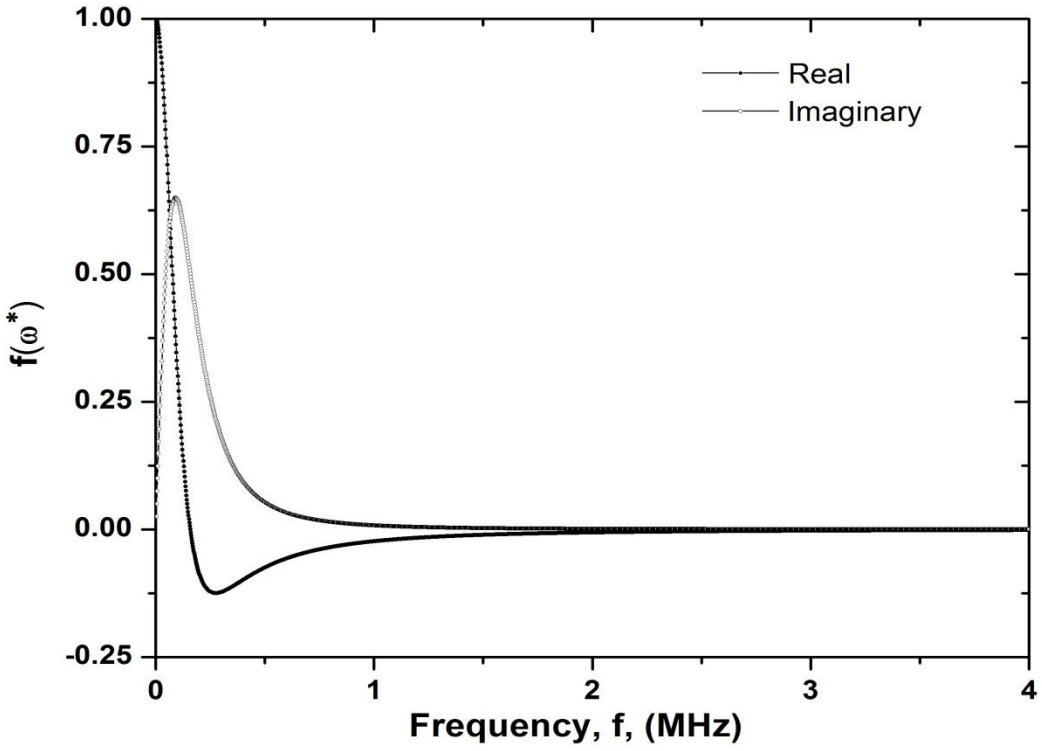

Figure 3.2(b): Frequency spectrum of *f(t)*

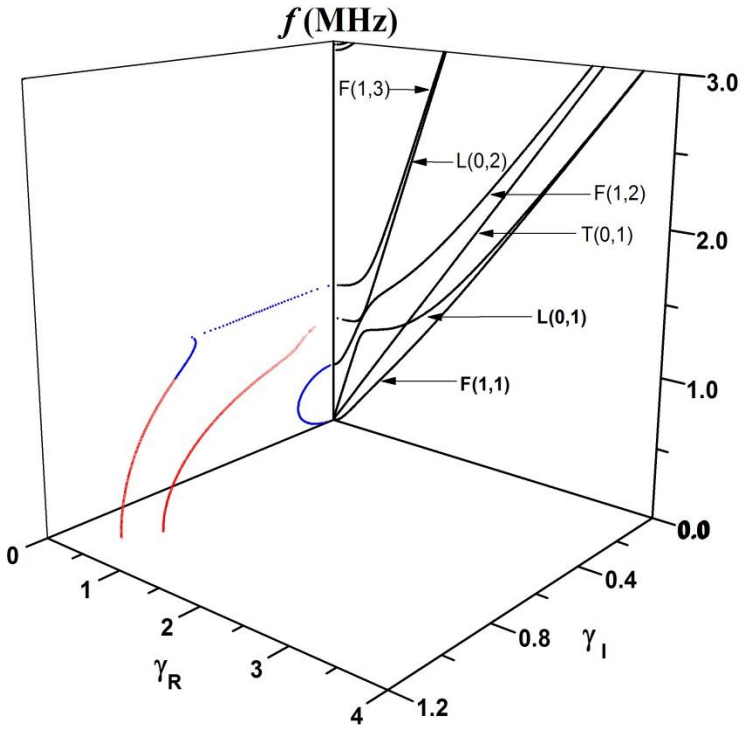

Figure 3.3(a): Frequency wave number plots for a silicon nitride tube when n=0 and n=1

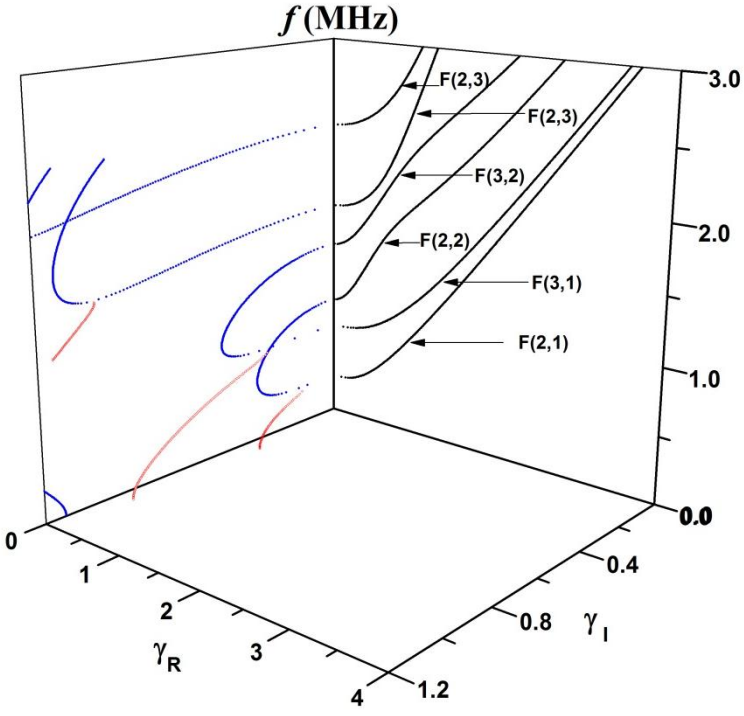

Figure 3.3(b): Frequency wave number plots for a silicon nitride tube when n=2 and n=3

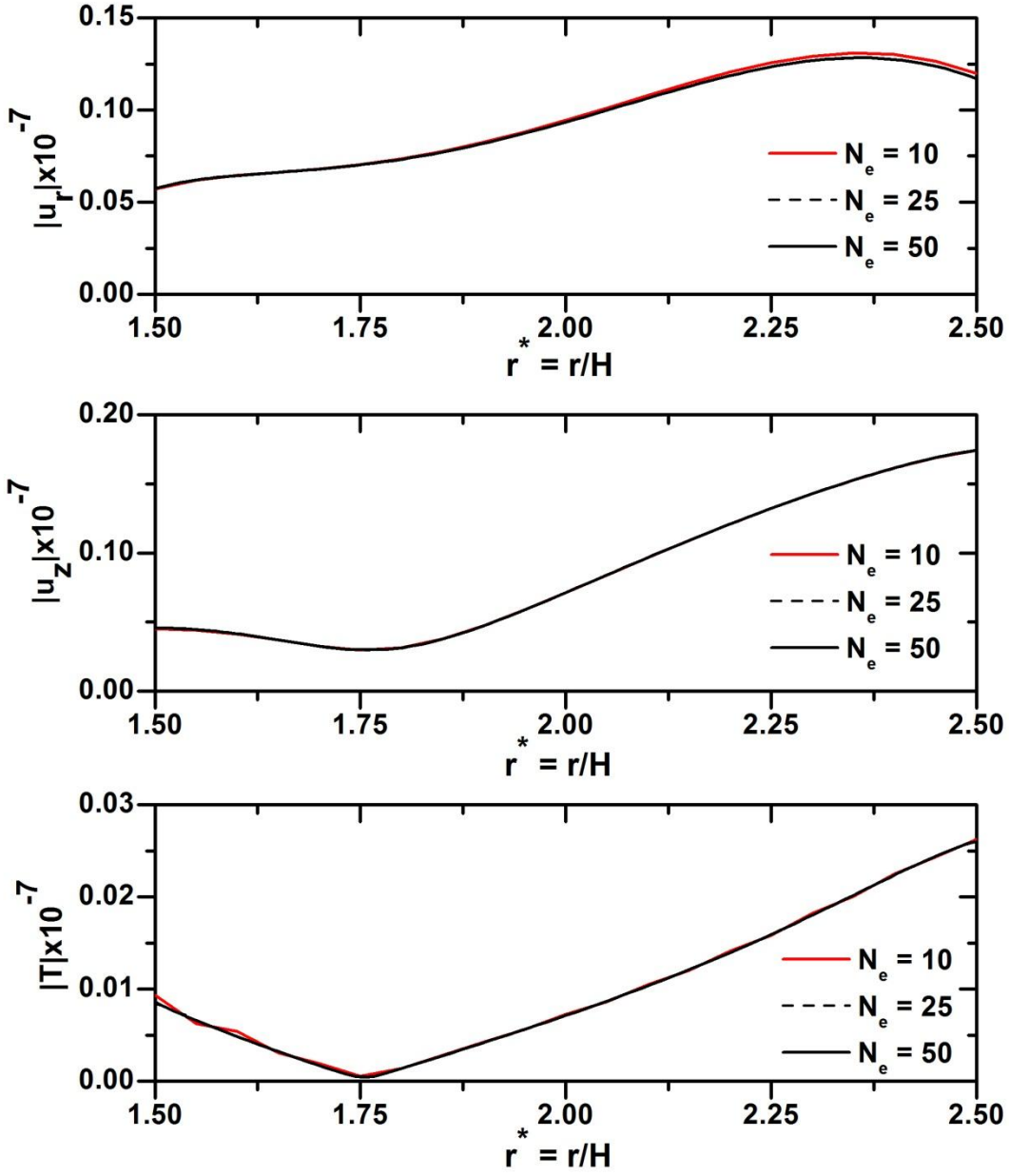

Figure 3.4(a): Comparison of displacement components and temperature distribution for a silicon nitride cylinder at $\omega^* = 100.0$ (~4 MHz) with different number of elements (Ne) at an observation point, θ = 0 and z = 100H

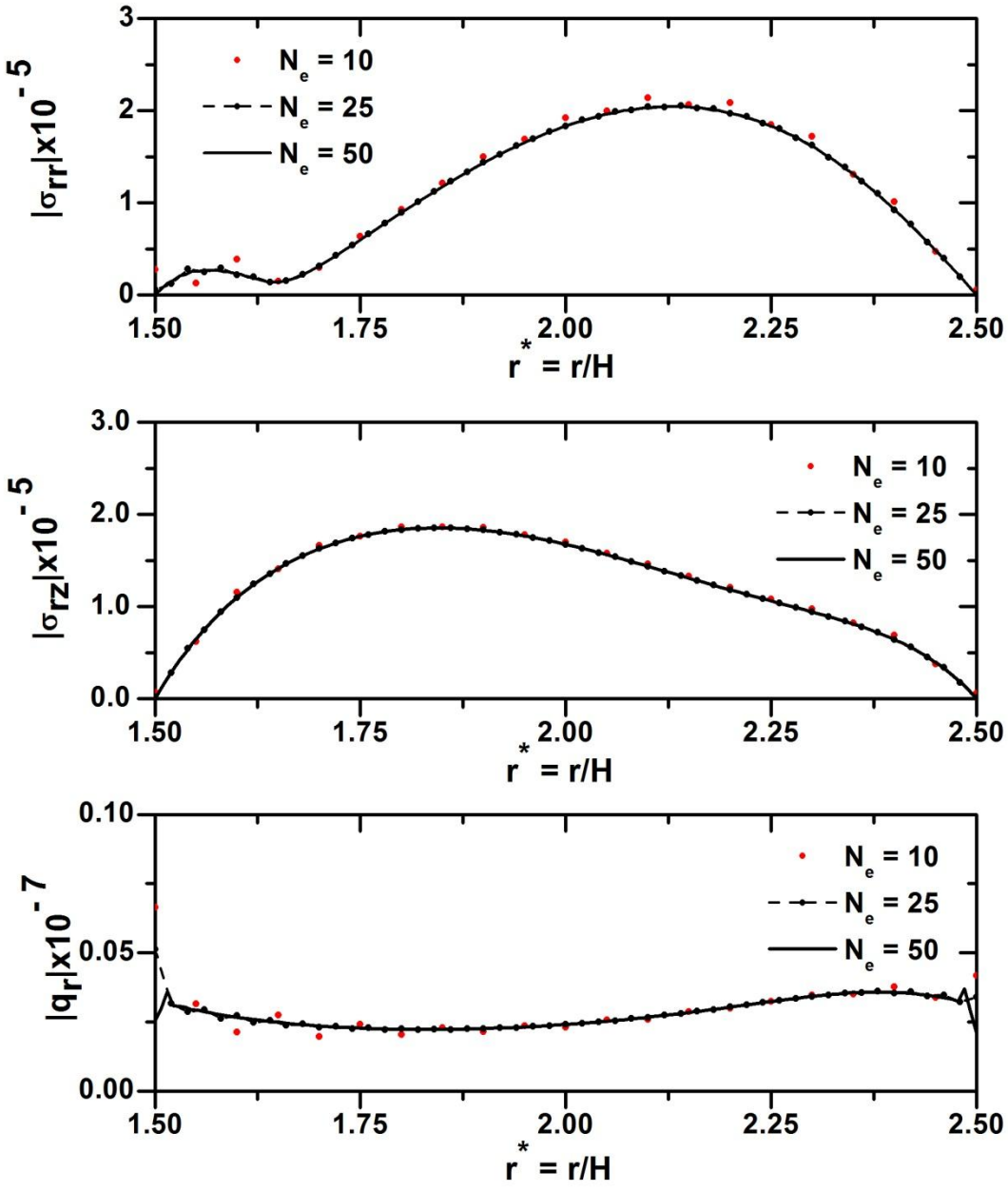

Figure 3.4(b): Comparison of stress components and temperature gradient for a silicon nitride cylinder at $\omega^* = 100.0$ (~4 MHz) with different number of elements (Ne) at an observation point, θ = 0 and z = 100H

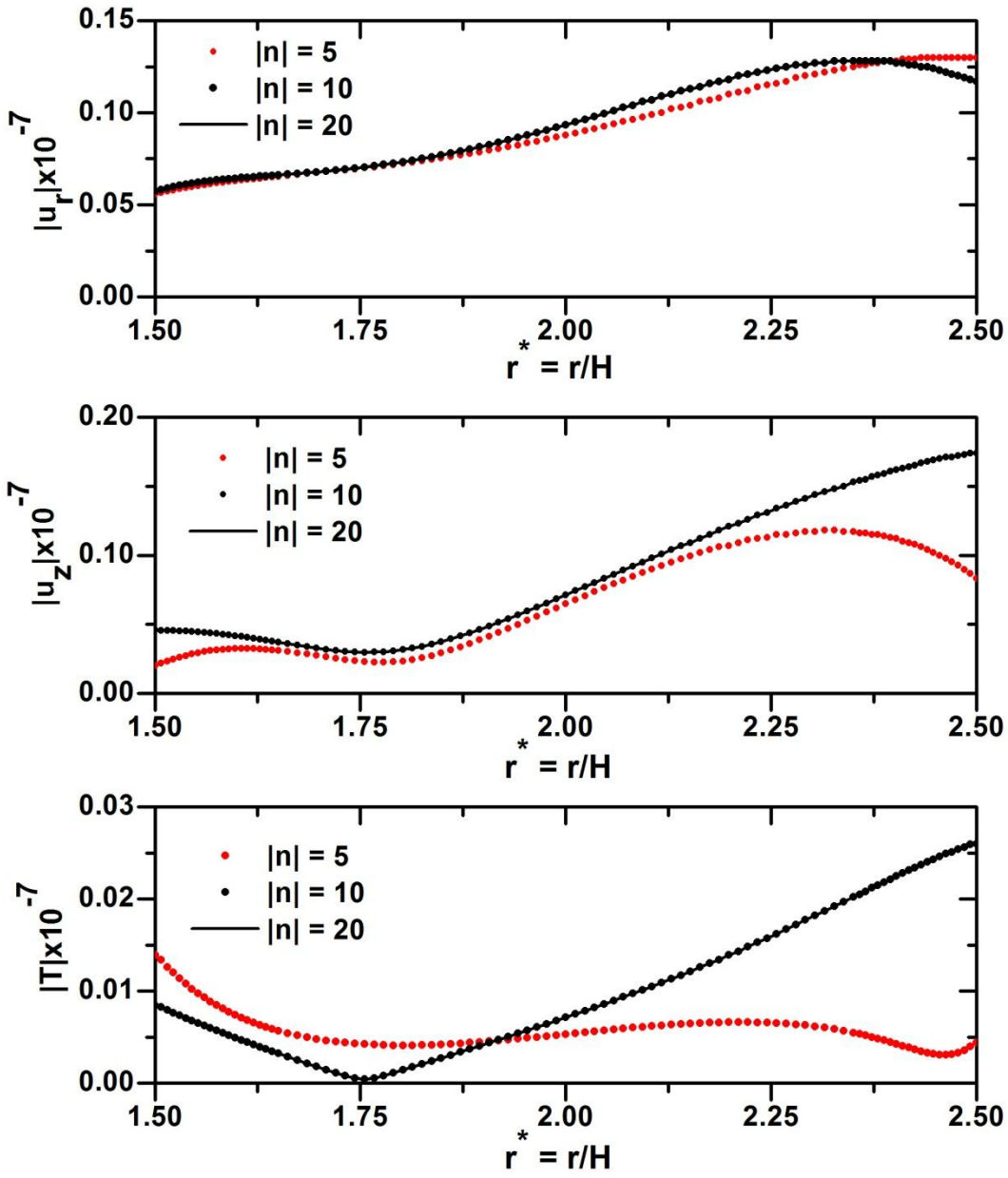

Figure 3.5(a): Comparison of displacement components and temperature distribution for a silicon nitride cylinder at $\omega^* = 100.0$ (~4 MHz) with $|n| = 5,10$ and 20 at an observation point θ = 0 and z = 100H

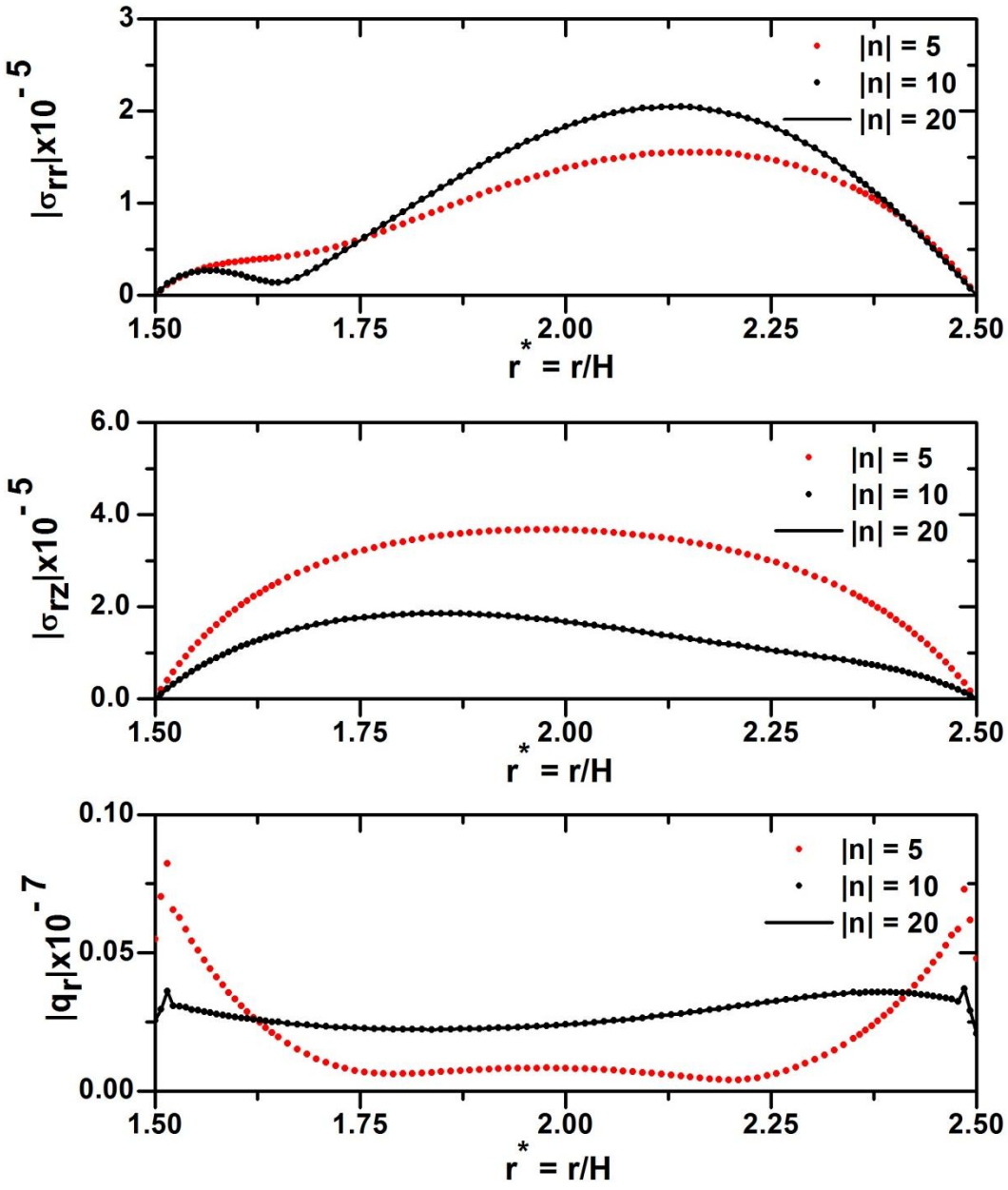

Figure 3.5(b): Comparison of stress components and temperature gradient for a silicon nitride cylinder at $\omega^* = 100.0$ (~4 MHz) with $|n| = 5,10$ and 20 at an observation point θ = 0 and z = 100H

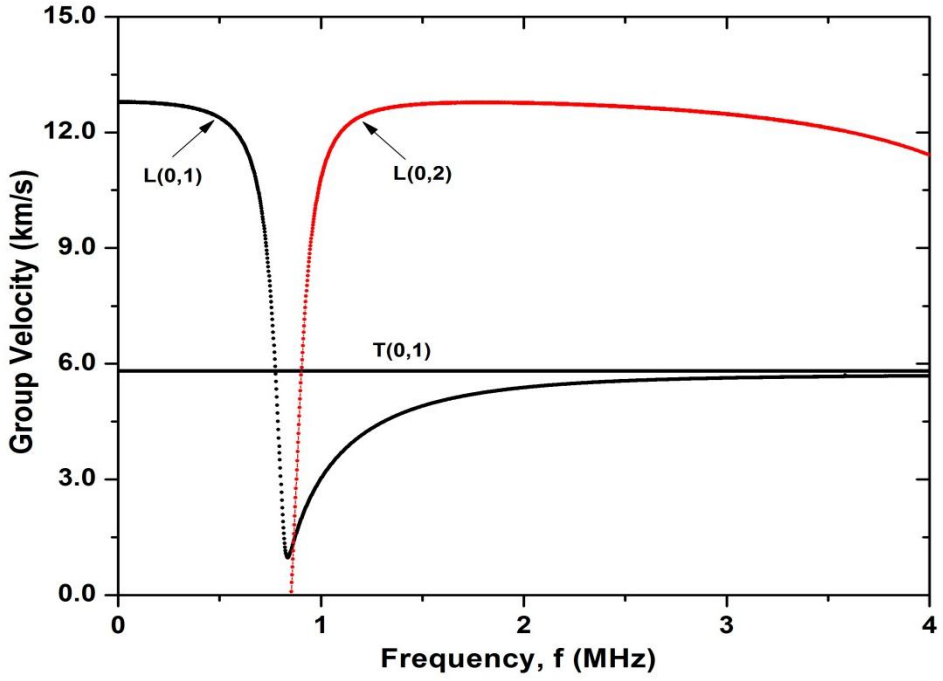

Figure 3.6(a): Group velocity diagram for n = 0

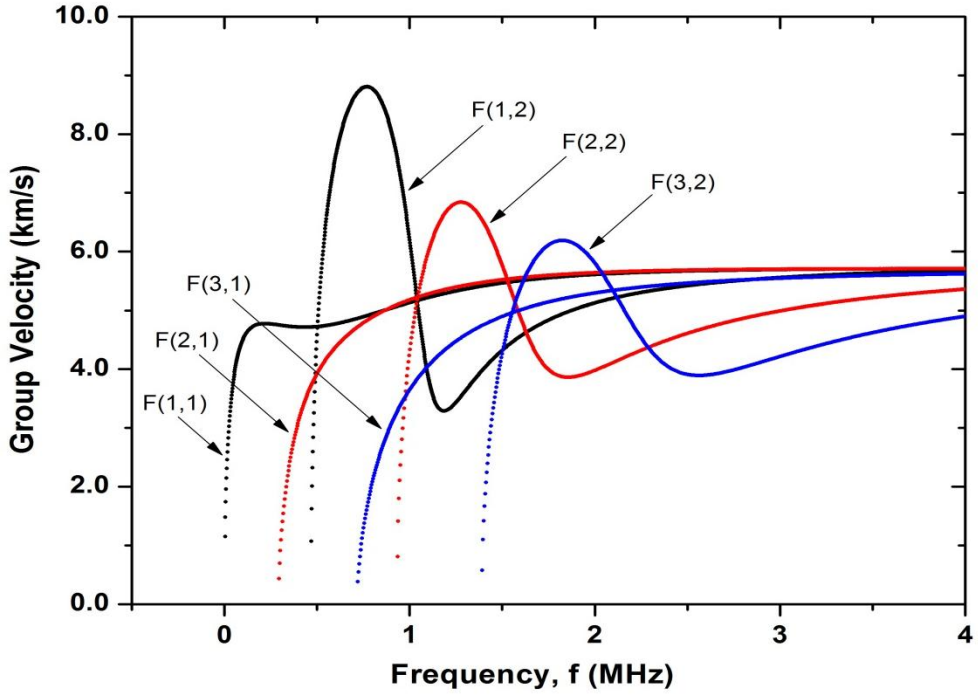

Figure 3.6(b): Group velocity diagram for n = 1, n = 2 and n = 3

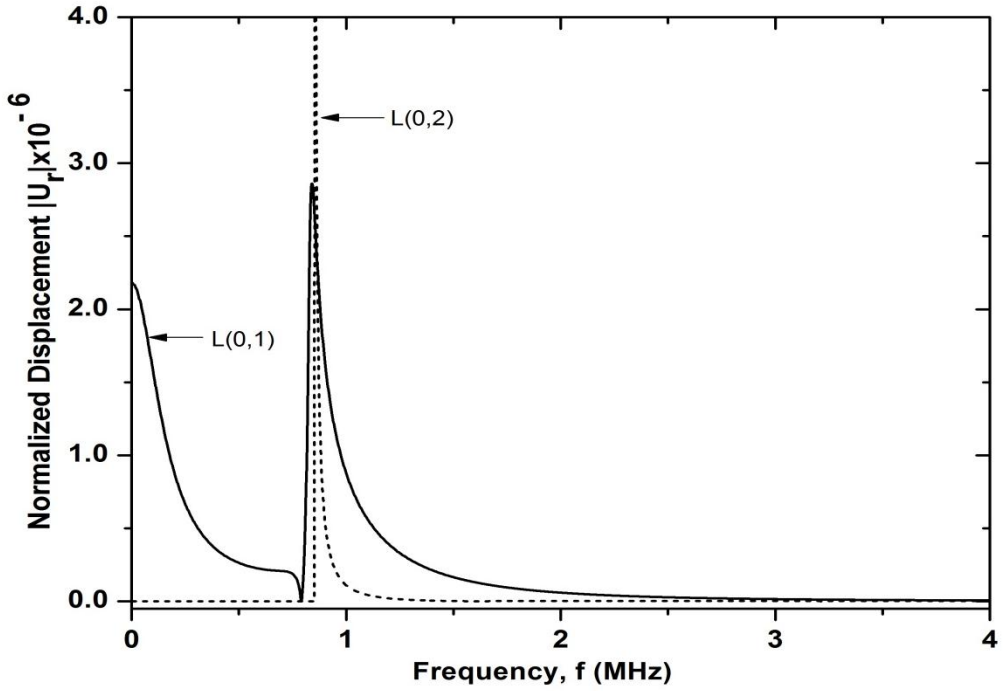

Figure 3.7(a): Frequency displacement response spectra of a silicon nitride cylinder for L(0, 1) and L(0, 2) modes at an observation point, θ = 0 and z = 100H

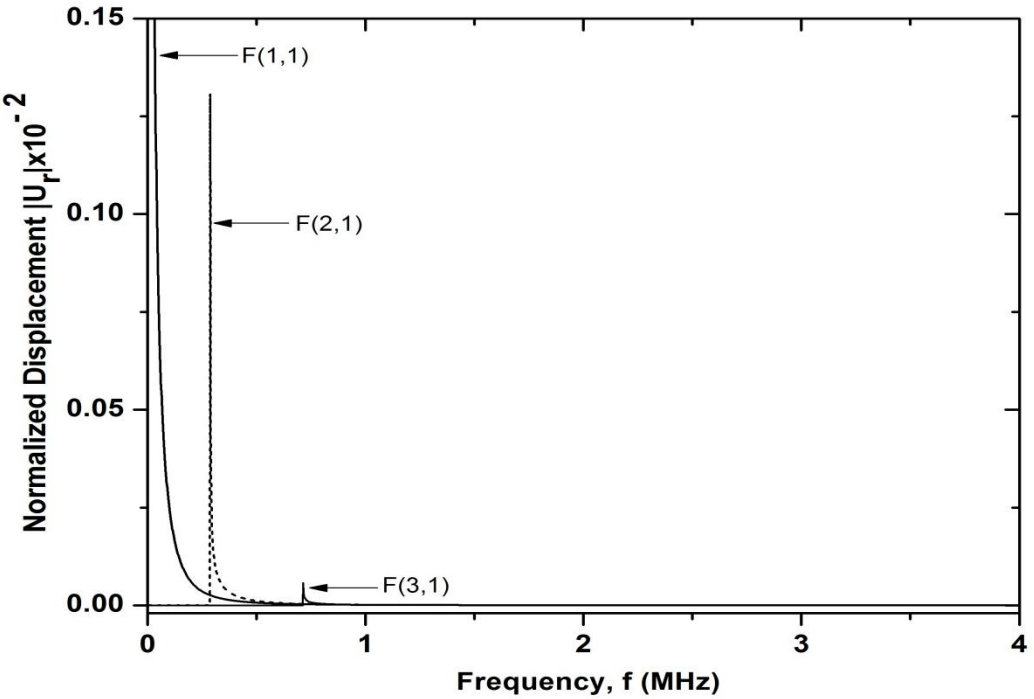

Figure 3.7(b): Frequency displacement response spectra of a silicon nitride cylinder for F(1, 1), F(2,1) and F(3,1) modes at an observation point, θ = 0 and z = 100H

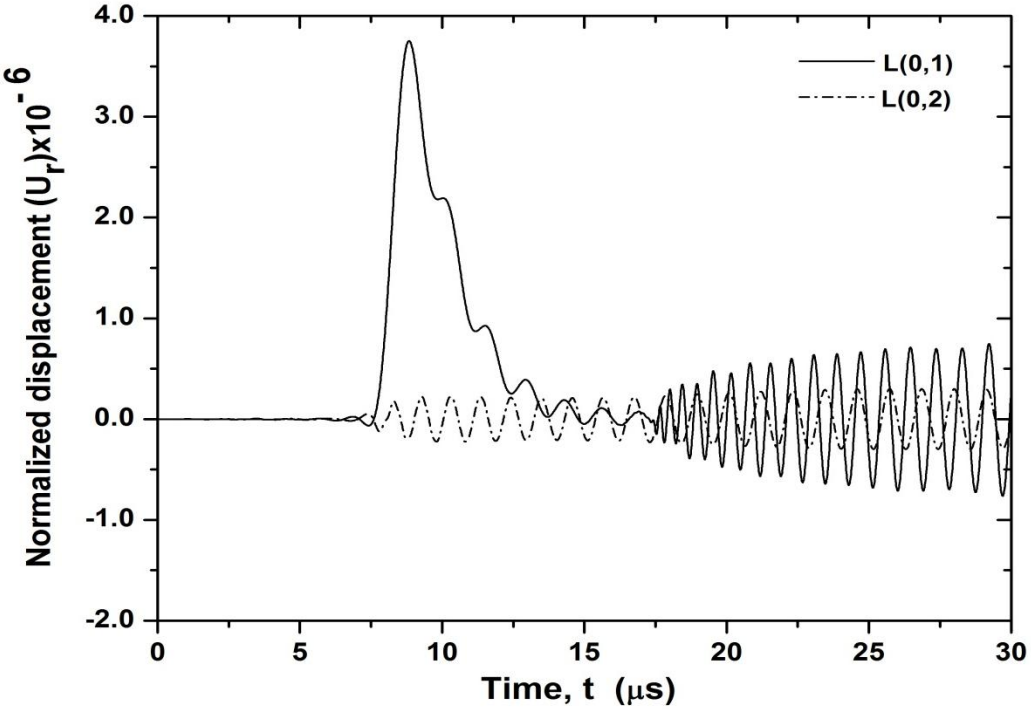

Figure 3.8(a): Displacement response time history of the L(0, 1) and L(0,2) modes at an observation point, θ = 0 and z = 100H

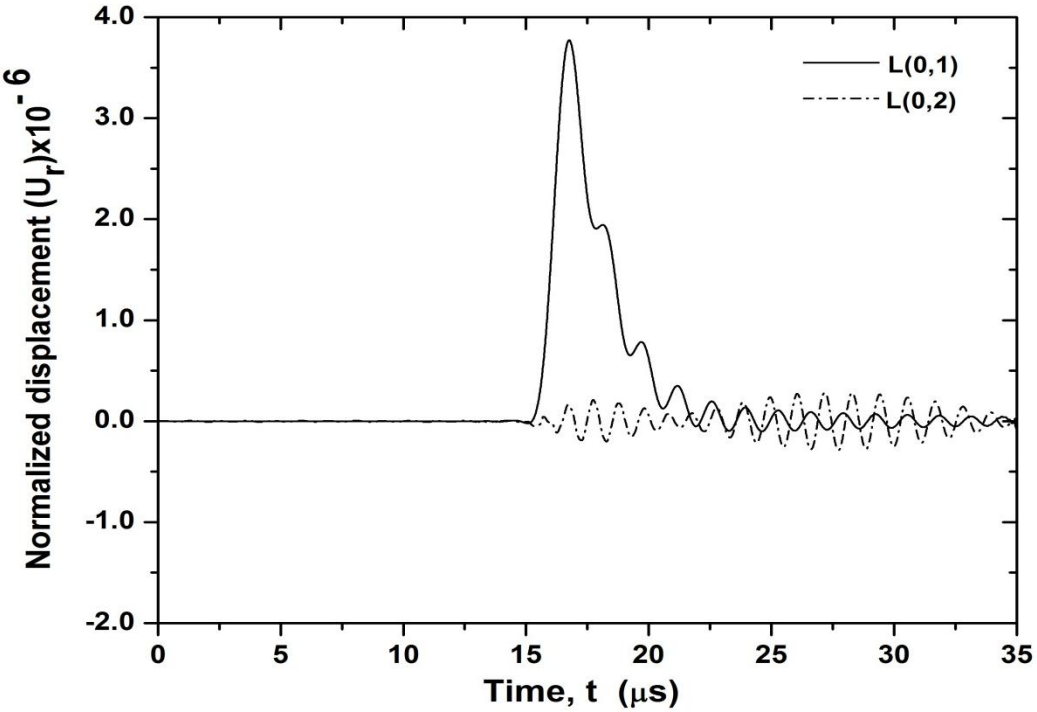

Figure 3.8(b): Displacement response time history of the L(0, 1) and L(0,2) modes at an observation point, θ = 0 and z = 200H

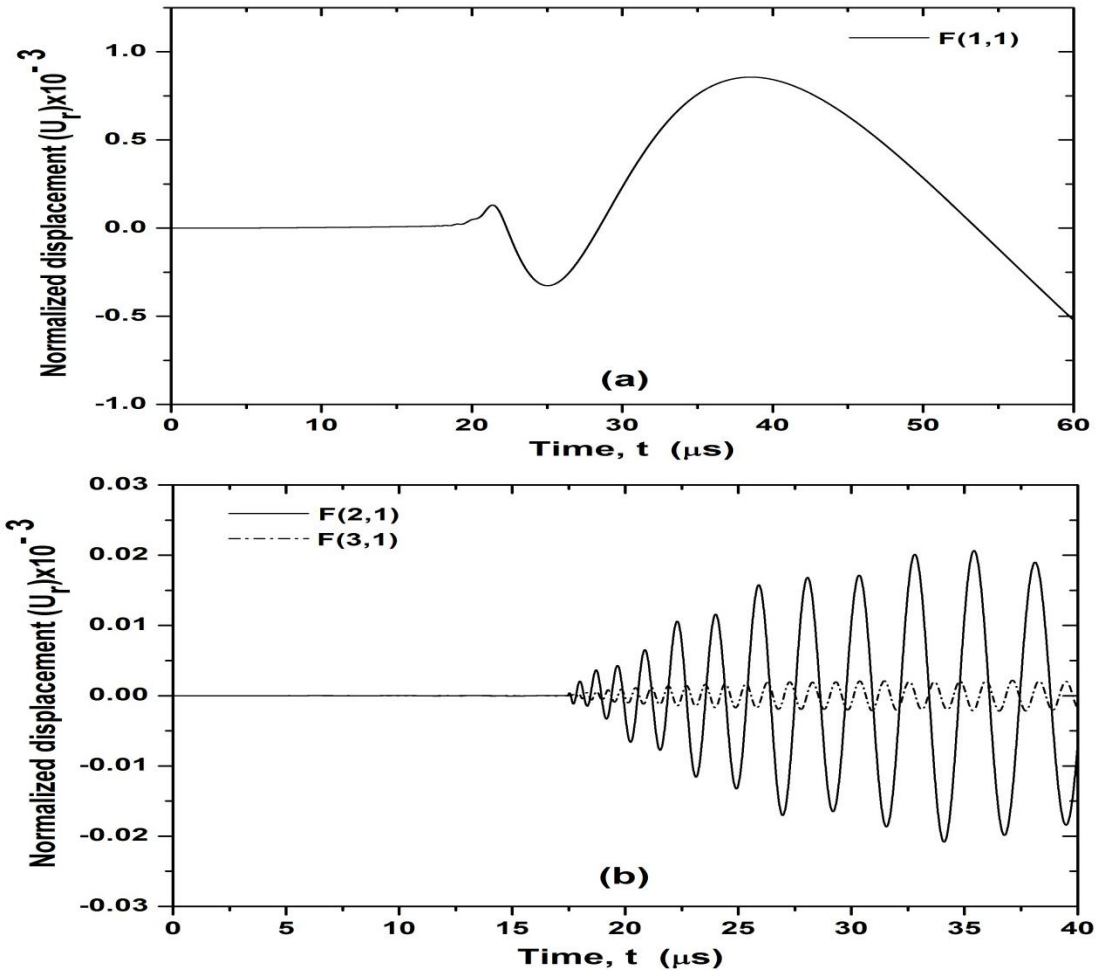

Figure 3.9: (a) Displacement response time history of the F(1, 1) mode; and (b) F(2,1) and F(3,1) modes at an observation point, θ = 0 and z = 100H

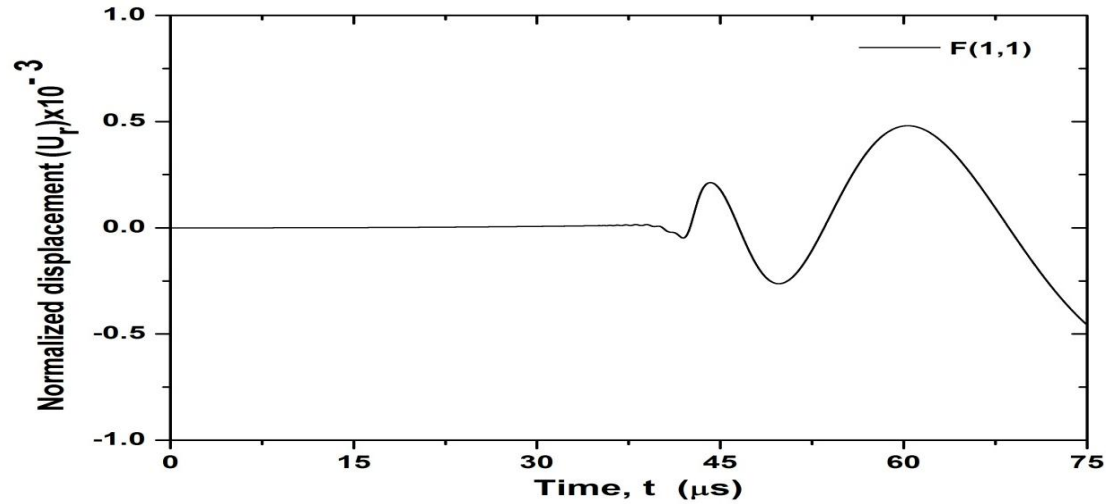

Figure 3.10 (a): Displacement response time history of the F(1, 1) mode at an observation point, θ = 0 and z = 200H

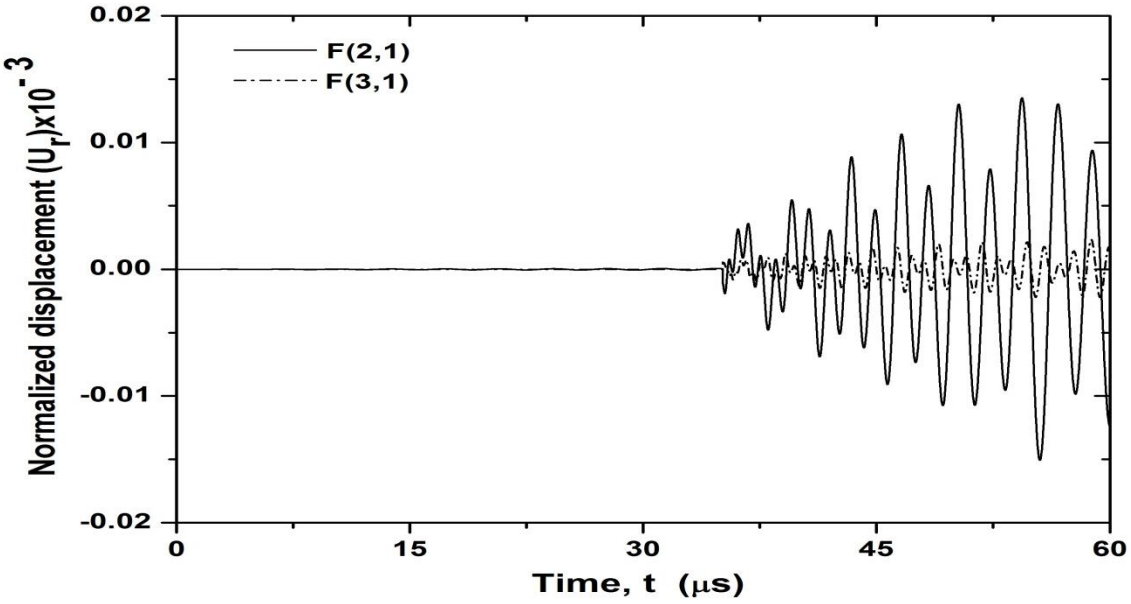

Figure 3.10(b): Displacement response time history of the F(2,1) and F(3,1) modes at an observation point, θ = 0 and z = 200H

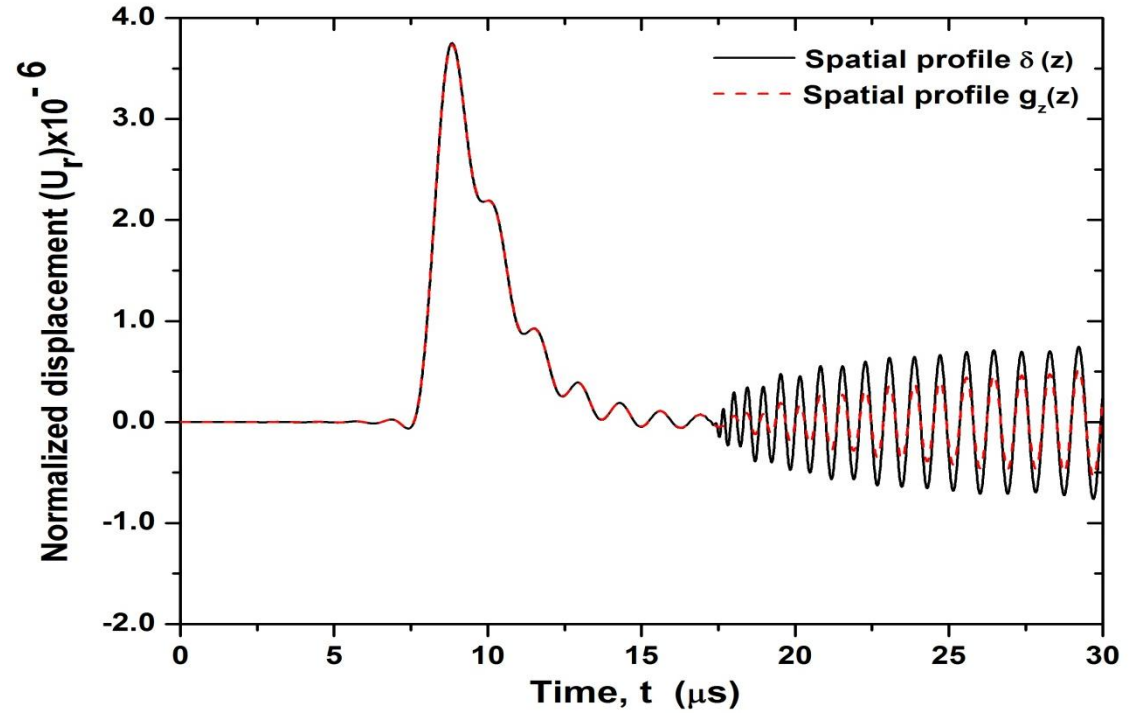

Figure 3.11: Comparison of time history responses due to δ(z) and that due to a Gaussian spatial distribution of $g_z(z)$ for L(0,1) mode at an observation point, θ = 0º and z = 100H

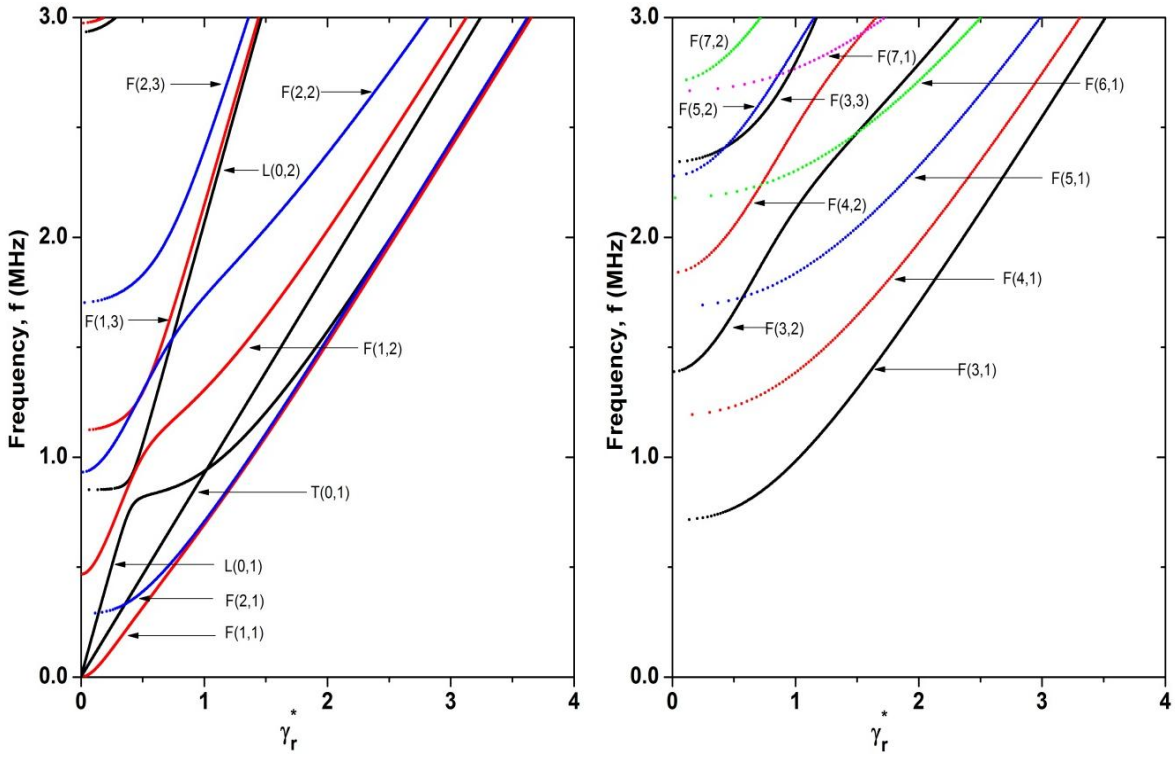

Figure 3.12: Propagating modes within the frequency range 0 to 3 MHz

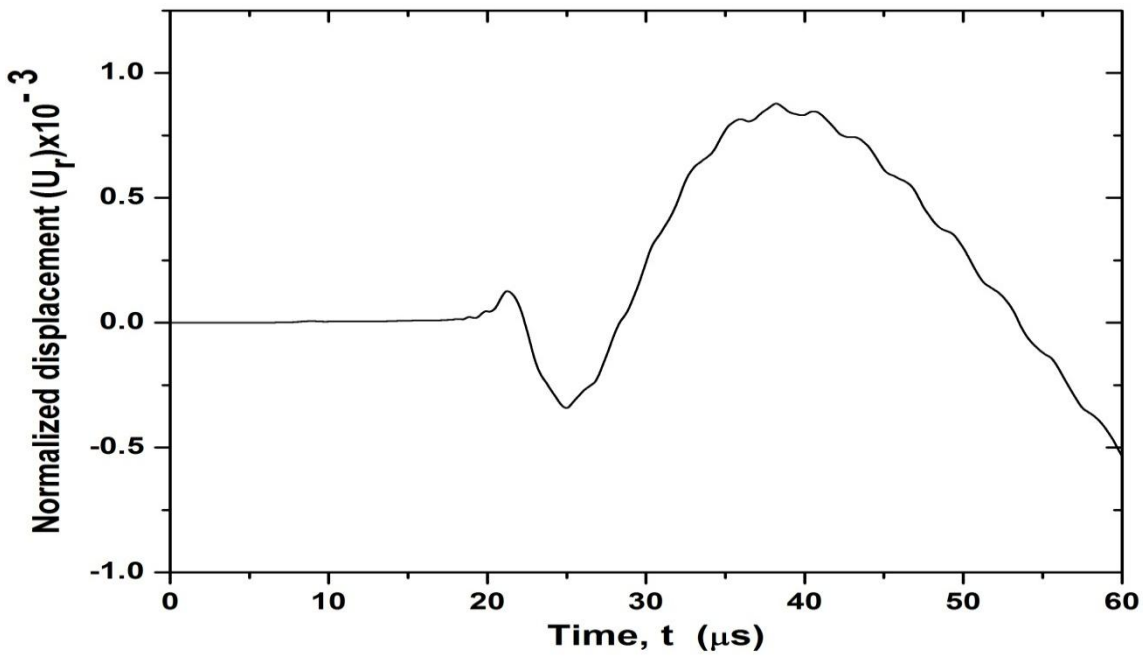

Figure 3.13: Total transient response of the cylinder at an observation point, $\theta = 0^{o}$ and $z = 100H$

Chapter 4

Thermoelastic Waves in Finite Cylinders

4.1 Introduction

Cylindrical shells are frequently used in aerospace, submarine and offshore structures, chemical and gas pipelines, civil engineering structures, and other industrial applications. Therefore, it is important to know their dynamic and vibration characteristics for practical design. Since exact analytical solutions for a finite-length vibrating cylinder cannot be obtained in general, several approximate solutions have been proposed to estimate natural frequencies of finite isotropic circular cylinders by McMahon (1964, 1970), Hutchinson (1972), Gladwell and Tahbildar (1972), and Gladwell and Vijay (1975).

If the material of the cylinder is anisotropic, the solution of the free vibration problem becomes more complex. Lusher and Hardy (1988) used separation of variables technique used by Morse (1954) to study the axisymmetric vibrations of transversely isotropic cylinders and presented experimental results for sapphire rods. Heyliger (1991) estimated natural frequencies of axisymmetric modes of finite length transversely

isotropic cylinders by applying the Ritz method. Chau (1994) and Honarvar et al. (2009) studied axisymmetric and asymmetric vibrations of a finite transversely isotropic cylinder using potential functions and compared their results with the experimental observations of Lusher and Hardy (1988). Chen et al. (1996) studied free vibrations of finite orthotropic thin cylindrical shells by employing shell theory. Liu and Qu (1998) studied analytically the two-dimension problem of guided circumferential waves in a circular annulus.

To our knowledge, propagating and evanescent modes of circumferential waves in a finite transversely isotropic cylinder have not been studied in the past. As mentioned before, finite sized cylinders are common structural components in practical applications. The safety of these structural components must be assessed regularly for their continual usage or for their repair. In order to monitor the health, it is necessary to detect critical cracks or defects. Guided ultrasonic waves have proven to be very efficient for structural health monitoring (SHM). In recent years, laser based ultrasonic techniques for material property measurements and defect characterizations have proven to be very reliable. The coupled theory of thermoelasticity must be used to find complete solutions for the guided waves generated by pulsed lasers.

In this chapter, propagation of thermoelastic waves in a circular annulus and in finite length circular cylindrical shells have been studied in the context of LS (Lord and Shulman, 1967) generalized theory of thermoelasticity. A semi-analytical finite element (SAFE) method is employed to study characteristics of guided wave modes in the cylinder. The dispersion equation governing the modes is obtained in the form of an eigenvalue problem. Solutions obtained by the SAFE formulation are validated by

comparing the numerical results for finite length transversely isotropic elastic cylinders (isothermal case) with those published by Chau (1994) and Honarvar et al. (2009). Results obtained for the (plane strain) circumferential wave propagation problem are shown to agree well with those published by Liu and Qu (1998) for an isotropic (isothermal) case. Numerical results are presented here for both propagating and evanescent modes in a transversely isotropic silicon nitride cylinder.

4.2 Description of the Problem

Consider a finite length transversely isotropic circular cylinder of inner radius r_i and outer radius r_o in the cylindrical coordinate system (r, θ, z) shown in Fig. 4.1. The cylinder is initially in the undisturbed state with uniform temperature T_0. The inner and outer surfaces of the cylinder are traction free and the heat flux vanishes at inner and outer surfaces in the radial direction. The ends of the cylinder are insulated thermally and also constrained by frictionless rigid walls.

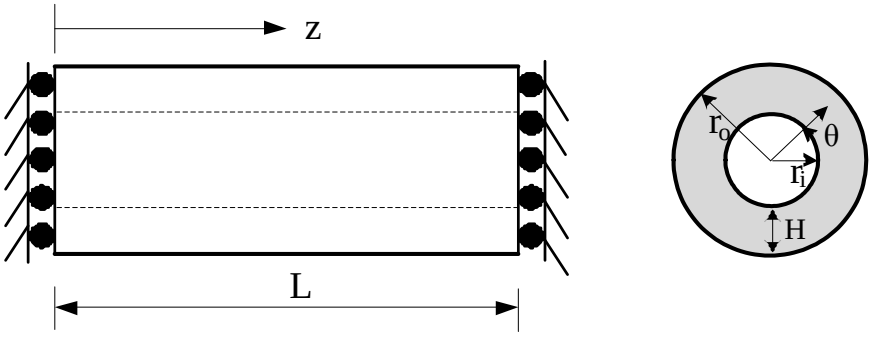

Figure 4.1: Geometry of the cylinder

4.3 Governing Equations

The generalized LS governing equations of thermoelasticity, in the absence of body forces and heat sources, are given by Al-Qahtani and Datta (2004) as,

$$\sigma_{ij,j} = \rho \ddot{u}_i \tag{4.1}$$

$$T_0 \rho \dot{\eta} = -q_{i,i} \tag{4.2}$$

$$\sigma_{ij} = C_{ijkl}\varepsilon_{kl} - \beta_{ij} T \tag{4.3}$$

$$\rho \dot{\eta} = \beta_{ij}\dot{\varepsilon}_{ij} + \frac{\rho c_E}{T_0}\dot{T} \tag{4.4}$$

$$q_i + \tau_0 \dot{q}_i = -k_{ij} T_{,j} \tag{4.5}$$

Various physical quantities and material constants appearing in the above equations are: σ_{ij}, the components of the stress tensor; u_i, the components of the displacement; ε_{ij}, the components of the strain tensor; C_{ijkl}, the elastic constants; q_i, components of the heat flux vector; ρ, the mass density; T_0, the reference temperature; η, the entropy density; T, the temperature change; c_E, the specific heat at constant deformation; τ_0, the thermal relaxation time; β_{ij}, the thermal coefficients; k_{ij}, the coefficients of thermal conductivity. In the above equations, the superposed dot indicates the derivative with respect to time.

Nondimensional quantities used by Al-Qahtani and Datta (2004) and many others are only suitable for the single layer cylinder since equations of motion have a different

form after normalization. A set of normalized quantities is presented here and they are given by

$$
\begin{aligned}
&r_i^* = \frac{r_i}{H}, \quad u_i^* = \frac{u_i}{\delta H}, \quad T^* = \frac{T}{\bar{T}}, \quad t^* = \frac{\bar{v}}{H}t, \\
&\sigma_{ij}^* = \frac{\sigma_{ij}}{\delta \bar{c}}, \quad q_i^* = \frac{q_i}{\bar{q}}, \quad \varepsilon_{ij}^* = \frac{\varepsilon_{ij}}{\delta}, \quad \rho^* = \frac{\rho}{\bar{\rho}}, \quad c_E^* = \frac{c_E}{\bar{c}_E}, \\
&\beta_{ij}^* = \frac{\beta_{ij}}{\bar{\beta}}, \quad k_{ij}^* = \frac{k_{ij}}{\bar{k}}, \quad c_{ijkl}^* = \frac{c_{ijkl}}{\bar{c}}, \quad \tau_0^* = \frac{\bar{v}}{H}\tau_0, \quad T_0^* = \frac{T_0}{\bar{T}}
\end{aligned}
\tag{4.6}
$$

where

$$
\bar{v} = \sqrt{\frac{\bar{c}}{\bar{\rho}}}, \quad \delta = \sqrt{\frac{\bar{k}\bar{T}}{H\bar{v}\bar{c}}}, \quad \bar{q} = \frac{\bar{k}\bar{T}}{H}, \quad \bar{\beta} = \frac{\delta \bar{c}}{\bar{T}}, \quad \bar{c}_E = \frac{\bar{k}}{\bar{\rho}\bar{v}H} \tag{4.7}
$$

In the sequel, two more nondimensional quantities are defined: the angular wave number $k^* = kH$ and frequency $\omega^* = \frac{\omega H}{\bar{v}}$. Here $\bar{\rho}, \bar{k}, \bar{c}, H$ and $\bar{T}$ are the basic normalization quantities and the rest could be derived from them as shown above. Note that, $\bar{\rho}, \bar{k}, \bar{c}$ and $\bar{T}$ can be suitably taken depending upon the material properties of the cylinder. This non-dimensional scheme yields all dimensionless equations in the same form as their dimensional counterparts. Therefore, this normalization could be used to solve multilayer cylinders.

Using equations (4.1) to (4.5), the equations governing coupled thermoelastic deformations can be written as

$$
c_{ijkl}u_{k,lj} - \beta_{ij}T_{,j} = \rho \ddot{u}_i \tag{4.8}
$$

$$(1+\tau_0 \frac{\partial}{\partial t})[T_0 \beta_{ij} \dot{\varepsilon}_{ij} + \rho c_E \dot{T}] = k_{ij} T_{,ij} \tag{4.9}$$

Writing these equations in terms of the nondimensional quantities defined by (4.6), the following are obtained

$$c^*_{ijkl} u^*_{k,lj} - \beta^*_{ij} T^*_{,j} = \rho^* \ddot{u}^*_i \tag{4.10}$$

$$\beta^*_{ij} T^*_0 (1+\tau^*_0 \frac{\partial}{\partial t^*}) \dot{u}^*_{i,j} - k^*_{ij} T^*_{,ij} + \rho^* c^*_E (1+\tau^*_0 \frac{\partial}{\partial t^*}) \dot{T}^* = 0 \tag{4.11}$$

Equations (4.10) and (4.11) have to be solved using some numerical techniques for a generally anisotropic medium. In the following, the SAFE method is used to solve the problem. For convenience, the superscript (*) will be dropped in the sequel.

4.4 Semi-Analytical Finite Element Formulation

In this method, for a finite cylinder of length L, the radial dependence of the displacement $\mathbf{u}$ and temperature T is approximated by one dimensional isoparametric finite elements. The total thickness of the cylinder H is composed of cylindrical layers and each layer can have distinct thermoelastic properties and thickness. By using the SAFE method, thickness of the cylinder is discretized into N laminas. Quadratic interpolation polynomials are used to approximate the displacement and temperature fields over each lamina in the radial direction.

The displacements and temperature of the k^{th} lamina are expressed as

$$\begin{aligned} \mathbf{u}(r,\theta,z,t) &= Z\mathbf{N}_1(\zeta)\mathbf{u}^e(\theta,t) \\ \mathbf{T}(r,\theta,z,t) &= c\mathbf{N}_2(\zeta)\mathbf{T}^e(\theta,t) \end{aligned} \tag{4.12}$$

and

$$r = \mathbf{N}_2(\zeta)\mathbf{R}^e \tag{4.13}$$

Here

$$\mathbf{N}_1(\zeta) = \begin{bmatrix} n_1 & 0 & 0 & n_2 & 0 & 0 & n_3 & 0 & 0 \\ 0 & n_1 & 0 & 0 & n_2 & 0 & 0 & n_3 & 0 \\ 0 & 0 & n_1 & 0 & 0 & n_2 & 0 & 0 & n_3 \end{bmatrix},$$
$$\mathbf{N}_2(\zeta) = \begin{bmatrix} n_1 & n_2 & n_3 \end{bmatrix} \tag{4.14}$$

$$\mathbf{u}^e = \left(u_{r1}, u_{\theta 1}, u_{z1}, u_{r2}, u_{\theta 2}, u_{z2}, u_{r3}, u_{\theta 3}, u_{z3}\right)^T,$$
$$\mathbf{T}^e = \left(T_1, T_2, T_3\right)^T, \tag{4.15}$$
$$\mathbf{R}^e = \left(R_b, R_m, R_f\right)^T$$

and

$$\mathbf{Z} = \begin{bmatrix} c & 0 & 0 \\ 0 & c & 0 \\ 0 & 0 & s \end{bmatrix} \tag{4.16}$$

where $s = \sin(pz)$, $c = \cos(pz)$, $p = \dfrac{m\pi}{L}$ and L is the length of the cylinder and, m is axial wave number.

In equation (4.14), the shape functions are

$$n_1 = \tfrac{1}{2}\zeta(\zeta - 1), \quad n_2 = 1 - \zeta^2, \quad n_3 = \tfrac{1}{2}\zeta(\zeta + 1), \quad -1 \le \zeta \le 1 \tag{4.17}$$

where

$$\zeta = \frac{2r - R_b - R_f}{R_f - R_b} \qquad (R_b \le r \le R_f) \tag{4.18}$$

In equation (4.15), the nodal displacements $u_{rj}, u_{\theta j}, u_{zj}$, and temperature T_j, where j = 1, 2, 3, are taken at the inner surface $\left(r = R_b\right)$, middle layer $\left(r = R_m = \left(R_b + R_f\right)/2\right)$, and the outer surface $\left(r = R_f\right)$ of the k[th] lamina.

The strain tensor and temperature gradient are expressed as

$$\boldsymbol{\varepsilon} = \mathbf{D}_1\mathbf{u}^e + \mathbf{D}_2\mathbf{u}^e_{,\theta} \tag{4.19}$$

$$\mathbf{T}' = \mathbf{B}_1\mathbf{T}^e + \mathbf{B}_2\mathbf{T}^e_{,\theta} \tag{4.20}$$

where

$$\begin{aligned} \mathbf{D}_1 &= c\mathbf{D}_{11} + s\mathbf{D}_{12} \\ \mathbf{D}_2 &= c\mathbf{D}_{21} + s\mathbf{D}_{22} \end{aligned} \tag{4.21}$$

$$\begin{aligned} \mathbf{B}_1 &= c\mathbf{B}_{11} + s\mathbf{B}_{12} \\ \mathbf{B}_2 &= c\mathbf{B}_{21} \end{aligned} \tag{4.22}$$

The stress vector is given by

$$\boldsymbol{\sigma} = \mathbf{C}\left(\mathbf{D}_1\mathbf{u}^e + \mathbf{D}_2\mathbf{u}^e_{,\theta}\right) - s\boldsymbol{\beta}\mathbf{N}_2\mathbf{T}^e \tag{4.23}$$

Matrices $\boldsymbol{\varepsilon}, \boldsymbol{\sigma}, \mathbf{C}, \boldsymbol{\beta}, \mathbf{B}_1, \mathbf{B}_{11}, \mathbf{B}_{12}, \mathbf{B}_2, \mathbf{B}_{21}, \mathbf{D}_1, \mathbf{D}_{11}, \mathbf{D}_{12}, \mathbf{D}_2, \mathbf{D}_{21}$ and $\mathbf{D}_{22}$ are defined in Appendix C. The variational principle of thermoelasticity, Al-Qahtani and Datta (2004), is

$$\int_{t_0}^{t_1}\int_V \left(\delta\boldsymbol{\varepsilon}^T\boldsymbol{\sigma} - \delta\mathbf{T}'^T\mathbf{K}\mathbf{T}' - \delta\mathbf{T}'^T\left(\mathbf{q} + \tau_0\dot{\mathbf{q}}\right)\right)dVdt = \int_{t_0}^{t_1}\int_V \left(-\delta\mathbf{u}^T\rho\ddot{\mathbf{u}}\right)dVdt \tag{4.24}$$

The first term in the left hand side of equation (4.24) is

$$\begin{aligned}\int_{t_0}^{t_1}\int_V \delta\boldsymbol{\varepsilon}^T\boldsymbol{\sigma}dVdt &= \int_{t_0}^{t_1}\int_V \left(\mathbf{D}_1\delta\mathbf{u}^e + \mathbf{D}_2\delta\mathbf{u}^e_{,\theta}\right)^T\left[\mathbf{C}\left(\mathbf{D}_1\mathbf{u}^e + \mathbf{D}_2\mathbf{u}^e_{,\theta}\right) - s\boldsymbol{\beta}\mathbf{N}_2\mathbf{T}^e\right]dVdt \\ &= \int_{t_0}^{t_1}\int_\theta \delta\mathbf{u}^{eT}\left[\mathbf{K}_{11}\mathbf{u}^e + \left(\mathbf{K}_{12} - \mathbf{K}_{21}\right)\mathbf{u}^e_{,\theta} - \mathbf{K}_{22}\mathbf{u}^e_{,\theta\theta} - \mathbf{K}^e_{01}\mathbf{T}^e + \mathbf{K}^e_{02}\mathbf{T}^e_{,\theta}\right]d\theta dt\end{aligned} \tag{4.25}$$

The second term in equation (4.24) is

$$\begin{aligned}\int_{t_0}^{t_1}\int_V \delta\mathbf{T}'^T\mathbf{K}\mathbf{T}'dVdt &= \int_{t_0}^{t_1}\int_V \left(\delta\mathbf{T}^{eT}\mathbf{B}_1^T + \delta\mathbf{T}^{eT}_{,\theta}\mathbf{B}_2^T\right)\mathbf{K}\left(\mathbf{B}_1\mathbf{T}^e + \mathbf{B}_2\mathbf{T}^e_{,\theta}\right)dVdt \\ &= \int_{t_0}^{t_1}\int_\theta \delta\mathbf{T}^{eT}\left(\mathbf{g}_{11}\mathbf{T}^e - \mathbf{g}_{22}\mathbf{T}^e_{,\theta\theta}\right)d\theta dt\end{aligned} \tag{4.26}$$

The third term in equation (4.24) is

$$\begin{aligned}\int_{t_0}^{t_1}\int_V \delta\mathbf{T}'^T\left(\mathbf{q} + \tau_0\dot{\mathbf{q}}\right)dVdt &= -\int_{t_0}^{t_1}\int_V \delta T^T\left(\nabla\cdot\mathbf{q} + \tau_0\nabla\cdot\dot{\mathbf{q}}\right)dVdt \\ &= \int_{t_0}^{t_1}\int_V \delta T\left(T_0\rho\dot{\eta} + \tau_0 T_0\rho\ddot{\eta}\right)dVdt \\ &= \int_{t_0}^{t_1}\int_V \delta T\left[T_0\boldsymbol{\beta}^T\dot{\boldsymbol{\varepsilon}} + \rho c_E\dot{T} + \tau_0\left(T_0\boldsymbol{\beta}^T\ddot{\boldsymbol{\varepsilon}} + \rho c_E\ddot{T}\right)\right]dVdt \\ &= \int_{t_0}^{t_1}\int_\theta \delta\mathbf{T}^{eT}\left[\left(\mathbf{f}_1\dot{\mathbf{u}}^e + \mathbf{f}_2\dot{\mathbf{u}}^e_{,\theta} + \mathbf{m}_0\dot{\mathbf{T}}^e\right) + \tau_0\left(\mathbf{f}_1\ddot{\mathbf{u}}^e + \mathbf{f}_2\ddot{\mathbf{u}}^e_{,\theta} + \mathbf{m}_0\ddot{\mathbf{T}}^e\right)\right]d\theta dt\end{aligned} \tag{4.27}$$

The right hand side of equation (4.24) has the form

$$\int_{t_0}^{t_1}\int_V \delta\mathbf{u}^T\left(-\rho\ddot{\mathbf{u}}\right)dVdt = \int_{t_0}^{t_1}\int_z\int_\theta \delta\mathbf{u}^{eT}\left(-\mathbf{M}\ddot{\mathbf{u}}^e\right)d\theta dzdt \tag{4.28}$$

The element matrices appearing in equations (4.25) to (4.28) are defined in Appendix C.

Equating the coefficients of $\delta\mathbf{u}^e$ in equation (4.24) to zero gives the following equation

$$\mathbf{M}\ddot{\mathbf{u}}^e + \mathbf{K}_{11}\mathbf{u}^e + \left(\mathbf{K}_{12} - \mathbf{K}_{21}\right)\mathbf{u}^e_{,\theta} - \mathbf{K}_{22}\mathbf{u}^e_{,\theta\theta} - \mathbf{K}_{01}\mathbf{T}^e + \mathbf{K}_{02}\mathbf{T}^e_{,\theta} = 0 \tag{4.29}$$

Similarly, equating the coefficients of $\delta\mathbf{T}^e$ in equation (4.24) yields

$$\tau_0\mathbf{f}_1\ddot{\mathbf{u}}^e + \tau_0\mathbf{m}_0\ddot{\mathbf{T}}^e + \tau_0\mathbf{f}_2\ddot{\mathbf{u}}^e_{,\theta} + \mathbf{f}_1\dot{\mathbf{u}}^e + \mathbf{m}_0\dot{\mathbf{T}}^e + \mathbf{f}_2\dot{\mathbf{u}}^e_{,\theta} + \mathbf{g}_{11}\mathbf{T}^e - \mathbf{g}_{22}\mathbf{T}^e_{,\theta\theta} = 0 \tag{4.30}$$

Combining equations (4.29) and (4.30), and assembling the element matrices into global matrices lead to the following governing equations of motion,

$$\mathbf{E}_1\ddot{\mathbf{V}} + \mathbf{E}_2\ddot{\mathbf{V}}_{,\theta} + \mathbf{E}_3\dot{\mathbf{V}} + \mathbf{E}_4\dot{\mathbf{V}}_{,\theta} + \mathbf{E}_5\mathbf{V} + \mathbf{E}_6\mathbf{V}_{,\theta} + \mathbf{E}_7\mathbf{V}_{,\theta\theta} = 0 \tag{4.31}$$

where $\mathbf{E}_i\left(i = 1, 2, ..., 7\right)$ are the global matrices, given in Appendix C, $\mathbf{V}$ is the global nodal displacement and temperature vector

Traction free boundary conditions on surfaces of cylinder require that the stresses at the inner and outer surfaces of the cylinder are zero

$$\sigma_{rr} = \sigma_{r\theta} = \sigma_{rz} = 0 \quad \text{at} \quad r = r_i \text{ and } r = r_o \tag{4.32}$$

End boundary conditions of the cylinder are

$$u_z = \sigma_{rz} = \sigma_{\theta z} = 0 \qquad \text{at} \quad z = 0, L \tag{4.33}$$

Thermal boundary conditions are considered as

$$\begin{aligned} T_{,z} &= 0 \quad \text{at} \quad z = 0, L \\ T_{,r} &= 0 \quad \text{at} \quad r = r_i \text{ and } r = r_o \end{aligned} \tag{4.34}$$

The solution of equation (4.31) is assumed as

$$\mathbf{V} = \mathbf{V}_0 e^{i(n\theta - \omega t)} \tag{4.35}$$

where $\mathbf{V}_0$ is the nodal amplitude vector and ω is the nondimensional circular frequency. For waves propagating in the θ - direction, $e^{in\theta}$ is defined as $e^{in\theta} = e^{i(kr_o)\theta}$, where k is the wave number defined as, $k = \dfrac{\omega}{c(r_o)}$. $c(r)$ is the phase velocity of the circumferential wave travelling along the surface at a distance r.

Substitution of equation (4.35) into equation (4.31) results in a set of linear homogeneous equations

$$\left(-\omega^2\mathbf{E}_1 - \omega^2(in)\mathbf{E}_2 - i\omega\mathbf{E}_3 + \omega n\mathbf{E}_4 + \mathbf{E}_5 + in\mathbf{E}_6 - n^2\mathbf{E}_7\right)\mathbf{V}_0 = 0 \tag{4.36}$$

For integer values of m, two eigenvalue problems can be obtained depending on whether n or ω is chosen as the eigenvalue. If n serves as the eigenvalue with assigned values for ω, equation (4.36) gives a quadratic eigenvalue problem:

$$\left(-n^2\mathbf{E}_7 + n\mathbf{E}_B + \mathbf{E}_A\right)\mathbf{V}_0 = 0 \tag{4.37}$$

where

$$\begin{aligned} \mathbf{E}_A &= -\omega^2\mathbf{E}_1 - i\omega\mathbf{E}_3 + \mathbf{E}_5 \\ \mathbf{E}_B &= -\omega^2(i)\mathbf{E}_2 + \omega\mathbf{E}_4 + i\mathbf{E}_6 \end{aligned} \tag{4.38}$$

Equation (4.38) can be converted into a first order equation in the form

$$\begin{bmatrix} 0 & I \\ \mathbf{E}_A & \mathbf{E}_B \end{bmatrix} \begin{Bmatrix} \mathbf{V}_0 \\ n\mathbf{V}_0 \end{Bmatrix} = n \begin{bmatrix} I & 0 \\ 0 & \mathbf{E}_7 \end{bmatrix} \begin{Bmatrix} \mathbf{V}_0 \\ n\mathbf{V}_0 \end{Bmatrix} \tag{4.39}$$

Solution of the generalized eigenvalue problem (4.39) gives the dispersion relation for guided circumferential thermoelastic waves in the cylinder.

On the other hand, for given integer values of *m* and *n*, equation (4.36) gives the frequencies of free thermoelastic vibration of the shell.

In Appendix D, relevant dispersion equations for the plane strain case are presented.

4.5 Numerical Results and Discussion

In order to validate the SAFE formulation, guided circumferential waves for the isothermal plane strain problem are obtained. Liu and Qu (1998) presented exact analytical solutions for this case. Geometry and material properties of the circular annulus considered by Liu and Qu (1998) are,

$$H = r_o - r_i, \quad \eta_s = \frac{r_i}{r_o}, \quad \nu = 0.2817, \quad c_T = \sqrt{\frac{\mu}{\rho}} = 3200 \text{ m/s}, \quad c_L = \sqrt{\frac{\lambda + 2\mu}{\rho}} = 5660 \text{ m/s}$$

Here, H is the thickness of the annulus; η_s is the shape factor; ν is Poisson's ratio; c_T and c_L are shear and longitudinal wave velocities, respectively. The nondimensional wave number, k^*, and nondimensional frequency, $\Omega\,(=\omega^*)$, are defined as $k^* = kH$ and $\omega^* = \omega H / c_T$, respectively. Figures 4.2(a) and 4.2(b) show the comparison between SAFE results and those obtained by Liu and Qu (1998) for $\eta_s = 0.1$ and 0.5. These figures show excellent agreement between the results obtained here by the SAFE method and those presented by Liu and Qu (1998).

As further validation of the SAFE method, the three dimensional problem of vibration of a finite transversely isotropic cylinder was also considered. Calculated

frequency spectra for axisymmetric (n = 0) and asymmetric (n = 1) modes for a sapphire solid cylinder (isothermal case) are shown in Figs. 4.3(a) and 4.3(b). Also shown in these figures are the results presented by Chau (1994) and Honarvar et al. (2009) using analytical methods. Material properties of the sapphire solid cylinder having radius $r_o = 1.4986\ cm$ and length $L = 2.97815\ cm,$ are (see Chau (1994),

$$c_{11} = 4.968\times10^{11}\ \ N/m^2, \qquad c_{12} = 1.636\times10^{11}\ \ N/m^2, \qquad c_{13} = 1.109\times10^{11}\ \ N/m^2,$$
$$c_{33} = 4.981\times10^{11}\ \ N/m^2, \qquad c_{44} = 1.474\times10^{11}\ \ N/m^2, \qquad \rho = 3986\ \ kg/m^3$$

The corresponding nondimensional quantities are

$$r_o^* = \frac{r_o}{H} = 1.0, \qquad \mathrm{L}^* = \frac{L}{r_o} = 1.987, \qquad \bar{v} = \sqrt{\frac{c_{44}}{\rho}}, \qquad \rho^* = 1.0, \qquad c_{11}^* = \frac{c_{11}}{c_{44}} = 3.3704,$$

$$c_{12}^* = \frac{c_{12}}{c_{44}} = 1.1099, \qquad c_{13}^* = \frac{c_{13}}{c_{44}} = 0.7523, \qquad c_{33}^* = \frac{c_{33}}{c_{44}} = 3.3792, \qquad c_{44}^* = \frac{c_{44}}{c_{44}} = 1.0$$

Figures 4.3(a) and 4.3(b) show excellent agreement between the results presented in this study and those obtained earlier by Chau (1994) and Honarvar et al. (1999). They confirm the validity of the SAFE formulation employed in this chapter. In the following, thermoelastic waves in a circular annulus and in a finite cylindrical tube are discussed.

A cylindrical tube with thickness 1 mm and inner radius 1.5 mm is considered. Thus, the nondimensional inner and outer radii are, $r_i = 1.5$ and $r_o = 2.5,$ respectively. The material of the tube is taken to be transversely isotropic silicon nitride (Si_3N_4), whose properties are listed in Table 2.1 (see Al-Qahtani and Datta, 2004). The symmetry axis of the material is aligned with the axis of the cylinder.

For the purpose of nondimensionalization, normalizing velocity $\bar{v}$ is chosen to be 0.25 km/s. Furthermore, the normalized density ρ^* is taken to be 1. Then, the nondimensional material properties of the tube are given by

$$T_0^* = 1.0, \quad \tau_0^* = 1.081\times10^{-7}, \quad \beta_{rr}^* = \beta_{\theta\theta}^* = 70.03, \quad \beta_{zz}^* = 83.21$$

$$k_{rr}^* = k_{\theta\theta}^* = 0.0785, \quad k_{zz}^* = 0.10, \quad c_E^* = 967.50, \quad c_{11}^* = \frac{c_{11}}{\bar{c}} = 2165,$$

$$c_{12}^* = \frac{c_{12}}{\bar{c}} = 975, \quad c_{13}^* = \frac{c_{13}}{\bar{c}} = 635, \quad c_{33}^* = \frac{c_{33}}{\bar{c}} = 2870, \quad c_{44}^* = \frac{c_{44}}{\bar{c}} = 540$$

The plain strain problem of circumferential guided waves is considered first. For a fixed real Ω the wavenumbers k^* $(=\eta_R^* + i\eta_I^*)$ are calculated and presented graphically in Fig. 4.4(a). Figure 4.4 (b) shows group velocities, respectively, of the circumferential propagating modes at the outer surface. From Fig. 4.4 (b), it is noticed that, the first propagating elastic mode tends asymptotically to a straight line at high frequencies with a group velocity 5.75km/s, indicating that it becomes non-dispersive. It is also observed that the influence of temperature change on circumferential propagating modes is negligible. The second mode has a low cutoff frequency $\Omega = 21.40$ and travels much faster than the first mode at low frequencies. Note that it reaches the first plateau at the velocity 6.37 km/s and both modes approach the Rayleigh wave velocity 5.40km/s at high frequencies.

A finite cylindrical tube of length 15 mm with inner and outer radii of 1.5 mm and 2.5 mm, respectively, is considered here. Thus, the nondimensional length is 15 and, nondimensional inner and outer radii are, respectively, $r_i = 1.5$ and $r_o = 2.5$. As mentioned previously, equation (4.39) yields dispersion curves for thermoelastic waves in

a cylinder of finite length. The curves (see Figs. 4.5 (a), 4.6 (a), and 4.7 (a)) for mode numbers (m = 1, 2, 3) in the *z* direction are obtained by keeping ω^* $(=\Omega)$ real and angular wave number k^* $(=\eta_R^* + i\eta_I^*)$ complex. Group velocities of the circumferential waves when m = 1, 2, 3, are computed at the outer surface of the cylinder and shown in Figs. 4.5(b), 4.6(b) and 4.7(b), respectively. From these curves it is observed that first two modes are almost non-dispersive at high frequencies and approach the Rayleigh wave velocity. It is found that elastic modes are not much affected by the thermal effects within the frequency range considered here. Thermal modes are found to have very high attenuation when compared with elastic modes. Higher order thermal modes originate with high imaginary values of the wave number when $\omega^* = 0$. It is also found that the higher order thermal modes approach the first thermal mode as the frequency increases. This is evident from Table 4.1.

Natural frequencies of the finite cylinder depend on the geometry ratio $(L^* = L/H)$ and the material properties of the cylinder. To study the dependence of ω on geometry ratio, frequencies are obtained as functions of L^* from 0 to 150 and presented graphically. The frequency spectra for axisymmetric modes (n = 0) with the first three longitudinal modes (m = 1, 2, 3) are shown in Figs. 4.8, 4.9 and 4.10, respectively. Also, frequencies for the first asymmetric modes (n = 1) with three flexural modes (m = 1, 2, 3) are presented in Figs. 4.11, 4.12 and 4.13, respectively. In Figs 4.9 to 4.14, thickness of the cylinder *H* = 1 mm is fixed with a varying value of *L*. For n = 0, the longitudinal and torsional modes are uncoupled and it is evidenced by the intersection of the torsional modes with that of the longitudinal modes which are shown in Figs. 4.8 to 4.10. From

Figs. 4.8 to 4.13 and Table 4.2, it was observed that the lowest frequency is not an axisymmetric type for all geometry ratios $\left(L^*\right)$ of the cylinder.

Natural frequencies for the first axisymmetric (n = 0) and asymmetric (n = 1) modes with axial mode number (m = 1) are also obtained for a composite cylinder which are shown in Figs. 4.14 and 4.15, respectively. The inner and outer layers of the composite cylinder are zinc and silicon nitride, respectively. Both layers of the cylinder are bonded perfectly with each other and the thickness of each layer is 1 mm. The inner radius of the cylinder is 1.5 mm. The length of the composite cylinder is 15 mm and the material properties of silicon nitride and Zinc are listed in Table 2.1.

4.6 Concluding Remarks

The natural frequencies of vibration of finite length cylinders and circumferential waves in such cylinders have been studied in the context of the L-S generalized theory of thermoelasticity. The proposed SAFE formulation is validated by comparing predicted numerical results with those obtained in earlier investigations by Chau (1994), Honarvar et al. (2009) and Liu and Qu (1998). Frequency spectra obtained for the first three longitudinal and circumferential modes (m, n = 1, 2, 3) for a silicon nitride cylinder are also presented here. Frequency spectra with n = 0 and n = 1 show that the lowest frequency corresponds to first asymmetric mode for all L/H ratios of the cylinder. Thermal modes have much higher attenuation than the elastic modes and the influence of thermal effects on elastic modes is not significant. Circumferential guided waves for a plane strain case for silicon nitride cylinder are also presented in this chapter. It is found that first mode is non-dispersive at high frequencies. The guided waves studied in this

chapter can be used for detecting cracks predominantly in the axial direction in finite cylinders. The semi-analytical finite element (SAFE) method that has been used here can also be used to calculate dispersion relations for other isotropic and transversely isotropic cylinders with and without a thermal coupling effect.

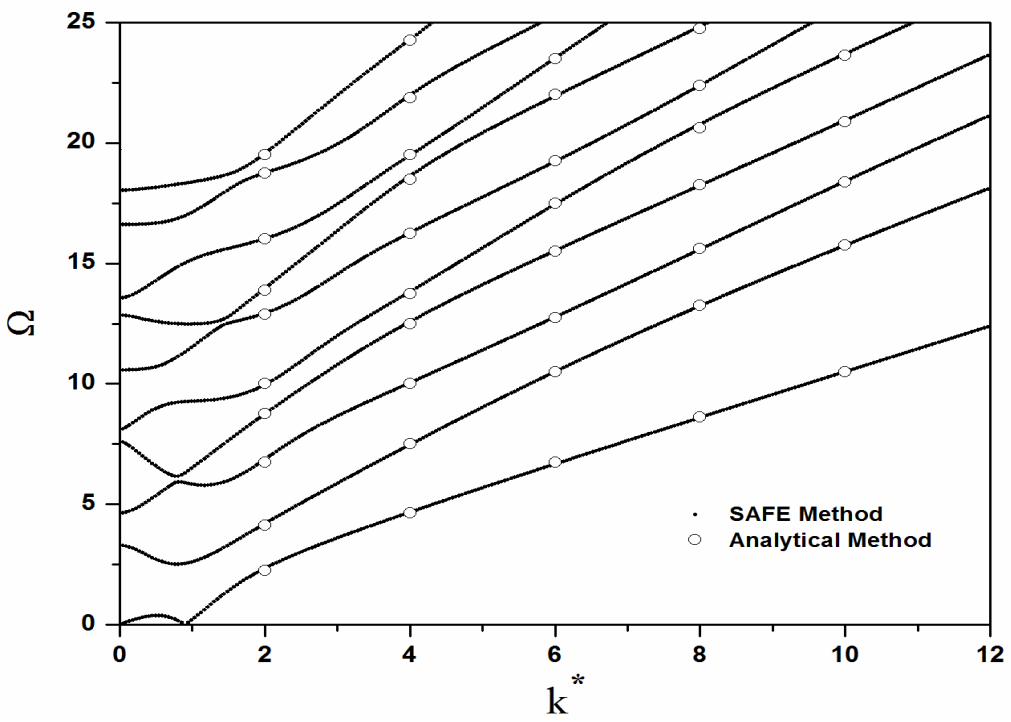

Fig. 4.2(a): 2D view of propagating modes for η_s = 0.1 (Liu and Qu, 1998, fig. 2(a))

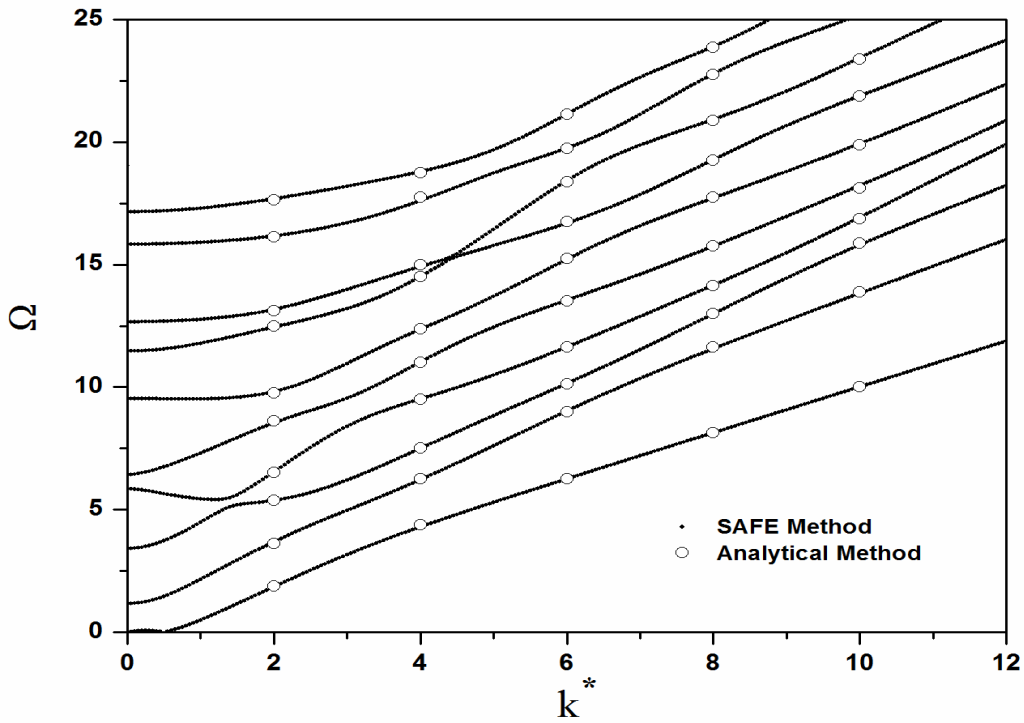

Fig. 4.2(b): 2D view of propagating modes for η_s = 0.5 (Liu and Qu, 1998, fig. 2(b))

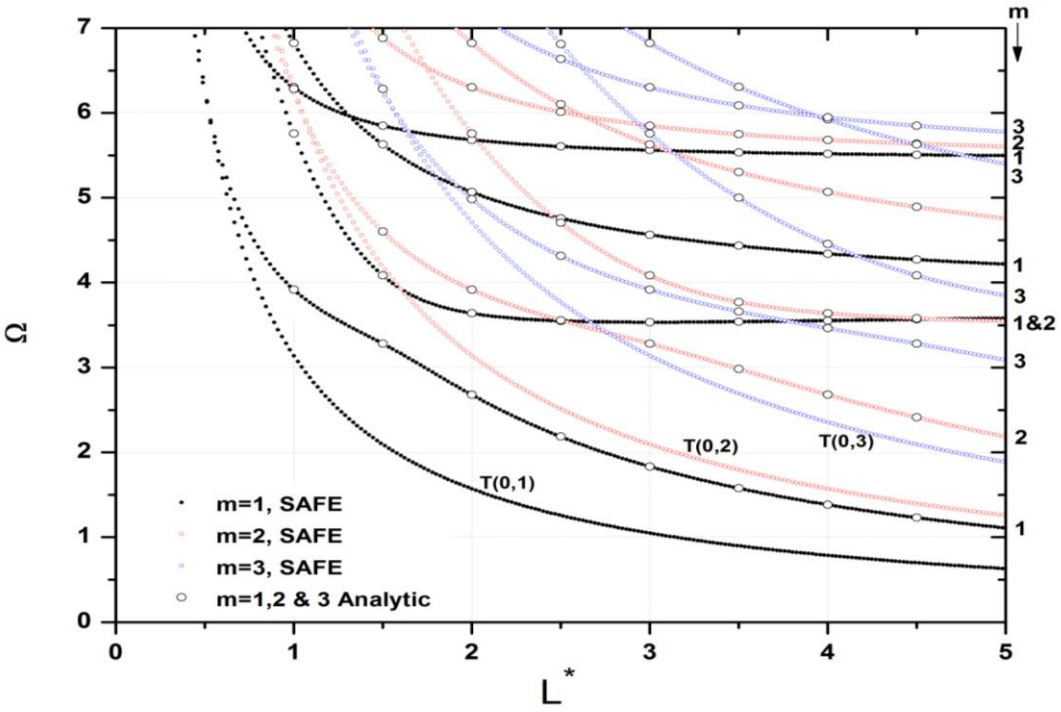

Figure 4.3(a): Frequency spectrum of a sapphire cylinder for n = 0 and m = 1, 2, 3 (Chau, 1994, fig. 1 and Honarvar et al. 2009, fig. 2)

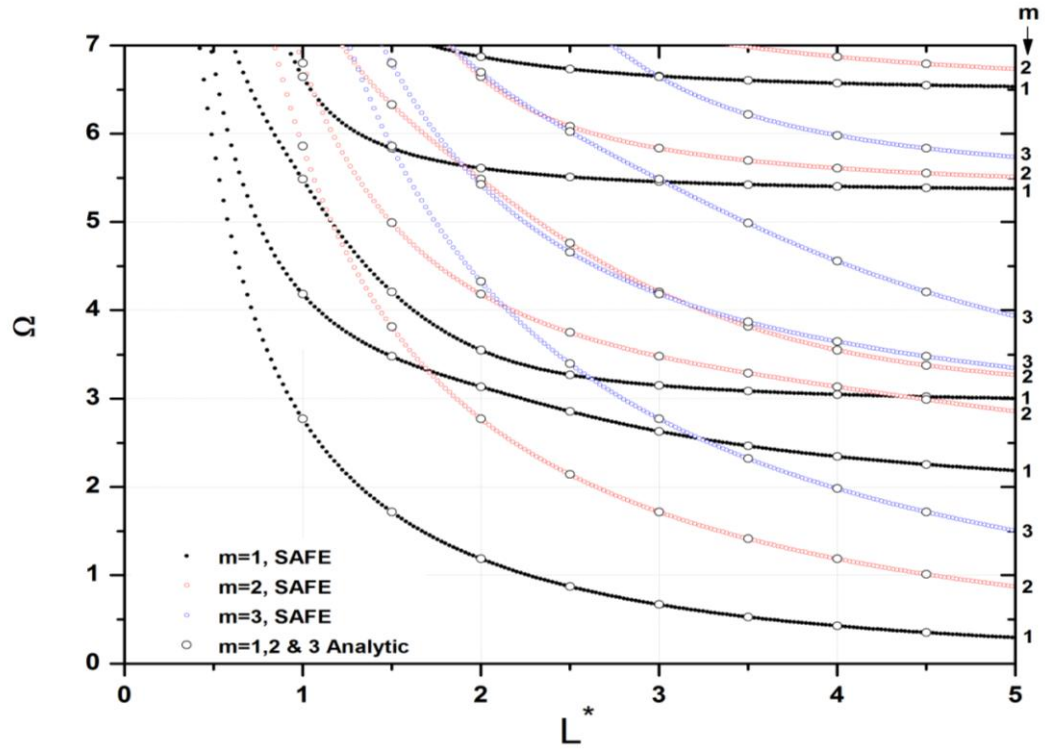

Figure 4.3(b): Frequency spectrum of a sapphire cylinder for n = 1 and for m = 1, 2, 3 (Chau, 1994, fig. 2 and Honarvar et al. 2009, fig. 3)

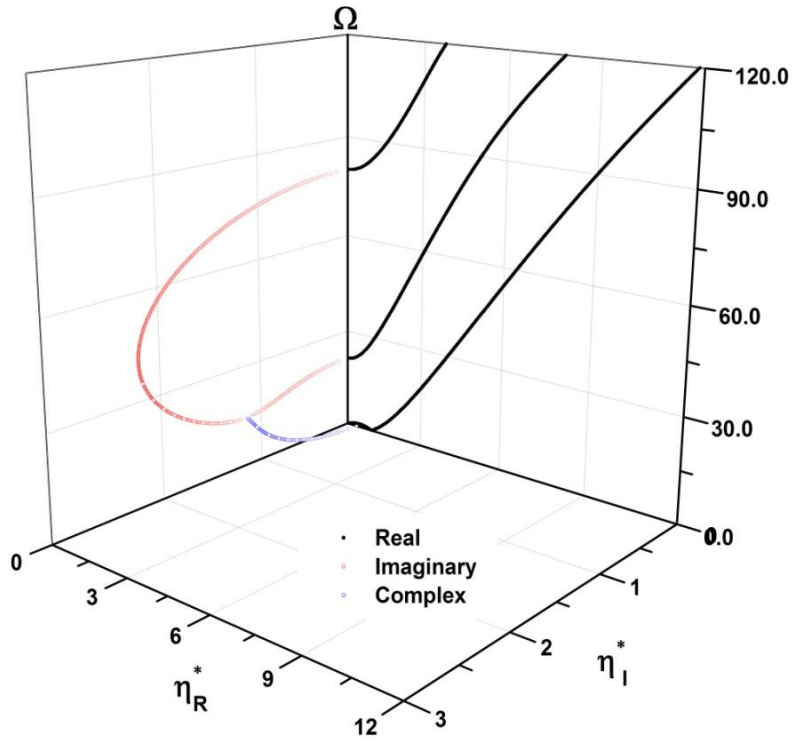

Figure 4.4(a): 3D view of frequency – circumferential wave number plots for the silicon nitride cylinder for plane strain problem

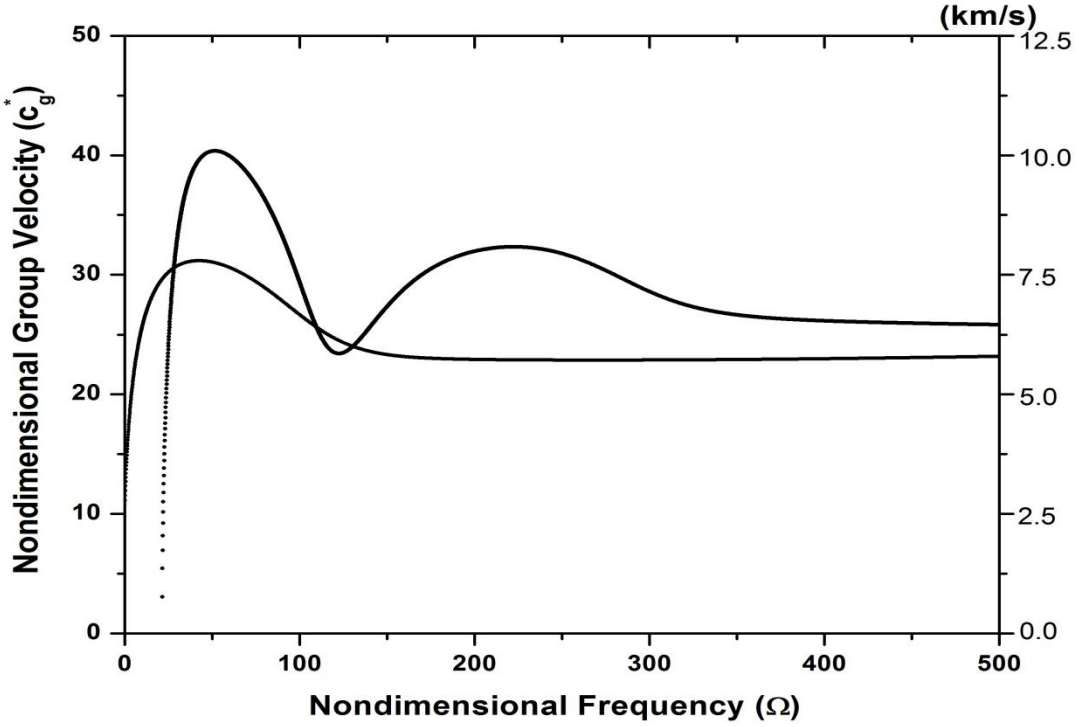

Figure 4.4 (b): Group velocity of a silicon nitride cylinder for plane strain problem

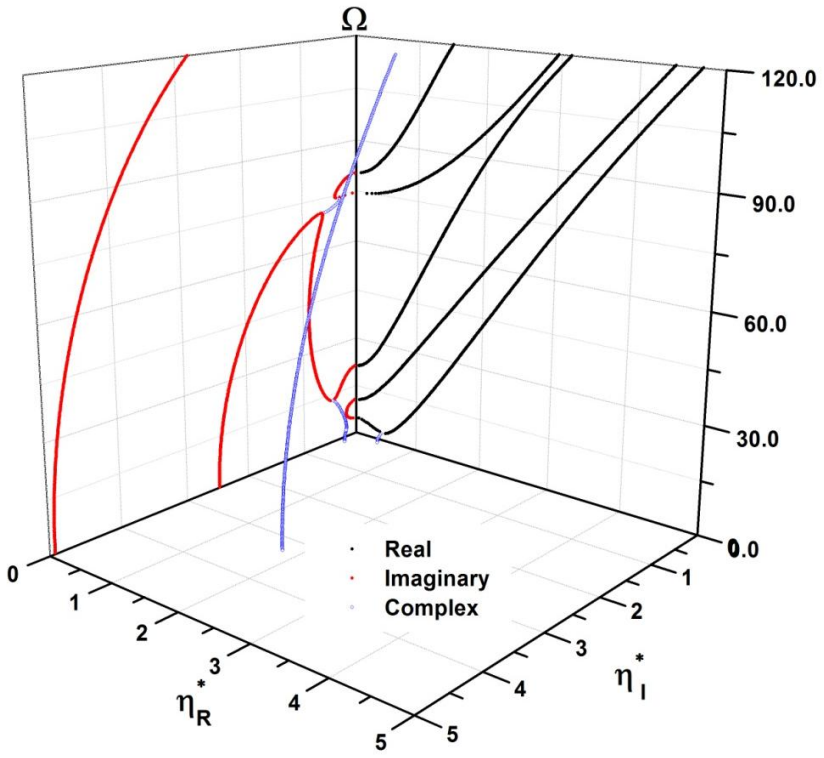

Figure 4.5(a): 3D view of frequency – circumferential wave number plots for the silicon nitride cylinder when axial wave number, m = 1

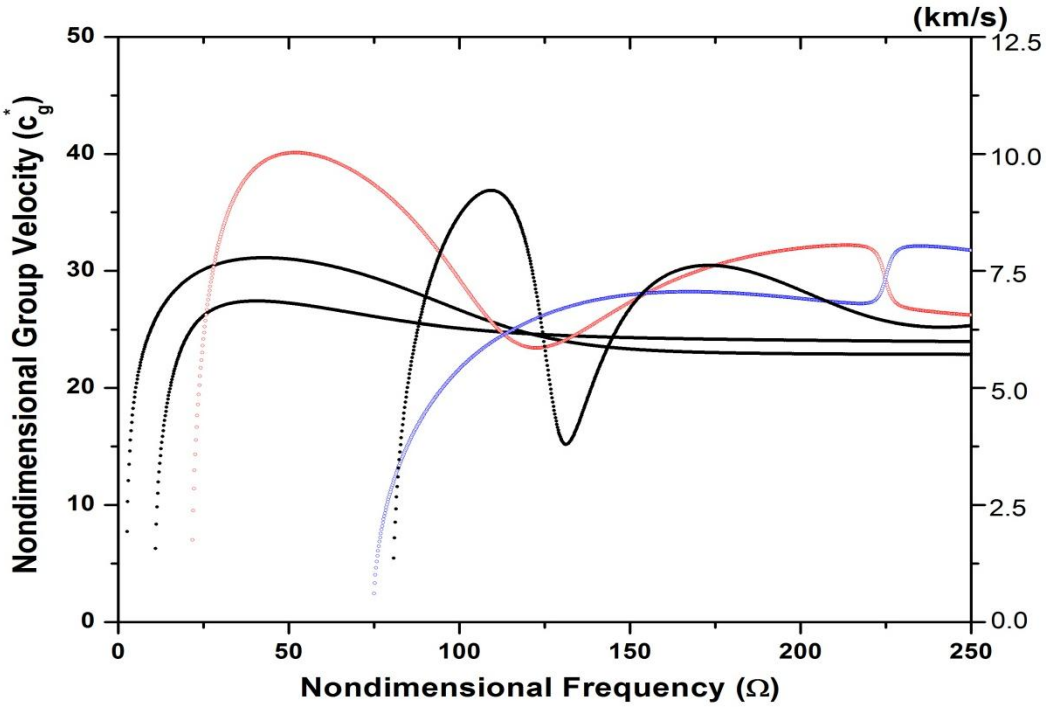

Figure 4.5(b): Group velocity of circumferential propagating waves of the silicon nitride cylinder when axial wave number, m = 1

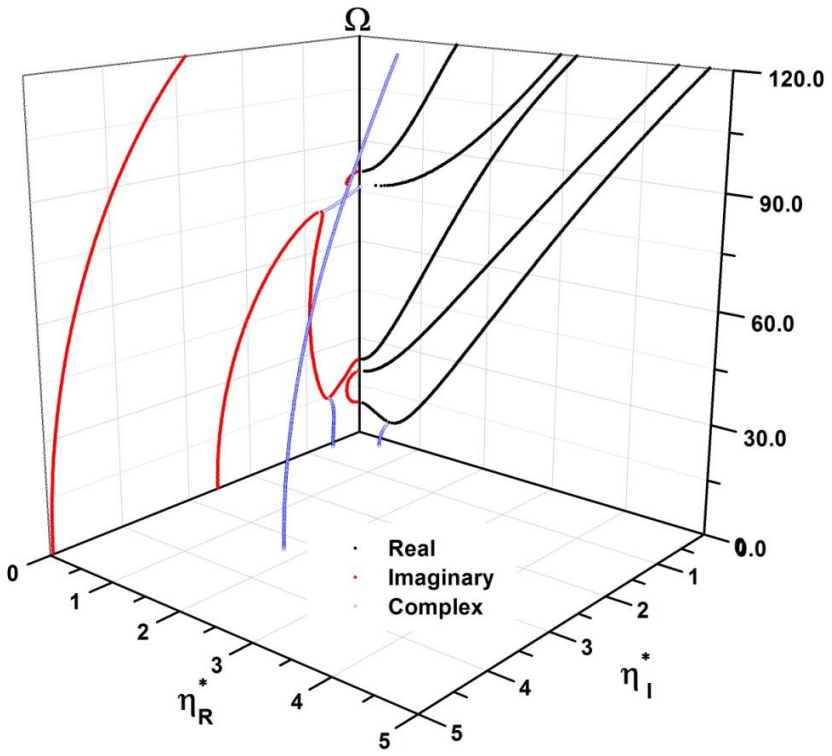

Figure 4.6(a): 3D view of frequency – circumferential wave number plots for the silicon nitride cylinder when axial wave number, m = 2

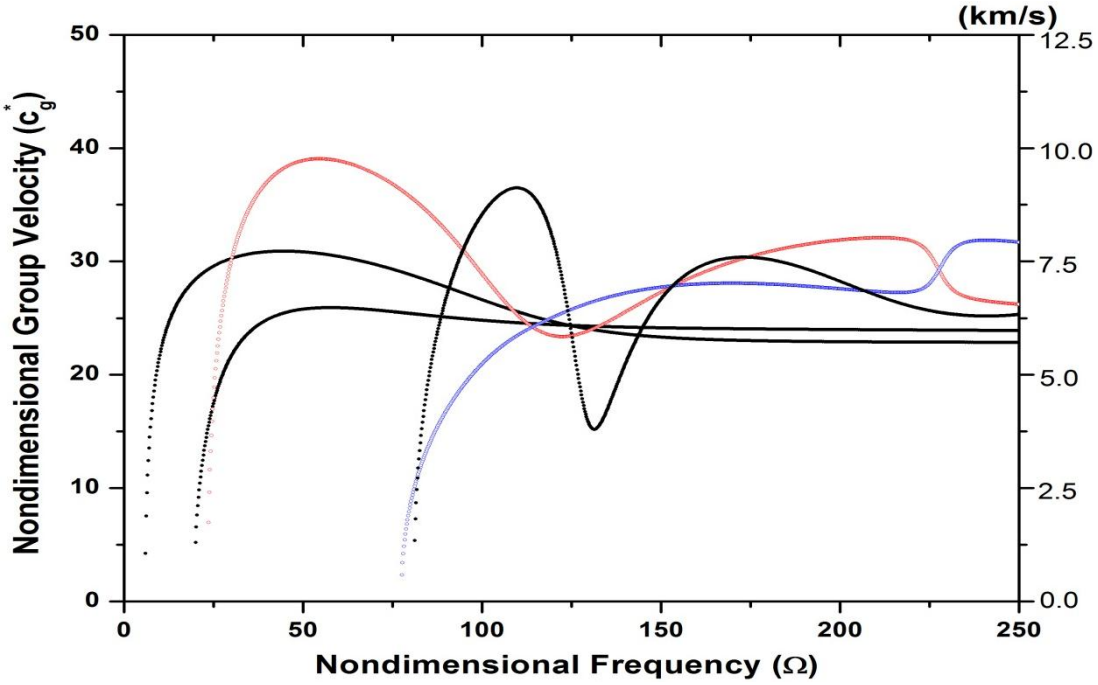

Figure 4.6(b): Group velocity of circumferential propagating waves of the silicon nitride cylinder when axial wave number, m = 2

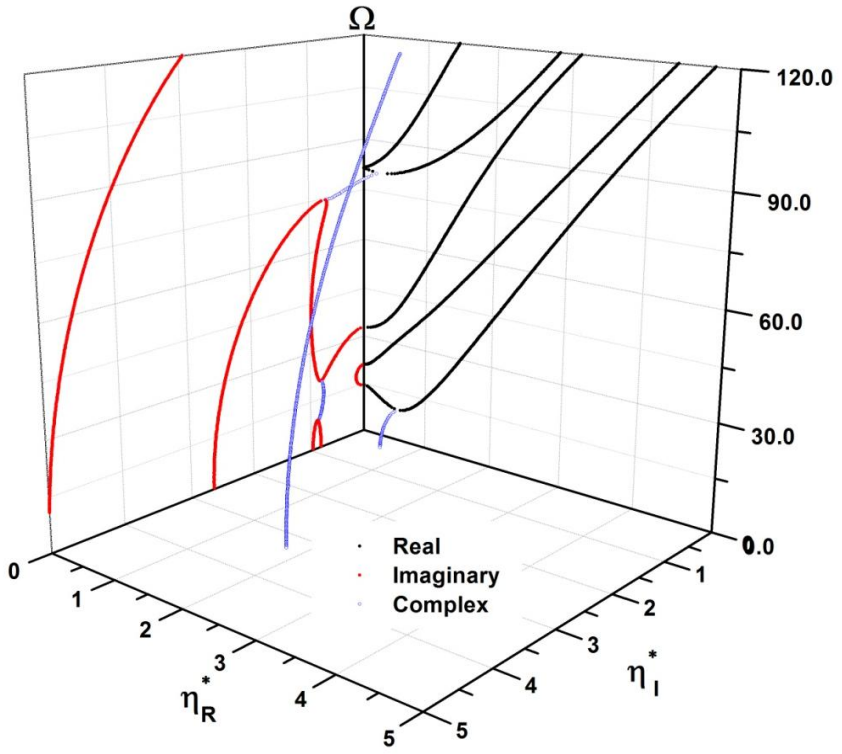

Figure 4.7(a): 3D view of frequency – circumferential wave number plots for the silicon nitride cylinder when axial wave number, m = 3

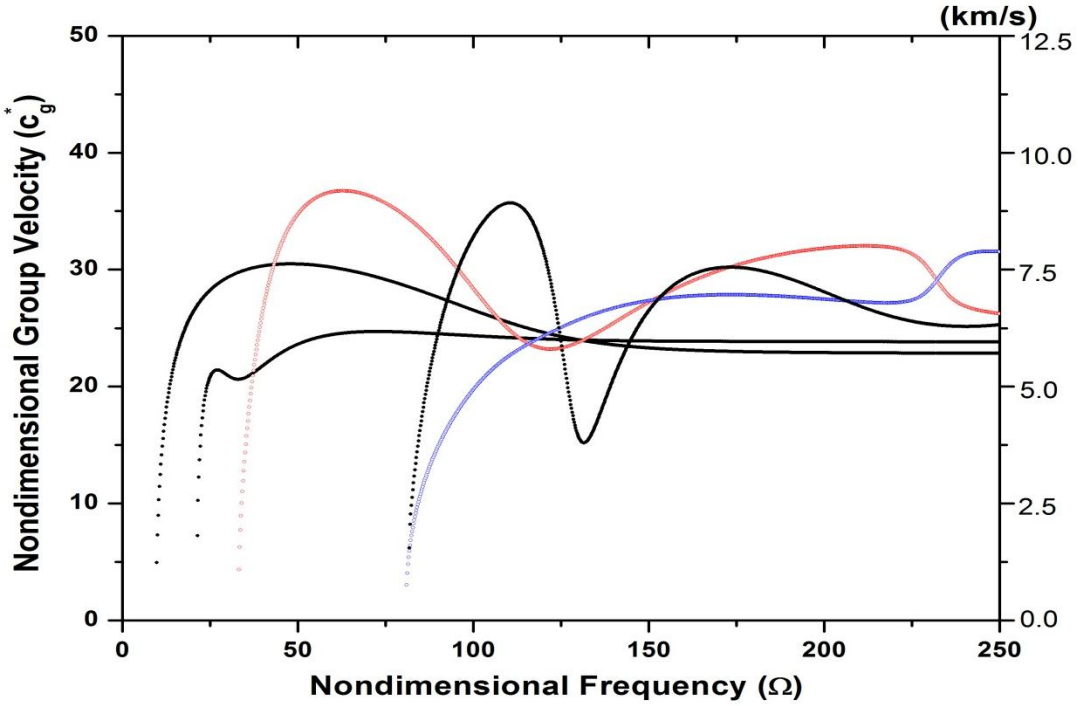

Figure 4.7(b): Group velocity of circumferential propagating waves of the silicon nitride cylinder when axial wave number, m = 3

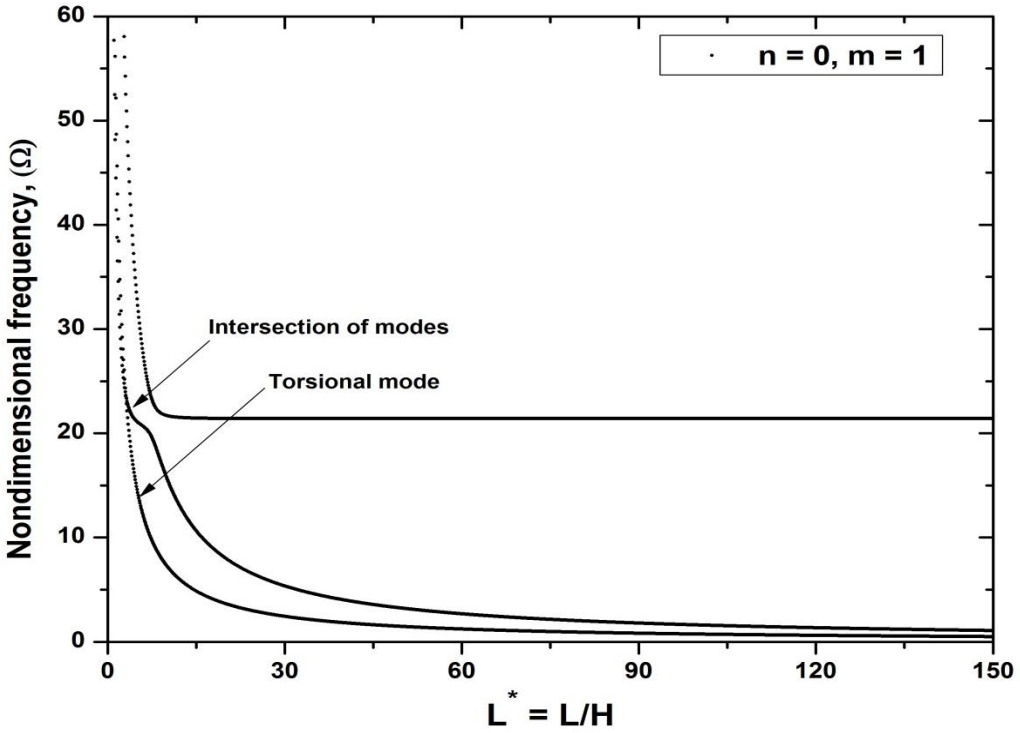

Figure 4.8: Frequency spectrum of the silicon nitride cylinder when n = 0 and m = 1

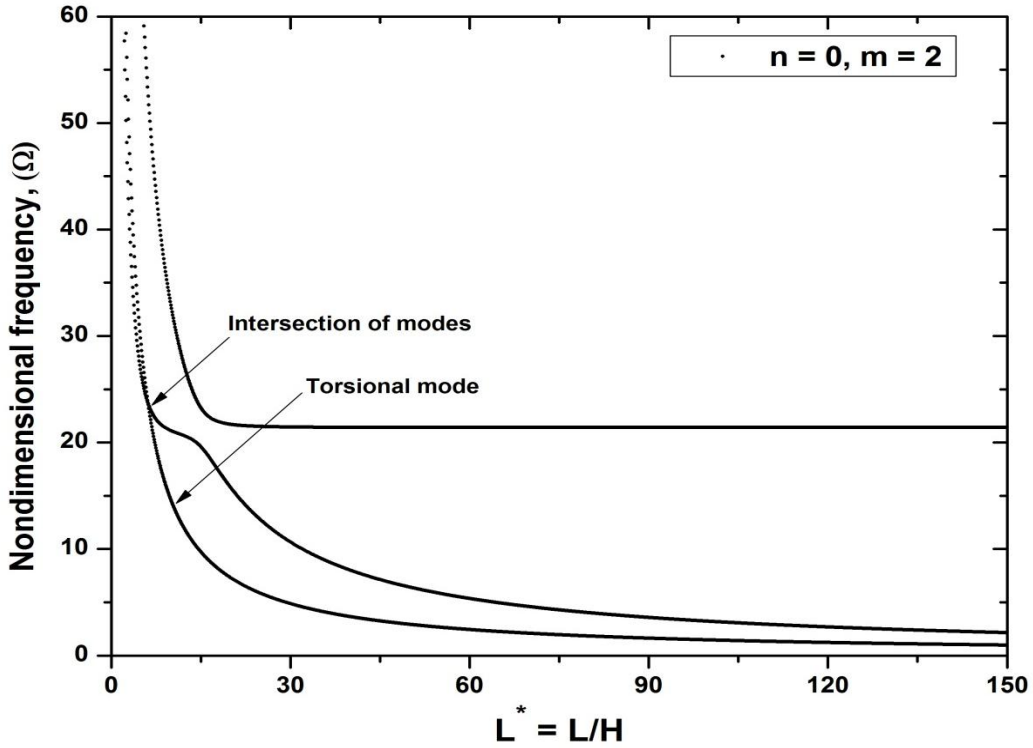

Figure 4.9: Frequency spectrum of the silicon nitride cylinder when n = 0 and m = 2

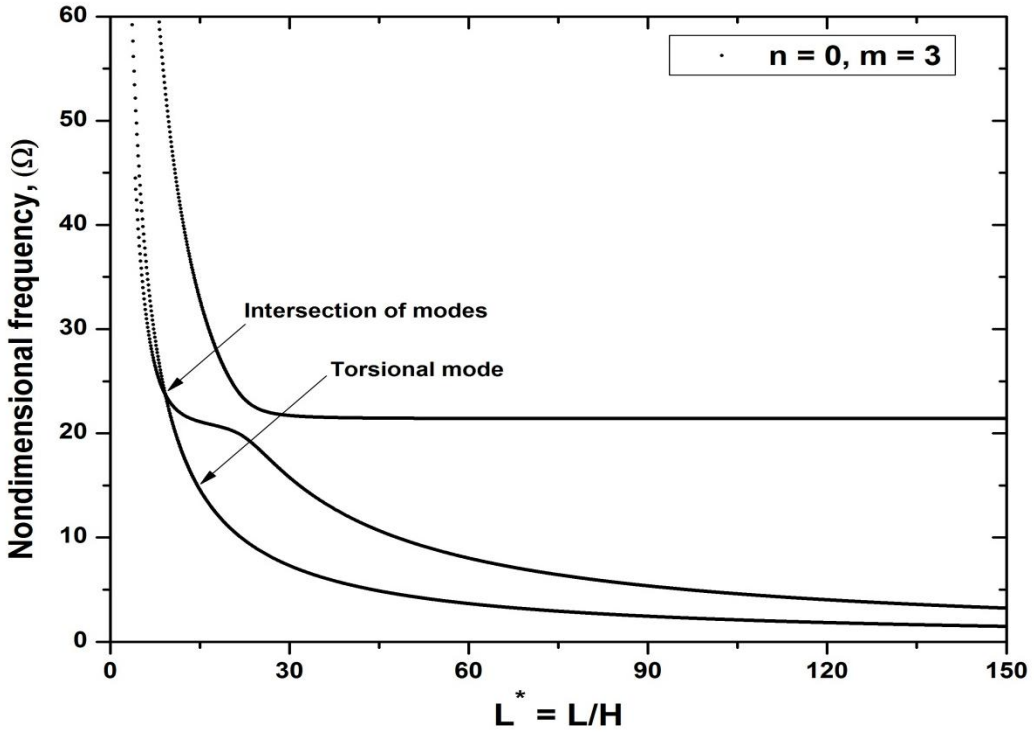

Figure 4.10: Frequency spectrum of the silicon nitride cylinder when n = 0 and m = 3

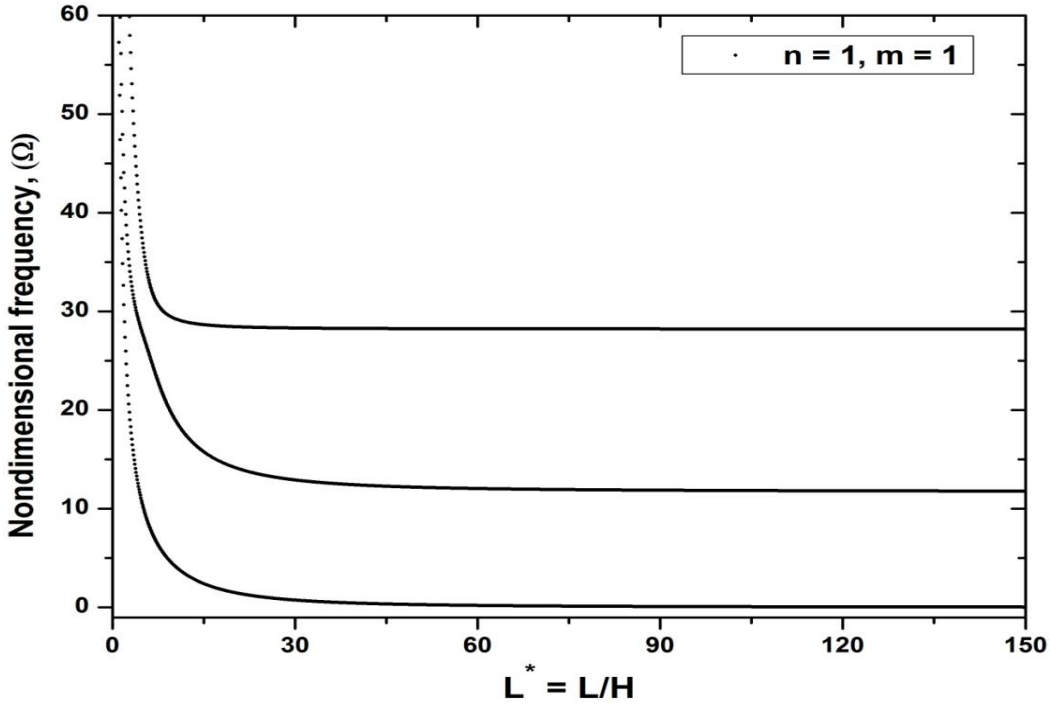

Figure 11: Frequency spectrum of the silicon nitride cylinder when n = 1 and m = 1

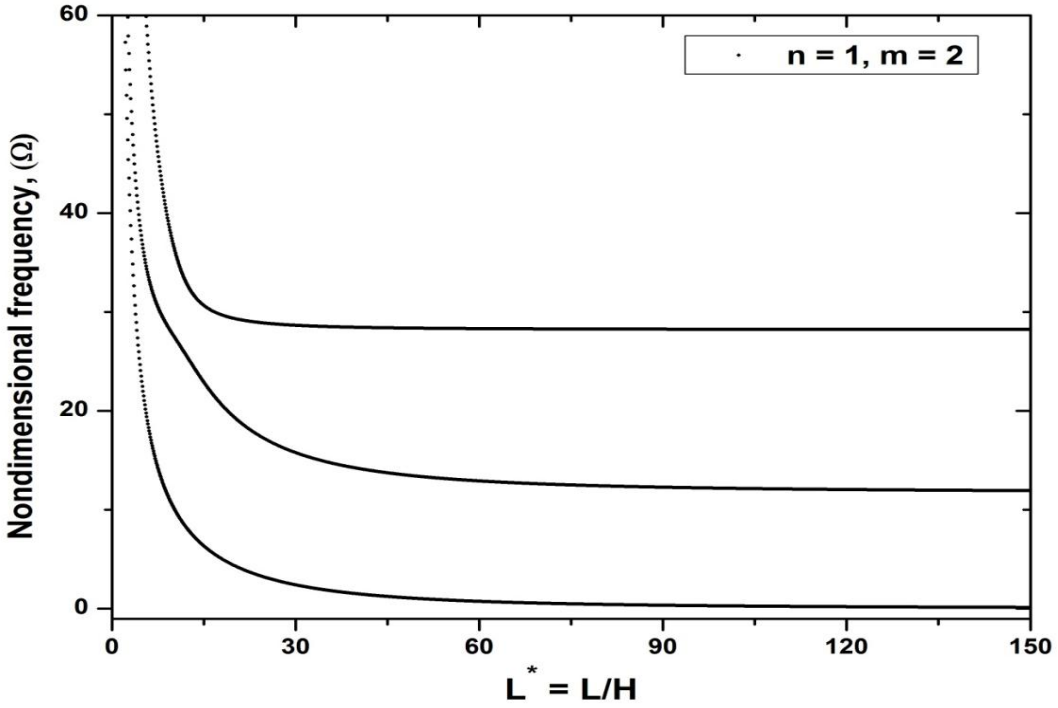

Figure 12: Frequency spectrum of the silicon nitride cylinder when n = 1 and m = 2

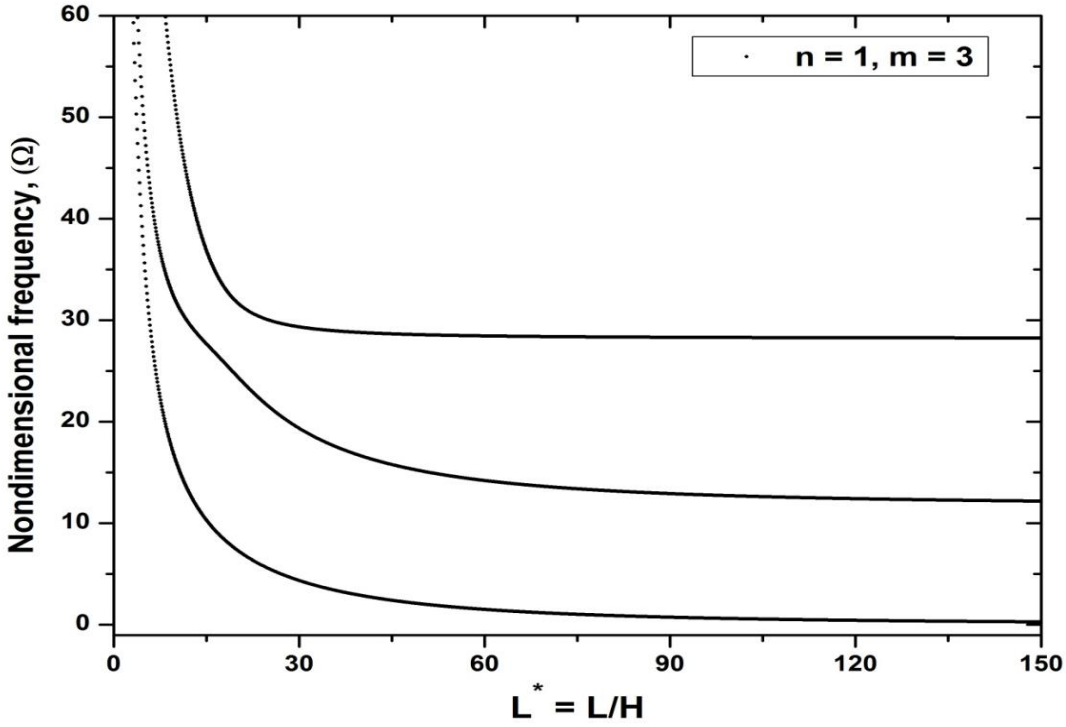

Figure 13: frequency spectrum of the silicon nitride cylinder when n = 1 and m = 3

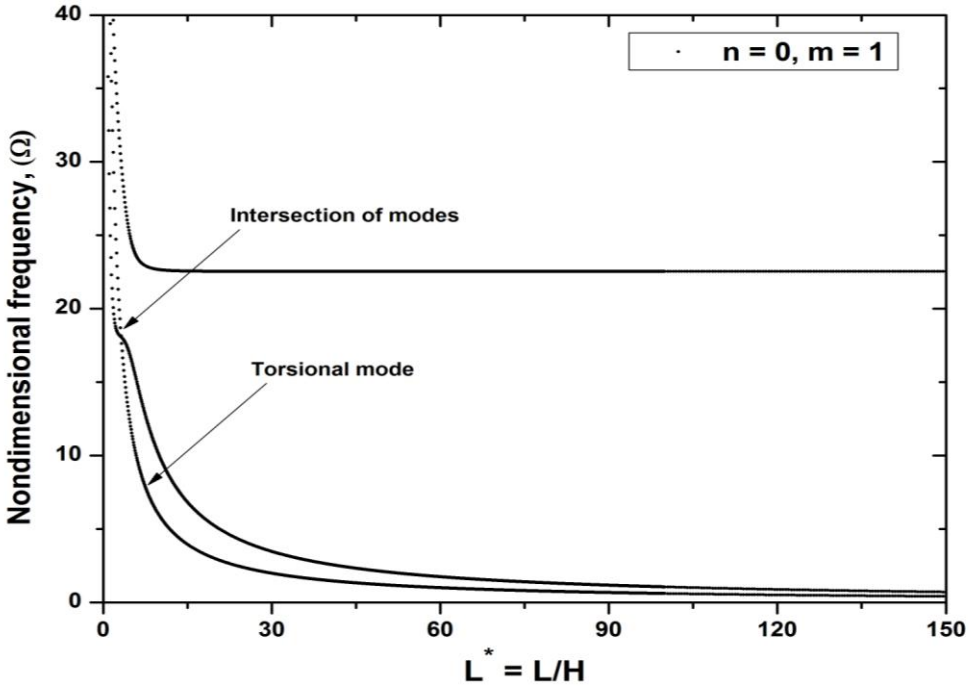

Figure 4.14: Frequency spectrum of the composite cylinder when n = 0 and m = 1

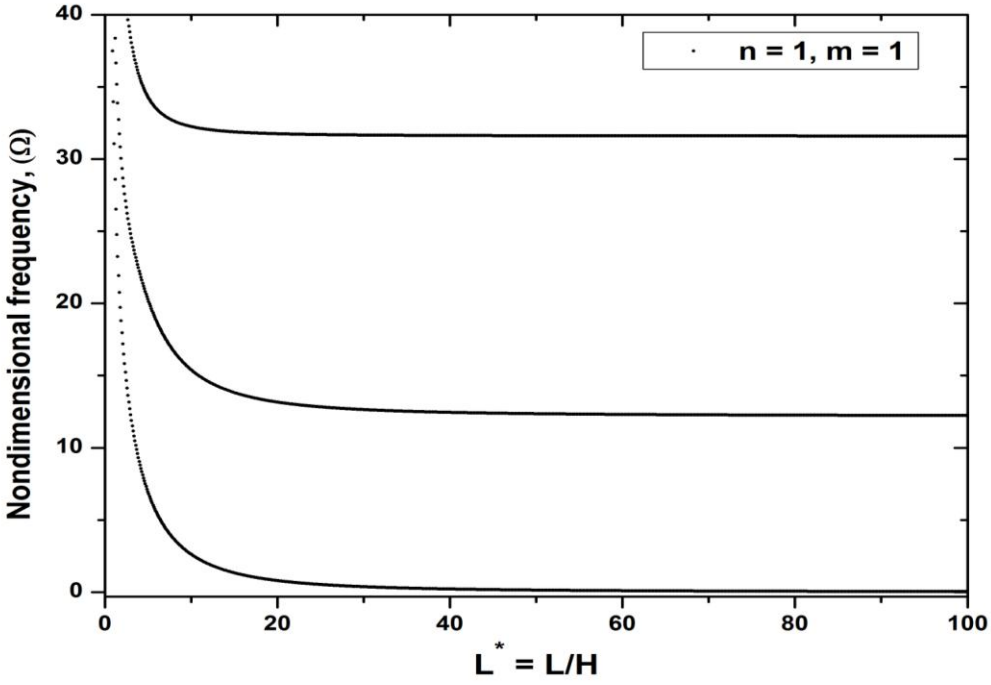

Figure 15: Frequency spectrum of the composite cylinder when n = 1 and m = 1

Table 4.1: Nondimensional wave numbers of thermal modes at low and high frequency level

At Low Level Frequency (4.0 Hz)			**At High Level Frequency (20 MHz)**		
Mode Number	Real Wave Number	Imaginary Wave Number	Mode Number	Real Wave Number	Imaginary Wave Number
1	0.6049	0.6395	1	1548.103	1548.511
2	0.1609	2.4746	2	1583.298	1583.674
3	0.0795	5.0143	3	1618.464	1618.892
4	0.0469	8.0553	4	1653.618	1654.018
5	0.0352	11.3162	5	1688.374	1688.866
6	0.0247	14.9497	6	1721.965	1722.56
7	0.0253	20.0187	7	1750.937	1751.312

Table 4.2: Natural frequencies of first axisymmetric and asymmetric modes

Axisymmetric mode (n = 0, m = 1)		**Asymmetric mode (n = 1, m = 1)**	
Nondimensional length (L^*)	Nondimensional frequency	Nondimensional length (L^*)	Nondimensional frequency
15	4.867	15	2.412
30	2.433	30	0.741
45	1.622	45	0.347
60	1.217	60	0.199
75	0.973	75	0.129
90	0.811	90	0.090
105	0.695	105	0.066
120	0.608	120	0.051
135	0.541	135	0.040
150	0.487	150	0.033

Chapter 5

Conclusions and Recommendations

5.1 Concluding Remarks

In this thesis, a theoretical modelling of thermoelastic guided waves in a transversely isotropic cylinder has been presented using the Lord-Shulman generalized theory of thermoelasticity. This theory was the modification of the Fourier law of heat conduction by the inclusion of thermal relaxation time to model the finite speed of a thermal wave. Dispersion relations in infinite cylinders are studied first. The approximate dispersion equation has been formulated as a generalized eigenvalue problem by treating radial displacement and temperature with a one dimensional finite element model through the thickness of the cylinder. An analytical formulation of dispersion relation, based on introducing potential functions, is also obtained for an isotropic cylinder to validate the semi analytical finite element (SAFE) method. Frequency spectra obtained by both methods for an isotropic copper cylinder have shown excellent agreement with each other. Dispersion curves are also presented for anisotropic and composite cylinders using the SAFE method.

Frequency spectra show that both elastic and thermal modes are attenuated; thermal modes have a very high attenuation when compared with elastic modes. It is noticed that higher order thermal modes originate with high imaginary values of the wave number when $\Omega = \omega^* = 0$ and these higher order thermal modes approach the first thermal mode as the frequency increases.

It is observed that the effect of temperature on elastic modes is found to be negligible. Therefore, materials having a small thermal coupling term can be neglected in the analysis. Neglecting coupling term simplifies the analysis procedure and reduces computational time to obtain a frequency spectrum without noticeable effect. This is shown in Chapter 2.

The transient analysis of thermoelastic waves in an anisotropic circular cylindrical shell excited by a focused laser beam has also been studied. The SAFE method is employed to model the response of a circular cylinder due to a pulsed laser focused on its surface. The heat input, due to a pulsed laser beam focused at the outer radius $r = r_o,\ \theta = 0,\ z = 0$, is assumed to decay exponentially in the radial direction and has a Gaussian profile in the axial direction. The solution can then be used for more general dependence on z and θ. Green's functions are constructed numerically by superposition of guided wave modes in frequency and wave number domains. Time histories of the propagating modes are then calculated by applying inverse Fourier transformation in the time domain.

The total response is found by summation of all modes in the frequency range of the pulse. Time history responses of propagating longitudinal and flexural modes in a

silicon nitride (Si_3N_4) tube are presented. Longitudinal modes travel faster than the flexural modes, the latter having larger amplitudes than the former. It is found that the response is dominated by the flexural modes. These results can be used along with experiments to characterize the anisotropic material properties.

Dispersion characteristics of thermoelastic waves in a circular annulus and in finite length circular cylindrical shells have been studied also. The SAFE method is used to simulate the guided wave modes in the cylinder. The plain strain problem of circumferential guided waves is studied first. It is found that the first circumferential propagating elastic mode is non-dispersive and approaches the Rayleigh wave velocity at high frequencies. Frequency spectra for axisymmetric and asymmetric modes, of a finite cylinder with both ends insulted and constrained by frictionless rigid walls, are computed and presented graphically. Frequency spectra show that the lowest frequency corresponds to first asymmetric mode independent of L/H ratio (where L is the length and H is the thickness) of the cylinder. Here also, it is observed that the influence of temperature change on elastic modes is negligible.

5.2 Recommendations for Future Work

The following recommendations for future research work are suggested:

1. Steady state Green's functions to be formulated in a finite cylinder.

2. Scattering of waves by cracks predominantly in longitudinal directions in a finite cylinder to be investigated by wave superposition method as well as by boundary element method.

3. The scope of this thesis is confined to the theoretical simulation of thermoelastic waves in cylinders. An experimental program should be carried out to validate the findings of the present study.

References

Alleyne, D.N., Lowe, M.J.S., Cawley, P., 1998. The reflection of guided waves from circumferential notches in pipes. Journal of Applied Mechanics 65, 635-641.

Al-Qahtani, H.M., Datta, S.K., 2004. Thermoelastic waves in an anisotropic infinite plate. Journal of Applied Physics 96, 3645-3658.

Al-Qahtani, H.M., Datta, S.K., Mukdadi, O.M., 2005. Laser generated thermoelastic waves in an anisotropic infinite plate: FEM Analysis. Journal of Thermal Stresses 28, 1099-1122.

Bai, H., Taciroglu, E., Dong, S. B., Shah, A. H., 2004. Elastodynamic Green's functions for a laminated piezoelectric cylinder. International Journal of Solids and Structures, 41, 6335-6350.

Bai, H, Shah, A. H., Popplewell, N., Datta, S.K., 2001. Scattering of guided waves by circumferential cracks in steel pipes, Journal of applied mechanics, 68, 619-631.

Bai, H, Shah, A. H., Popplewell, N., Datta, S.K., 2002. Scattering of guided waves by circumferential cracks in composite cylinders, International Journal of Solids and Structures, 39, 4583-4603.

Chau, K. T., 1994. Vibrations of transversely isotropic finite circular cylinders. ASME Journal of Applied Mechanics 61, 964– 970.

Chen, W., Cai, J., Ye, G., Ding, H., 1996. Vibration analysis of orthotropic cylindrical shells with free ends by the Rayleigh-Ritz method. Journal of Sound and Vibration 195, 117–135.

Chester, M., 1963. Second sound in solids. Physical Review 131, 2013 – 2015.

Chree, C., 1889. The Equations of an Isotropic Elastic Solid in Polar and Cylindrical Coordinates, their Solutions and Applications. Trans. Cambridge Philosophical Society, 14, 250-269.

Clorennec, D., Royer, D., 2003. Analysis of surface acoustic wave propagation on a cylinder using laser ultrasonics. Applied Physics Letters 82, 4608-4610.

Datta, S. K., 2000. Wave Propagation in Composite Plates and Shells. Comprehensive Composite Materials, Vol. 1, Ed. T.W. Chou, Elsevier Science Publishers, Oxford, 463-471.

Datta, S.K., Shah, A.H., 2009. Elastic waves in composite media and structures: with applications to ultrasonic nondestructive evaluation, CRC Press, Boca Raton.

Elnagar, A.M., Abd-Alla, A.M., 1987. On a generalized thermo-elastic problem in an infinite cylinder under initial stress. Earth, Moon and Plates 37, 213-223.

Erbay, S., Suhubi, E.S., 1986. Longitudinal wave propagation in a generalized thermoelastic cylinder. Journal of Thermal Stresses 9, 279-295.

Gazis, D. C., 1959. Three-dimensional investigation of the propagation of waves in hallow circular cylinders. I – Analytical foundation. II – Numerical results. The Journal of Acoustical Society of America 31(5), 568 – 578.

Gladwell, G. M. L., Tahbildar, U. C., 1972. Finite element analysis of the axisymmetric vibrations of cylinders. Journal of Sound and Vibration 22, 143–157.

Gladwell, G. M. L., Vijay, D. K., 1975. Natural frequencies of free finite-length circular cylinders. Journal of Sound and Vibration 42, 387–397.

Green, A.E., Lindsay, K.A., 1972. Thermoelasticity. Journal of Elasticity 2, 1-7.

Green, A.E., Naghdi, P.M., 1993. Thermoelasticity without energy dissipation. Journal of Elasticity 31, 189-208.

Gsell, D., Profunser, D., Dual, J., 2000. Measurement of the dispersion relation of guided non-axisymmetric waves in filament-wound cylindrical structures. Ultrasonics 38, 517-521.

Gsell, D., Dual, J., 2004. Non-destructive evaluation of elastic material properties in anisotropic circular cylindrical structures. Ultrasoincs 43, 123-132.

Heyliger, P. R., 1991. Axisymmetric free vibrations of finite anisotropic cylinders. Journal of Sound and Vibration 148, 507–520.

Honarvar, F., Enjilela, E., Sinclair, A. N., 2009. Asymmetric and axisymmetric vibrations of finite transversely isotropic circular cylinders. Acoustical Physics 55, 708–714.

Hutchinson, J. R., 1972. Axisymmetric vibrations of a free finite length rod. Journal of the Acoustical Society of America 51, 233–240.

Huang K.H., Dong, S.B., 1984. Propagating waves and edge vibrations in anisotropic cylinders. Journal of Sound and Vibrations 96(3), 363-379.

Ignaczak, J., Ostoja, M., 2010. Thermoelasticity with Finite Wave Speeds, Oxford, New York.

Jiangong, Y., Bin, W., Cunfu, H., 2010. Circumferential thermoelastic waves in orthotropic cylindrical curved plated without energy dissipation. Ultrasonics 50, 416-423.

Kitayama, M., Hirao, K., Toriyama, M., Kanazaki, S., 1999. Thermal conductivity of β-Si_3N_4: I, Effects of various microstructural factors. Journal of the American Ceramic Society 82, 3105-3112.

Lin, F-H., Hsu, C-K., Tang, T-P., Lee, J-S., Lin, J-Y., Kang, P-K., 2005. A study of silicon nitride nanotube synthesis at relative low temperature by thermal-heating chemical-vapor deposition method. Materials Chemistry and Physics 93, 10-15.

Liu, G., Qu, J., 1998. Guided circumferential waves in a circular annulus. ASME Journal of Applied Mechanics 65, 424 – 430.

Lord, H.W., Shulman, Y., 1967. A generalized dynamical theory of thermoelasticity. Journal of the Mechanics and Physics of Solids 15, 299-309.

Lusher, C. P., Hardy, W. N., 1988. Axisymmetric free vibrations of a transversely isotropic finite cylindrical rod, ASME Journal of Applied Mechanics 55, 855–862.

McMahon, G. W., 1964. Experimental study of the vibrations of solid, isotropic, elastic cylinders. Journal of the Acoustical Society of America 36, 85–92.

McMahon, G. W., 1970. Finite difference analysis of the vibrations of solid cylinders. Journal of the Acoustical Society of America 48, 307–312.

Morse, R. W., 1954. Compressional waves along an anisotropic circular cylinder having hexagonal symmetry. Journal of the Acoustical Society of America 26, 1018–1021.

Nelson, R. B., Dong, S. B., Kalra, R. D., 1971. Vibration and Waves in Laminated Orthotropic Circular Cylinders. Journal of Sound and Vibration, 18, 429 – 444.

Onoe, M., McNiven, H. D., Mindlin, R. D., 1962. Dispersion of Axially Symmetric Waves in Elastic Rods. ASME Journal of Applied Mechanics, 29, 729-734.

Pan, Y., Perton, M., Audoin, B., Rossignol, C., 2006. Acoustic waves generated by a laser point source in a transversely isotropic cylinder. Journal of the Acoustical Society of America 119(1), 243-250.

Pan, Y., Rossignol, C., Audoin, B., 2004. Acoustic waves generated by a laser point source in an isotropic cylinder. Journal of the Acoustical Society of America 116(2), 814-820.

Pochhammer, L., 1876. Ueber die Fortpflanzungsgeschwindigkeiten Schwingungen in einem Unbegrenzten Isotropen Kreiscylinder. Zeitschrift für Mathematik, 81, 324-336.

Ponnusamy, P., 2007. Wave propagation in a generalized thermoelastic solid cylinder of arbitrary cross-section. International Journal of Solids and Structures 44, 5336-5348.

Rose, J.L., 2004. Ultrasonic Waves in Solid Media, Cambridge University Press, UK.

Rattanawangcharoen, N., Datta, S.K., Shah, A. H., 1994a. Non-aximsymmetric Guided Waves in a Composite Cylinder with Transversely Isotropic Core. Geophysical Journal International, 118(2), 317-324.

Rattanawangcharoen N., Shah, A.H., Datta, S.K., 1994. Reflection of waves at the free edge of a laminated circular cylinder. ASME Journal of Applied Mechanics 61, 323-329.

Rattanawangcharoen, N., Shah, A. H., Datta, S.K., 1992. Wave Propagation in Laminated Composite Circular Cylinders. International Journal of Solids and Structures, 29(6), 767-781.

Scruby, C.B., Drain, L.E., 1990. Laser Ultrasonics: Techniques and Applications, Adam Hilger, New York.

Sharma, J.N., 2001. Three-dimensional analysis of a homogeneous transversely isotropic thermoelastic cylindrical panel. Journal of the Acoustical Society of America 110, 254-259.

Sharma, J.N., Singh, D., Kumar, R., 2000. Generalized thermoelastic waves in homogeneous isotropic plates. Journal of the Acoustical Society of America 108, 848-851.

Sharma, J.N., Sharma, P.K., 2002. Free vibration analysis of homogeneous transversely isotropic thermoelastic cylindrical panel. Journal of Thermal Stresses 25, 169-182.

Soldatos, K. P., 1994. Review of Three Dimensional Dynamic Analysis of Circular Cylinders and Cylindrical Shells. ASME Applied Mechanics Review, 47(10), 501-516.

Spicer, J.B., Mckie, A.D.W., Wagner, J.W., 1990. Quantitative theory for laser ultrasonic waves in a thin plate. Applied Physics Letters 57, 1882-1884.

Verma, K.L., 2002. On the propagation of waves in layered anisotropic media in generalized thermoelasticity. International Journal of Engineering Science 40, 2077-2096.

Verma, K.L., Hasebe, N., 2001. Dispersion of thermoelastic waves in a plate with and without energy dissipation. International Journal of Thermophysics 22, 957-978.

Vogelgesang, R., Grimsditch, M., Wallace, J.S., 2000. The elastic constants of single crystal β-Si_3N_4. Applied Physics Letters 76, 982-984.

White, R.M., 1963. Generation of elastic waves by transient surface heating. Journal of Applied Physics 34, 3559-3567.

Xu, B., Feng, J., Xu, G., Wang, J., Sun, H., Cao, G., 2008. Laser generated thermoelastic acoustic sources and lamb waves in anisotropic plates. Applied Physics A 91, 173-179.

Yokota, H., Ibukiyama, M., 2003. Microstructure tailoring for high thermal conductivity of β-Si_3N_4 ceramics. Journal of the American Ceramic Society 86, 197-199.

Zhuang, W., Shah, A.H., Datta, S.K., 1997. Axisymmetric guided wave scattering by cracks in welded steel pipes. ASME Journal of pressure vessel technology 19, 401-406.

Zhuang, W., Shah, A.H., Dong, S.B., 1999. Elastodynamic Green's function for laminated anisotropic circular cylinders. ASME Journal of Applied Mechanics 66, 665-673.

Zhu, X., Sakka, Y., 2008. Textured silicon nitride: processing and anisotropic properties. Science and Technology of Advanced Materials 9, 1-47.

Appendix A

$$\boldsymbol{\varepsilon}=\begin{bmatrix}\varepsilon_{rr}\\ \varepsilon_{\theta\theta}\\ \varepsilon_{zz}\\ \gamma_{\theta z}\\ \gamma_{rz}\\ \gamma_{r\theta}\end{bmatrix},\quad \boldsymbol{\sigma}=\begin{bmatrix}\sigma_{rr}\\ \sigma_{\theta\theta}\\ \sigma_{zz}\\ \sigma_{\theta z}\\ \sigma_{rz}\\ \sigma_{r\theta}\end{bmatrix},\quad \mathbf{C}=\begin{bmatrix}c_{11} & c_{12} & c_{13} & 0 & 0 & 0\\ c_{12} & c_{11} & c_{13} & 0 & 0 & 0\\ c_{13} & c_{13} & c_{33} & 0 & 0 & 0\\ 0 & 0 & 0 & c_{44} & 0 & 0\\ 0 & 0 & 0 & 0 & c_{44} & 0\\ 0 & 0 & 0 & 0 & 0 & (c_{11}-c_{12})/2\end{bmatrix},\quad \boldsymbol{\beta}=\begin{bmatrix}\beta_{rr}\\ \beta_{rr}\\ \beta_{zz}\\ 0\\ 0\\ 0\end{bmatrix}$$

$$\mathbf{B}_1=\begin{bmatrix}n_{1,r} & n_{2,r} & n_{3,r}\\ 0 & 0 & 0\\ 0 & 0 & 0\end{bmatrix},\quad \mathbf{B}_2=\begin{bmatrix}0 & 0 & 0\\ \frac{n_1}{r} & \frac{n_2}{r} & \frac{n_3}{r}\\ 0 & 0 & 0\end{bmatrix},\quad \mathbf{B}_3=\begin{bmatrix}0 & 0 & 0\\ 0 & 0 & 0\\ n_1 & n_2 & n_3\end{bmatrix}$$

$$\mathbf{D}_1=\begin{bmatrix}n_{1,r} & 0 & 0 & n_{2,r} & 0 & 0 & n_{3,r} & 0 & 0\\ \frac{n_1}{r} & 0 & 0 & \frac{n_2}{r} & 0 & 0 & \frac{n_3}{r} & 0 & 0\\ 0 & 0 & 0 & 0 & 0 & 0 & 0 & 0 & 0\\ 0 & 0 & 0 & 0 & 0 & 0 & 0 & 0 & 0\\ 0 & 0 & n_{1,r} & 0 & 0 & n_{2,r} & 0 & 0 & n_{3,r}\\ 0 & n_{1,r}-\frac{n_1}{r} & 0 & 0 & n_{2,r}-\frac{n_2}{r} & 0 & 0 & n_{3,r}-\frac{n_3}{r} & 0\end{bmatrix}$$

$$\mathbf{D}_2=\begin{bmatrix}0 & 0 & 0 & 0 & 0 & 0 & 0 & 0 & 0\\ 0 & \frac{n_1}{r} & 0 & 0 & \frac{n_2}{r} & 0 & 0 & \frac{n_3}{r} & 0\\ 0 & 0 & 0 & 0 & 0 & 0 & 0 & 0 & 0\\ 0 & 0 & \frac{n_1}{r} & 0 & 0 & \frac{n_2}{r} & 0 & 0 & \frac{n_3}{r}\\ 0 & 0 & 0 & 0 & 0 & 0 & 0 & 0 & 0\\ \frac{n_1}{r} & 0 & 0 & \frac{n_2}{r} & 0 & 0 & \frac{n_3}{r} & 0 & 0\end{bmatrix}$$

$$\mathbf{D}_3 = \begin{bmatrix} 0 & 0 & 0 & 0 & 0 & 0 & 0 & 0 & 0 \\ 0 & 0 & 0 & 0 & 0 & 0 & 0 & 0 & 0 \\ 0 & 0 & n_1 & 0 & 0 & n_2 & 0 & 0 & n_3 \\ 0 & n_1 & 0 & 0 & n_2 & 0 & 0 & n_3 & 0 \\ n_1 & 0 & 0 & n_2 & 0 & 0 & n_3 & 0 & 0 \\ 0 & 0 & 0 & 0 & 0 & 0 & 0 & 0 & 0 \end{bmatrix}$$

$$\mathbf{K}_{jk} = \int_r \mathbf{D}_j^T \mathbf{C} \mathbf{D}_k r dr \qquad (j,k = 1,2,3)$$

$$\mathbf{K}_{0k} = \int_r \mathbf{D}_k^T \boldsymbol{\beta} \mathbf{N}_2 r dr \qquad (k = 1,2,3)$$

$$\mathbf{M} = \int_r \rho \mathbf{N}_1^T \mathbf{N}_1 r dr$$

$$\mathbf{g}_{jj} = \int_r \mathbf{B}_j^T \mathbf{K} \mathbf{B}_j r dr \qquad (j = 1,2,3)$$

$$\mathbf{f}_j = \int_r T_0 \mathbf{N}_2^T \boldsymbol{\beta}^T \mathbf{D}_j r dr \qquad (j = 1,2,3)$$

$$\mathbf{m}_0 = \int_r \rho c_E \mathbf{N}_2^T \mathbf{N}_2 r dr$$

$$\mathbf{f}^e = \int_r \mathbf{N}_2^T \mathbf{f} r dr$$

$$\mathbf{Q}_{th} = \int_r \mathbf{N}_2^T (Q + \tau_0 \dot{Q}) r dr$$

$$\mathbf{H}_1 = \begin{bmatrix} \mathbf{M} & 0 \\ \tau_0 \mathbf{f}_1 & \tau_0 \mathbf{m}_0 \end{bmatrix}, \qquad \mathbf{H}_2 = \begin{bmatrix} 0 & 0 \\ \tau_0 \mathbf{f}_2 & 0 \end{bmatrix}, \qquad \mathbf{H}_3 = \begin{bmatrix} 0 & 0 \\ \tau_0 \mathbf{f}_3 & 0 \end{bmatrix},$$

$$\mathbf{H}_4 = \begin{bmatrix} 0 & 0 \\ \mathbf{f}_1 & \mathbf{m}_0 \end{bmatrix}, \qquad \mathbf{H}_5 = \begin{bmatrix} 0 & 0 \\ \mathbf{f}_2 & 0 \end{bmatrix}, \qquad \mathbf{H}_6 = \begin{bmatrix} 0 & 0 \\ \mathbf{f}_3 & 0 \end{bmatrix},$$

$$\mathbf{H}_7 = \begin{bmatrix} \mathbf{K}_{11} & -\mathbf{K}_{01} \\ 0 & \mathbf{g}_{11} \end{bmatrix}, \qquad \mathbf{H}_8 = \begin{bmatrix} \mathbf{K}_{12} - \mathbf{K}_{21} & \mathbf{K}_{02} \\ 0 & 0 \end{bmatrix}, \qquad \mathbf{H}_9 = \begin{bmatrix} \mathbf{K}_{13} - \mathbf{K}_{31} & \mathbf{K}_{03} \\ 0 & 0 \end{bmatrix},$$

$$\mathbf{H}_{10} = \begin{bmatrix} -\mathbf{K}_{22} & 0 \\ 0 & -\mathbf{g}_{22} \end{bmatrix}, \qquad \mathbf{H}_{11} = \begin{bmatrix} -(\mathbf{K}_{23} + \mathbf{K}_{32}) & 0 \\ 0 & 0 \end{bmatrix}, \qquad \mathbf{H}_{12} = \begin{bmatrix} -\mathbf{K}_{33} & 0 \\ 0 & -\mathbf{g}_{33} \end{bmatrix}$$

Appendix B

Temperature gradient and Stresses:

$$\begin{bmatrix} T_{,r} \\ \sigma_{rr} \\ \sigma_{r\theta} \\ \sigma_{rz} \end{bmatrix} = \begin{bmatrix} a_{11} & a_{12} & a_{13} & a_{14} & 0 & 0 & 0 & 0 \\ a_{21} & a_{22} & a_{23} & a_{24} & a_{25} & a_{26} & a_{27} & a_{28} \\ a_{31} & a_{32} & a_{33} & a_{34} & a_{35} & a_{36} & a_{37} & a_{38} \\ a_{41} & a_{42} & a_{43} & a_{44} & a_{45} & a_{46} & a_{47} & a_{48} \end{bmatrix} \begin{bmatrix} A_1 \\ A_2 \\ A_3 \\ A_4 \\ B_1 \\ B_2 \\ C_1 \\ C_2 \end{bmatrix}$$

$$a_{11} = \frac{1}{\hat{\beta}}\left(\frac{c_p^2}{c_s^2} r_1 + \hat{\beta}^2 + \xi^2\right)\left(\frac{n}{r} J_n(\alpha_1 r) - \alpha_1 J_{n+1}(\alpha_1 r)\right)$$

$$a_{13} = \frac{1}{\hat{\beta}}\left(\frac{c_p^2}{c_s^2} r_2 + \hat{\beta}^2 + \xi^2\right)\left(\frac{n}{r} J_n(\alpha_2 r) - \alpha_2 J_{n+1}(\alpha_2 r)\right)$$

$$a_{21} = \mu\left[\left(2\frac{n(n-1)}{r^2} - \left(\hat{\beta}^2 - \xi^2\right)\right) J_n(\alpha_1 r) + 2\frac{\alpha_1}{r} J_{n+1}(\alpha_1 r)\right]$$

$$a_{23} = \mu\left[\left(2\frac{n(n-1)}{r^2} - \left(\hat{\beta}^2 - \xi^2\right)\right) J_n(\alpha_2 r) + 2\frac{\alpha_2}{r} J_{n+1}(\alpha_2 r)\right]$$

$$a_{25} = \mu\left[-2\xi\left(\hat{\beta} J_n(\hat{\beta} r) - \frac{(n+1)}{r} J_{n+1}(\hat{\beta} r)\right)\right]$$

$$a_{27} = \mu\left[2\frac{in}{r}\left(-\hat{\beta} J_{n+1}(\beta r) + \frac{(n-1)}{r} J_n(\hat{\beta} r)\right)\right]$$

$$a_{31} = \mu\left[\frac{2in}{r}\left(-\alpha_1 J_{n+1}(\alpha_1 r) + \frac{n-1}{r} J_n(\alpha_1 r)\right)\right]$$

$$a_{33} = \mu\left[\frac{2in}{r}\left(-\alpha_2 J_{n+1}(\alpha_2 r) + \frac{(n-1)}{r} J_n(\alpha_2 r)\right)\right]$$

$$a_{35} = \mu\left[i\xi\left(\hat{\beta} J_n(\hat{\beta} r) - \frac{2(n+1)}{r} J_{n+1}(\hat{\beta} r)\right)\right]$$

$$a_{37} = \mu\left[-\left(\frac{2n(n-1)}{r^2} - \hat{\beta}^2\right) J_n(\beta r) - \frac{2\hat{\beta}}{r} J_{n+1}(\hat{\beta} r)\right]$$

$$a_{41} = \mu(2i\xi)\left[-\alpha_1 J_{n+1}(\alpha_1 r) + \frac{n}{r} J_n(\alpha_1 r)\right]$$

$$a_{43} = \mu(2i\xi)\left[-\alpha_2 J_{n+1}(\alpha_2 r) + \frac{n}{r} J_n(\alpha_2 r)\right]$$

$$a_{45} = \mu\left[\frac{-in}{r}\hat{\beta} J_n(\hat{\beta} r) + i\left(\hat{\beta}^2 - \xi^2\right) J_{n+1}(\hat{\beta} r)\right]$$

$$a_{47} = \mu\left(\frac{-n\xi}{r} J_n(\hat{\beta} r)\right)$$

The elements a_{i2}, a_{i4}, a_{i6}, a_{i8} $(i = 1-4)$ are obtained from a_{i1}, a_{i3}, a_{i5}, a_{i7} $(i = 1-4)$ by replacing the Bessel function of the first kind, J_n, by the Bessel function of the second kind, Y_n.

Appendix C

$$\boldsymbol{\varepsilon}=\begin{bmatrix}\varepsilon_{rr}\\ \varepsilon_{\theta\theta}\\ \varepsilon_{zz}\\ \gamma_{\theta z}\\ \gamma_{rz}\\ \gamma_{r\theta}\end{bmatrix},\quad \boldsymbol{\sigma}=\begin{bmatrix}\sigma_{rr}\\ \sigma_{\theta\theta}\\ \sigma_{zz}\\ \sigma_{\theta z}\\ \sigma_{rz}\\ \sigma_{r\theta}\end{bmatrix},\quad \mathbf{C}=\begin{bmatrix}c_{11} & c_{12} & c_{13} & 0 & 0 & 0\\ c_{12} & c_{11} & c_{13} & 0 & 0 & 0\\ c_{13} & c_{13} & c_{33} & 0 & 0 & 0\\ 0 & 0 & 0 & c_{44} & 0 & 0\\ 0 & 0 & 0 & 0 & c_{44} & 0\\ 0 & 0 & 0 & 0 & 0 & (c_{11}-c_{12})/2\end{bmatrix},\quad \boldsymbol{\beta}=\begin{bmatrix}\beta_{rr}\\ \beta_{rr}\\ \beta_{zz}\\ 0\\ 0\\ 0\end{bmatrix}$$

$$\mathbf{B}_1=\begin{bmatrix}cn_{1,r} & cn_{2,r} & cn_{3,r}\\ 0 & 0 & 0\\ -spn_1 & -spn_2 & -spn_3\end{bmatrix},\quad \mathbf{B}_{11}=\begin{bmatrix}n_{1,r} & n_{2,r} & n_{3,r}\\ 0 & 0 & 0\\ 0 & 0 & 0\end{bmatrix},\quad \mathbf{B}_{12}=\begin{bmatrix}0 & 0 & 0\\ 0 & 0 & 0\\ -pn_1 & -pn_2 & -pn_3\end{bmatrix}$$

$$\mathbf{B}_2=\begin{bmatrix}0 & 0 & 0\\ c\dfrac{n_1}{r} & c\dfrac{n_2}{r} & c\dfrac{n_3}{r}\\ 0 & 0 & 0\end{bmatrix},\qquad \mathbf{B}_{21}=\begin{bmatrix}0 & 0 & 0\\ \dfrac{n_1}{r} & \dfrac{n_2}{r} & \dfrac{n_3}{r}\\ 0 & 0 & 0\end{bmatrix}$$

$$\mathbf{D}_1=\begin{bmatrix}cn_{1,r} & 0 & 0 & cn_{2,r} & 0 & 0 & cn_{3,r} & 0 & 0\\ c\dfrac{n_1}{r} & 0 & 0 & c\dfrac{n_2}{r} & 0 & 0 & c\dfrac{n_3}{r} & 0 & 0\\ 0 & 0 & pcn_1 & 0 & 0 & pcn_2 & 0 & 0 & pcn_3\\ 0 & -psn_1 & 0 & 0 & -psn_2 & 0 & 0 & -psn_3 & 0\\ -psn_1 & 0 & sn_{1,r} & -psn_2 & 0 & sn_{2,r} & -psn_3 & 0 & sn_{3,r}\\ 0 & c\left(n_{1,r}-\dfrac{n_1}{r}\right) & 0 & 0 & c\left(n_{2,r}-\dfrac{n_2}{r}\right) & 0 & 0 & c\left(n_{3,r}-\dfrac{n_3}{r}\right) & 0\end{bmatrix}$$

$$\mathbf{D}_{11} = \begin{bmatrix} n_{1,r} & 0 & 0 & n_{2,r} & 0 & 0 & n_{3,r} & 0 & 0 \\ n_1/r & 0 & 0 & n_2/r & 0 & 0 & n_3/r & 0 & 0 \\ 0 & 0 & pn_1 & 0 & 0 & pn_2 & 0 & 0 & pn_3 \\ 0 & 0 & 0 & 0 & 0 & 0 & 0 & 0 & 0 \\ 0 & 0 & 0 & 0 & 0 & 0 & 0 & 0 & 0 \\ 0 & \left(n_{1,r} - n_1/r\right) & 0 & 0 & \left(n_{2,r} - n_2/r\right) & 0 & 0 & \left(n_{3,r} - n_3/r\right) & 0 \end{bmatrix}$$

$$\mathbf{D}_{12} = \begin{bmatrix} 0 & 0 & 0 & 0 & 0 & 0 & 0 & 0 & 0 \\ 0 & 0 & 0 & 0 & 0 & 0 & 0 & 0 & 0 \\ 0 & 0 & 0 & 0 & 0 & 0 & 0 & 0 & 0 \\ 0 & -pn_1 & 0 & 0 & -pn_2 & 0 & 0 & -pn_3 & 0 \\ -pn_1 & 0 & n_{1,r} & -pn_2 & 0 & n_{2,r} & -pn_3 & 0 & n_{3,r} \\ 0 & 0 & 0 & 0 & 0 & 0 & 0 & 0 & 0 \end{bmatrix}$$

$$\mathbf{D}_2 = \begin{bmatrix} 0 & 0 & 0 & 0 & 0 & 0 & 0 & 0 & 0 \\ 0 & c\frac{n_1}{r} & 0 & 0 & c\frac{n_2}{r} & 0 & 0 & c\frac{n_3}{r} & 0 \\ 0 & 0 & 0 & 0 & 0 & 0 & 0 & 0 & 0 \\ 0 & 0 & s\frac{n_1}{r} & 0 & 0 & s\frac{n_2}{r} & 0 & 0 & s\frac{n_3}{r} \\ 0 & 0 & 0 & 0 & 0 & 0 & 0 & 0 & 0 \\ c\frac{n_1}{r} & 0 & 0 & c\frac{n_2}{r} & 0 & 0 & c\frac{n_3}{r} & 0 & 0 \end{bmatrix}$$

$$\mathbf{D}_{21} = \begin{bmatrix} 0 & 0 & 0 & 0 & 0 & 0 & 0 & 0 & 0 \\ 0 & n_1/r & 0 & 0 & n_2/r & 0 & 0 & n_3/r & 0 \\ 0 & 0 & 0 & 0 & 0 & 0 & 0 & 0 & 0 \\ 0 & 0 & 0 & 0 & 0 & 0 & 0 & 0 & 0 \\ 0 & 0 & 0 & 0 & 0 & 0 & 0 & 0 & 0 \\ n_1/r & 0 & 0 & n_2/r & 0 & 0 & n_3/r & 0 & 0 \end{bmatrix}$$

$$\mathbf{D}_{22}=\begin{bmatrix}0&0&0&0&0&0&0&0&0\\0&0&0&0&0&0&0&0&0\\0&0&0&0&0&0&0&0&0\\0&0&n_1/r&0&0&n_2/r&0&0&n_3/r\\0&0&0&0&0&0&0&0&0\\0&0&0&0&0&0&0&0&0\end{bmatrix}$$

$$\mathbf{K}_{jk}=\frac{L}{2}\int_r\left(\mathbf{D}_{j1}^T\mathbf{C}\mathbf{D}_{k1}+\mathbf{D}_{j2}^T\mathbf{C}\mathbf{D}_{k2}\right)rdr \qquad (j,k=1,2)$$

$$\mathbf{K}_{0k}=\frac{L}{2}\int_r\mathbf{D}^T{}_{k1}\boldsymbol{\beta}\mathbf{N}_2rdr \qquad (k=1,2)$$

$$\mathbf{g}_{jj}=\frac{L}{2}\int_r\left(\mathbf{B}_{j1}^T\mathbf{K}\mathbf{B}_{j1}+\mathbf{B}_{j2}^T\mathbf{K}\mathbf{B}_{j2}\right)rdr \qquad (j=1,2)$$

$$\mathbf{f}_j=\frac{L}{2}\int_r T_0\mathbf{N}_2^T\boldsymbol{\beta}^T\mathbf{D}_{j1}rdr \qquad (j=1,2)$$

$$\mathbf{m}_0=\frac{L}{2}\int_r\rho c_E\mathbf{N}_2^T\mathbf{N}_2rdr$$

$$\mathbf{M}=\frac{L}{2}\int_r\rho\mathbf{N}_1^T\mathbf{N}_1rdr$$

$$\mathbf{E}_1=\begin{bmatrix}\mathbf{M}&0\\\tau_0\mathbf{f}_1&\tau_0\mathbf{m}_0\end{bmatrix},\quad \mathbf{E}_2=\begin{bmatrix}0&0\\\tau_0\mathbf{f}_2&0\end{bmatrix},\quad \mathbf{E}_3=\begin{bmatrix}0&0\\\mathbf{f}_1&\mathbf{m}_0\end{bmatrix},\quad \mathbf{E}_4=\begin{bmatrix}0&0\\\mathbf{f}_2&0\end{bmatrix},$$

$$\mathbf{E}_5=\begin{bmatrix}\mathbf{K}_{11}&-\mathbf{K}_{01}\\0&\mathbf{g}_{11}\end{bmatrix},\quad \mathbf{E}_6=\begin{bmatrix}\mathbf{K}_{12}-\mathbf{K}_{21}&\mathbf{K}_{02}\\0&0\end{bmatrix},\quad \mathbf{E}_7=\begin{bmatrix}-\mathbf{K}_{22}&0\\0&-\mathbf{g}_{22}\end{bmatrix}$$

Appendix D

Equations for plane strain problem

The displacements and temperature of the k^{th} lamina are

$$\begin{aligned}\mathbf{u}(r,\theta,t) &= \mathbf{N}_1(\xi)\mathbf{u}^e(\theta,t)\\ T(r,\theta,t) &= \mathbf{N}_2(r)\mathbf{T}^e(\theta,t)\end{aligned} \tag{a}$$

where

$$\mathbf{N}_1 = \begin{bmatrix} n_1 & 0 & n_2 & 0 & n_3 & 0 \\ 0 & n_1 & 0 & n_2 & 0 & n_3 \end{bmatrix}$$

$$\mathbf{N}_2 = \begin{bmatrix} n_1 & n_2 & n_3 \end{bmatrix}$$

$$\mathbf{u}^e = (u_1, v_1, u_2, v_2, u_3, v_3)^T \text{ and } \mathbf{T}^e = (T_1, T_2, T_3)^T$$

The strain tensor and temperature gradient are

$$\begin{aligned}\boldsymbol{\varepsilon} &= \mathbf{D}_1\mathbf{u}^e + \mathbf{D}_2\mathbf{u}^e_{,\theta}\\ \mathbf{T}' &= \mathbf{B}_1\mathbf{T}^e + \mathbf{B}_2\mathbf{T}^e_{,\theta}\end{aligned} \tag{b}$$

where

$$\mathbf{D}_1 = \begin{bmatrix} n_{1,r} & 0 & n_{2,r} & 0 & n_{3,r} & 0 \\ \frac{n_1}{r} & 0 & \frac{n_2}{r} & 0 & \frac{n_3}{r} & 0 \\ 0 & n_{1,r} - \frac{n_1}{r} & 0 & n_{2,r} - \frac{n_2}{r} & 0 & n_{3,r} - \frac{n_3}{r} \end{bmatrix}, \quad \mathbf{D}_2 = \begin{bmatrix} 0 & 0 & 0 & 0 & 0 & 0 \\ 0 & \frac{n_1}{r} & 0 & \frac{n_2}{r} & 0 & \frac{n_3}{r} \\ \frac{n_1}{r} & 0 & \frac{n_2}{r} & 0 & \frac{n_3}{r} & 0 \end{bmatrix}$$

$$\mathbf{B}_1 = \begin{bmatrix} n_{1,r} & n_{2,r} & n_{3,r} \\ 0 & 0 & 0 \end{bmatrix}, \mathbf{B}_2 = \begin{bmatrix} 0 & 0 & 0 \\ \frac{n_1}{r} & \frac{n_2}{r} & \frac{n_3}{r} \end{bmatrix}$$

The stress vector is given by

$$\boldsymbol{\sigma} = \mathbf{C}\left(\mathbf{D}_1\mathbf{u}^e + \mathbf{D}_2\mathbf{u}^e_{,\theta}\right) - \boldsymbol{\beta}\mathbf{N}_2\mathbf{T}^e \tag{c}$$

The variational principle of thermoelasticity is

$$\int_{t_0}^{t_1}\int_A \left(\delta\boldsymbol{\varepsilon}^T\boldsymbol{\sigma} - \delta\mathbf{T}'^T\mathbf{K}\mathbf{T}' - \delta\mathbf{T}'^T\left(\mathbf{q}+\tau_0\dot{\mathbf{q}}\right)\right)dAdt = \int_{t_0}^{t_1}\int_A \left(-\delta\mathbf{u}^T\rho\ddot{\mathbf{u}}\right)dAdt \tag{d}$$

The first term in eq. (d) is

$$\begin{aligned}\int_{t_0}^{t_1}\int_A \delta\boldsymbol{\varepsilon}^T\boldsymbol{\sigma}dAdt &= \int_{t_0}^{t_1}\int_A \left(\mathbf{D}_1\delta\mathbf{u}^e + \mathbf{D}_2\delta\mathbf{u}^e_{,\theta}\right)^T\left[\mathbf{C}\left(\mathbf{D}_1\mathbf{u}^e + \mathbf{D}_2\mathbf{u}^e_{,\theta}\right) - \boldsymbol{\beta}\mathbf{N}_2\mathbf{T}^e\right]dAdt \\ &= \int_{t_0}^{t_1}\int_\theta \delta\mathbf{u}^{eT}\left[\mathbf{K}_{11}\mathbf{u}^e + \left(\mathbf{K}_{12}-\mathbf{K}_{21}\right)\mathbf{u}^e_{,\theta} - \mathbf{K}_{22}\mathbf{u}^e_{,\theta\theta} - \mathbf{K}^e_{01}\mathbf{T}^e + \mathbf{K}^e_{02}\mathbf{T}^e_{,\theta}\right]d\theta dt\end{aligned} \tag{e}$$

where

$$\mathbf{K}_{11} = \int_r \mathbf{D}_1^T\mathbf{C}\mathbf{D}_1 rdr, \quad \mathbf{K}_{12} = \int_r \mathbf{D}_1^T\mathbf{C}\mathbf{D}_2 rdr, \quad \mathbf{K}_{21} = \int_r \mathbf{D}_2^T\mathbf{C}\mathbf{D}_1 rdr, \quad \mathbf{K}_{22} = \int_r \mathbf{D}_2^T\mathbf{C}\mathbf{D}_2 rdr$$

$$\mathbf{K}_{01} = \int_r \mathbf{D}_1^T\boldsymbol{\beta}\mathbf{N}_2 rdr, \quad \mathbf{K}_{02} = \int_r \mathbf{D}_2^T\boldsymbol{\beta}\mathbf{N}_2 rdr$$

The second term in eq. (d) is

$$\begin{aligned}\int_{t_0}^{t_1}\int_A \delta\mathbf{T}'^T\mathbf{K}\mathbf{T}'dAdt &= \int_{t_0}^{t_1}\int_A \left(\delta\mathbf{T}^{eT}\mathbf{B}_1^T + \delta\mathbf{T}^{eT}_{,\theta}\mathbf{B}_2^T\right)\mathbf{K}\left(\mathbf{B}_1\mathbf{T}^e + \mathbf{B}_2\mathbf{T}^e_{,\theta}\right)dAdt \\ &= \int_{t_0}^{t_1}\int_\theta \delta\mathbf{T}^{eT}\left(\mathbf{g}_{11}\mathbf{T}^e - \mathbf{g}_{22}\mathbf{T}^e_{,\theta\theta}\right)d\theta dt\end{aligned} \tag{f}$$

where

$$\mathbf{g}_{11} = \int_r \mathbf{B}_1^T\mathbf{K}\mathbf{B}_1 rdr, \quad \mathbf{g}_{22} = \int_r \mathbf{B}_2^T\mathbf{K}\mathbf{B}_2 rdr$$

The third term in eq. (d) is

$$\begin{aligned}\int_{t_0}^{t_1}\int_A \delta\mathbf{T}'^T\left(\mathbf{q}+\tau_0\dot{\mathbf{q}}\right)dAdt &= -\int_{t_0}^{t_1}\int_A \delta\mathbf{T}^T\left(\nabla\cdot\mathbf{q} + \tau_0\nabla\cdot\dot{\mathbf{q}}\right)dAdt \\ &= \int_{t_0}^{t_1}\int_A \delta\mathbf{T}^T\left[T_0\boldsymbol{\beta}^T\dot{\boldsymbol{\varepsilon}} + \rho c_E\dot{T} + \tau_0\left(T_0\boldsymbol{\beta}^T\ddot{\boldsymbol{\varepsilon}} + \rho c_E\ddot{T}\right)\right]dAdt \\ &= \int_{t_0}^{t_1}\int_\theta \delta\mathbf{T}^{eT}\left[\left(\mathbf{f}_1\dot{\mathbf{u}}^e + \mathbf{f}_2\dot{\mathbf{u}}^e_{,\theta} + \mathbf{m}_0\dot{\mathbf{T}}^e\right) + \tau_0\left(\mathbf{f}_1\ddot{\mathbf{u}}^e + \mathbf{f}_2\ddot{\mathbf{u}}^e_{,\theta} + \mathbf{m}_0\ddot{\mathbf{T}}^e\right)\right]d\theta dt\end{aligned} \tag{g}$$

The right hand side of the in eq. (d) has the form

$$\int_{t_0}^{t_1}\int_{V}\delta\mathbf{u}^{T}\left(-\rho\ddot{\mathbf{u}}\right)dVdt=\int_{t_0}^{t_1}\int_{\theta}\delta\mathbf{u}^{eT}\left(-\mathbf{M}\ddot{\mathbf{u}}^{e}\right)d\theta dt \tag{h}$$

where $\mathbf{f}_1=\int_r T\mathbf{N}_2^{eT}\boldsymbol{\beta}^T\mathbf{D}_1 rdr,\ \ \mathbf{f}_2=\int_r T_0\mathbf{N}_2^{eT}\boldsymbol{\beta}^T\mathbf{D}_2 rdr,\ \ \mathbf{M}=\int_r \rho\mathbf{N}_1^T\mathbf{N}_1 rdr,\ \ \mathbf{m}_{\theta\theta},=\int_r \mathbf{N}_2^{eT}\rho c_E\mathbf{N}_2^{e} rdr$

Equating the coefficients of $\delta\mathbf{u}^e$ in equations (e) and (h) to zero gives the following equation

$$\mathbf{M}\ddot{\mathbf{u}}^{e}+\mathbf{K}_{11}\mathbf{u}^{e}-\mathbf{K}_{01}\mathbf{T}^{e}+\left(\mathbf{K}_{12}-\mathbf{K}_{21}\right)\mathbf{u}_{,\theta}^{e}+\mathbf{K}_{02}\mathbf{T}_{,\theta}^{e}-\mathbf{K}_{22}\mathbf{u}_{,\theta\theta}^{e}=0 \tag{i}$$

Similarly, equating the coefficients of $\delta\mathbf{T}^e$ in equations (f) and (g) yields

$$\tau_0\mathbf{f}_1\ddot{\mathbf{u}}^{e}+\tau_0\mathbf{m}_0\ddot{\mathbf{T}}^{e}+\tau_0\mathbf{f}_2\ddot{\mathbf{u}}_{,\theta}^{e}+\mathbf{f}_1\dot{\mathbf{u}}^{e}+\mathbf{m}_0\dot{\mathbf{T}}^{e}+\mathbf{f}_2\dot{\mathbf{u}}_{,\theta}^{e}+\mathbf{g}_{11}\mathbf{T}^{e}-\mathbf{g}_{22}\mathbf{T}_{,\theta\theta}^{e}=0 \tag{j}$$

Combining equations (i) and (j) and assembling the element matrices into global matrices lead to the following governing equations of motion,

$$\mathbf{P}_1\ddot{\mathbf{V}}+\mathbf{P}_2\ddot{\mathbf{V}}_{,\theta}+\mathbf{P}_3\dot{\mathbf{V}}+\mathbf{P}_4\dot{\mathbf{V}}_{,\theta}+\mathbf{P}_5\mathbf{V}+\mathbf{P}_6\mathbf{V}_{,\theta}+\mathbf{P}_7\mathbf{V}_{,\theta\theta}=0 \tag{k}$$

$$\mathbf{P}_1=\begin{bmatrix}\mathbf{M} & 0\\ \tau_0\mathbf{f}_1 & \tau_0\mathbf{m}_0\end{bmatrix},\quad \mathbf{P}_2=\begin{bmatrix}0 & 0\\ \tau_0\mathbf{f}_2 & 0\end{bmatrix},\quad \mathbf{P}_3=\begin{bmatrix}0 & 0\\ \mathbf{f}_1 & \mathbf{m}_0\end{bmatrix},\quad \mathbf{P}_4=\begin{bmatrix}0 & 0\\ \mathbf{f}_2 & 0\end{bmatrix},$$

$$\mathbf{P}_5=\begin{bmatrix}\mathbf{K}_{11} & -\mathbf{K}_{01}\\ 0 & \mathbf{g}_{11}\end{bmatrix},\quad \mathbf{P}_6=\begin{bmatrix}\mathbf{K}_{12}-\mathbf{K}_{21} & \mathbf{K}_{02}\\ 0 & 0\end{bmatrix},\quad \mathbf{P}_7=\begin{bmatrix}-\mathbf{K}_{22} & 0\\ 0 & -\mathbf{g}_{22}\end{bmatrix}$$

where $\mathbf{P}_i\left(i=1,2,...,7\right)$ are the global matrices, $\mathbf{V}$ is the global nodal displacement and temperature vector. The harmonic wave-form solution of equation (k) is assumed as

$$\mathbf{V}=\mathbf{V}_0e^{i(n\theta-\omega t)} \tag{l}$$

Substitution of equation (l) into equation (k) results a set of linear homogeneous equations

$$\left(-\omega^2\mathbf{P}_1-\omega^2(in)\mathbf{P}_2-i\omega\mathbf{P}_3+\omega n\mathbf{P}_4+\mathbf{P}_5+in\mathbf{P}_6-n^2\mathbf{P}_7\right)\mathbf{V}_0=0 \tag{m}$$

Solution of the generalized eigenvalue problem (m) gives the dispersion relation for plane strain problem.